International Ocean Discovery Program Expedition 403 Scientific Prospectus

Eastern Fram Strait Paleo-Archive (FRAME)

Renata Giulia Lucchi
Co-Chief Scientist
Department of Geophysics
National Institute of Oceanography and Applied Geophysics-OGS
Italy

Kristen St. John
Co-Chief Scientist
Department of Geology and Environmental Science
James Madison University
USA

Thomas A. Ronge
Expedition Project Manager/Staff Scientist
International Ocean Discovery Program
Texas A&M University
USA

Publisher's notes

This publication was prepared by the *JOIDES Resolution* Science Operator (JRSO) at Texas A&M University (TAMU) as an account of work performed under the International Ocean Discovery Program (IODP). This material is based upon work supported by the JRSO, which is a major facility funded by the National Science Foundation Cooperative Agreement Number OCE1326927. Funding for IODP is provided by the following international partners:

National Science Foundation (NSF), United States
Ministry of Education, Culture, Sports, Science and Technology (MEXT), Japan
European Consortium for Ocean Research Drilling (ECORD)
Ministry of Science and Technology (MOST), People's Republic of China
Australia-New Zealand IODP Consortium (ANZIC)
Ministry of Earth Sciences (MoES), India

Portions of this work may have been published in whole or in part in other IODP documents or publications.

This IODP *Scientific Prospectus* is based on precruise *JOIDES Resolution* Facility advisory panel discussions and scientific input from the designated Co-Chief Scientists on behalf of the drilling proponents. During the course of the cruise, actual site operations may indicate to the Co-Chief Scientists, the Expedition Project Manager/Staff Scientist, and the Operations Superintendent that it would be scientifically or operationally advantageous to amend the plan detailed in this prospectus. It should be understood that any substantial changes to the science deliverables outlined in the plan presented here are contingent upon the approval of the IODP JRSO Director and/or *JOIDES Resolution* Facility Board.

Disclaimer

The JRSO is supported by the NSF. Any opinions, findings, and conclusions or recommendations expressed in this material do not necessarily reflect the views of the NSF, the participating agencies, TAMU, or Texas A&M Research Foundation.

Copyright

Except where otherwise noted, this work is licensed under the Creative Commons Attribution 4.0 International (CC BY 4.0) license (**https://creativecommons.org/licenses/by/4.0/**). Unrestricted use, distribution, and reproduction are permitted, provided the original author and source are credited.

Citation

Lucchi, R.G., St. John, K., and Ronge, T.A., 2023. Expedition 403 Scientific Prospectus: Eastern Fram Strait Paleo-Archive (FRAME). International Ocean Discovery Program. https://doi.org/10.14379/iodp.sp.403.2023

ISSN

World Wide Web: 2332-1385

May 2023

Abstract

The North Atlantic and Arctic Oceans are unquestionably major players in the climatic evolution of the Northern Hemisphere and in the history of the meridional overturning circulation of the Atlantic Ocean. The establishment of the modern North Atlantic Water (NAW) transporting heat, salt, and moisture to the Northern Hemisphere has been indicated as one of the main forcing mechanisms for the onset of the Northern Hemisphere glaciation. NAW controls the extent and dynamics of circum-Arctic and circum-North Atlantic ice sheets and sea ice in addition to deep water and brine production. How the ocean system and cryosphere worked during past warmer intervals of high insolation and/or high atmospheric CO_2 content is still largely unknown and debated. The required information can only be attained by offshore scientific drilling in high-resolution, continuous, and undisturbed sedimentary sequences identified on the western continental margin of Svalbard (eastern side of the Fram Strait) along the main pathway and northern penetration of the NAW flowing into the Arctic Ocean. The area around Svalbard is very sensitive to climatic variability and it can be considered as a "sentinel of climate change." Further, the reconstruction of the dynamic history of the marine-based paleo-Svalbard-Barents Sea Ice Sheet is important because it is considered the best available analog to the modern, marine-based West Antarctic Ice Sheet, for which the loss of stability is presently the major uncertainty in projecting future global sea level rise in response to the present global climate warming.

Plain language summary

The Fram Strait is a special gateway for ocean currents to flow between the North Atlantic and Arctic Oceans. The northward flowing current system plays important roles in regional and global climate change because of the heat, salt, and moisture it brings to the Arctic region, which influence the formation and melting of ice sheets and sea ice, as well as the overturning circulation of the ocean itself. Thick deposits of ocean sediments (sediment drifts) have accumulated over millions of years under the effect of the warm current flowing along the seafloor in the eastern Fram Strait. Shaped by the bottom current, and fed by the input of marine biological activity and sediments delivered by advancing and retreating glaciers on the nearby continental margin, sediment drifts contain the record of the past (paleo) oceanographic and climatic changes that occurred over millions of years. The dynamic history of ocean-ice interactions during global climate transitions, such as the onset of Northern Hemisphere glaciation, and past periods of rapid warming and higher CO_2 levels than today can be reconstructed from the detailed record contained in these sediment drifts. These paleoclimate data are valuable for groundtruthing climate models of projected future CO_2, temperature, and ice sheet stability.

1. Schedule for Expedition 403

International Ocean Discovery Program (IODP) Expedition 403 (Eastern Fram Strait Paleo-Archive [FRAME]) is based on IODP drilling Proposal 985 (including versions 985-Full2 and 985-Add available at **http://iodp.tamu.edu/scienceops/expeditions/eastern_fram_strait_paleo_archive.html**). Following evaluation by the IODP Scientific Advisory Structure, the expedition was scheduled for the research vessel (R/V) *JOIDES Resolution*, operating under contract with the *JOIDES Resolution* Science Operator (JRSO). At the time of publication of this *Scientific Prospectus*, the expedition is scheduled to start in Reykjavík, Iceland, on 4 June 2024 and to end in Amsterdam, The Netherlands, on 2 August. A total of 60 days will be available for the transit, drilling, coring, and downhole measurements described in this report (for the current detailed schedule, see **http://iodp.tamu.edu/scienceops**). Further details about the facilities aboard *JOIDES Resolution* can be found at **http://iodp.tamu.edu/labs/index.html**.

2. Introduction

The Arctic and North Atlantic Oceans are unquestionably major players in the climatic evolution of the Northern Hemisphere (e.g., Overland et al., 2011; Mahajan et al., 2011). Many uncertainties remain about the establishment, evolution and role of the northern North Atlantic–Arctic Ocean circulation in relation to the opening of the Fram Strait, and its impact on the Earth's global climate during the major climatic transitions that occurred since the late Miocene. Further, the linkage among changes in insolation, atmospheric CO_2 levels, ocean dynamics, and cryosphere in the past and in the future remains unclear. A present major concern is the impact that meltwater release from Greenland and Antarctic ice sheets under the ongoing global climate warming will have at regional to global scales. The Arctic in particular is currently experiencing temperature changes that are two to four times faster than the global average (Intergovernmental Panel on Climate Change, 2014; Rantanen et al., 2022). Numerical simulations of past and current Greenland Ice Sheet melting have indicated the meltwater's potential to slow down the Atlantic meridional overturning circulation (AMOC) (Rahmstorf et al., 2015; Turney et al., 2020). The weakening of AMOC was shown to induce a bipolar seesaw by transferring the heat to Southern high latitudes, accelerating the demise of the West Antarctic Ice Sheet (WAIS) during the last interglacial (Turney et al., 2020). Antarctic ice sheet melting could then cause a cooling and a drying in the Northern Hemisphere high latitudes due to a reduction of Antarctic Bottom Water formation as one of major drivers of the AMOC (Golledge et al., 2019). Reconstructing the dynamic history of ocean and ice sheet interactions along the western margin of Svalbard and eastern side of the Fram Strait at the gateway to the Arctic is key to understanding the linkage among insolation, atmospheric CO_2 concentration, ocean circulation, and ice sheet dynamics.

Expedition 403 (Figure **F1**) is motivated by the necessity of retrieving continuous, high-resolution, and datable depositional sequences containing the record of the paleoceanographic characteristics and cryosphere evolution during past key climatic transitions that followed the opening of the Fram Strait. Such data are greatly needed to generate a FRAME of information to better constrain global climate connections, forcing mechanisms and climate models.

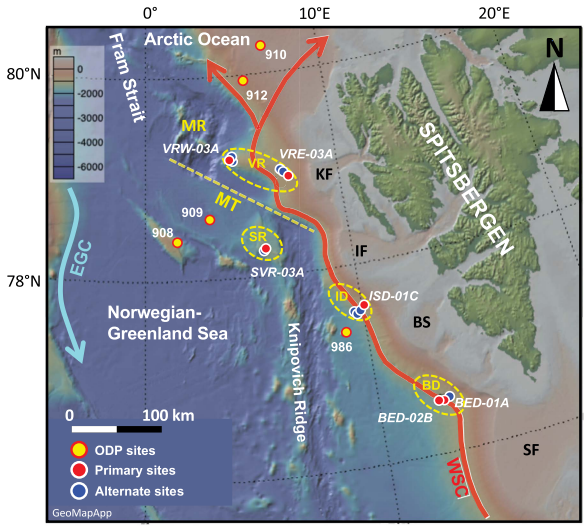

Figure F1. Location of Expedition 403 sites and relevant Leg 151 and 162 sites. Dashed yellow circles = location of sediment drifts that are the object of this study. WSC = West Spitsbergen Current, EGC = East Greenland Current, KF = Kongsfjorden Fjord, IF = Isfjorden Fjord, BS = Bellsund Fjord, SF = Storfjorden Fjord, MR = Molloy Ridge, VR = Vestnesa Ridge, SR = Svyatogor Ridge, ID = Isfjorden drift, BD = Bellsund drift, MT = Molloy transform. Scale shows North Atlantic circulation (red = warm Atlantic water; blue = cold Arctic water).

3. Background

3.1. Modern oceanography and climate

The Fram Strait is the only deepwater (~2600 m) passage between the Arctic and the subpolar oceans, and is crossed by two opposite oceanic currents (Figure F1). North Atlantic Water (NAW) flows into the Arctic via the West Spitsbergen Current (WSC), the northernmost branch of the North Atlantic Current, delivering heat, salt, and moisture to the Arctic Ocean (Teigen et al., 2010; Agarwal and Worster, 2021; Figure F2A). The heat from the WSC is a primary control on air temperature over Svalbard, and is the primary control enabling nearly sea-ice free conditions in the winter month in the eastern Fram Strait (western Svalbard margin). In contrast, cold, low-salinity water masses are brought southward along the western side of the Fram Strait by the East Greenland Current (EGC), which is responsible for the sea ice coverage along East Greenland, and contributes to the stability of the Greenland Ice Sheet.

The WSC is a bathymetrically controlled boundary current that hugs the continental slope of western Svalbard. The current extends from near the surface to >1500 m water depth and flows at an average rate of 30 cm/s along the 1000 m isobath (Beszczynska-Möller et al., 2012; Bensi et al., 2019). The WSC transports to the north both NAW, which is a subsurface water mass located between 300–400 and 800–1000 m water depth, and the Norwegian Sea Deep Water (NSDW) located below 1200 m water depth. The NAW is a saline and warm water mass that is 2°–6°C in the summer and 2°–4°C in the winter (von Appen et al., 2016; Beszczynska-Möller et al., 2012). It is estimated that the shallow core of the WSC composed of NAW loses 300 W/m^2 in the summer and 1000 W/m^2 in the winter, having a strong impact on the Arctic Ocean heat balance (Saloranta and Haugan, 2004). In addition to seasonal differences in temperature and heat loss, the waters transported by the WSC also exhibit seasonal cycles of stratification, velocity, and stability. Winter cooling and stronger winds lead to weaker stratification (greater convection), stronger flow (at times overshooting 40 cm/s in the shallow area; Bensi et al., 2019), and more vertical shear. These factors create more instability in the current and increase the formation of eddies, compared to summer (von Appen et al. 2016; Hattermann et al., 2016).

The colder (less than –0.9°C) and more saline (>34.91 ppt) NSDW fill the deep marine environment below 1200 m water depth underlying the NAW (Aagaard et al., 1985; Rudels et al., 2000;

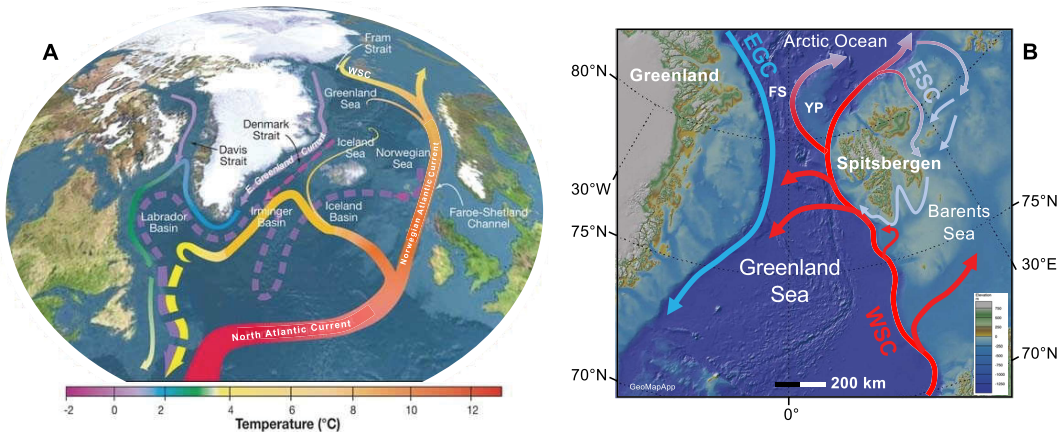

Figure F2. Modern oceanographic configuration of North Atlantic Ocean. A. Schematic circulation of surface currents (solid curves) and deep currents (dashed curves) that form portion of AMOC. Curve colors indicate approximate temperatures. North Atlantic Current transporting warm and salty NAW, derives from Caribbean Gulf Stream. Current changes name along European coasts, and northernmost tip flanking western margin of Spitsbergen is called West Spitsbergen Current (WSC). Modified after Curry (2010); **https://editors.eol.org/eoearth/wiki/File:OCP07_Fig-6.jpg**, permission for use via Creative Common 3.0). B. Details of northernmost part of Atlantic Ocean currents' configuration (see text for details). ESC = East Spitsbergen Current, EGC = East Greenland Current, YP = Yermak Plateau, FS = Fram Strait (Bathymetry IBCAO-v3; Jakobson et al. (2012).

Langehaug and Falck, 2012). At this depth, the WSC is slower (5–10 cm/s; Bensi et al., 2019) but still steering northward. Although the high-energy shallow core of WSC causes erosion of the upper slope and outer part of the shelf, the slower deeper core, moving within NSDW, allows for greater deposition contributing to the growth of sediment drifts along the seabed (Figure **F3**). Source water for the NSDW comes from the mixing of Greenland Sea Deep Water and Eurasian Basin Deep Water in the Fram Strait (Bensi et al., 2019) and is modified locally by turbulent mixing along the Barents Sea slope (Swift and Koltermann, 1988).

The proximity of the WSC to the continental shelf of western Svalbard sets up additional interactions that modify physical properties of the water, as well as nutrient availability. Cold freshwaters from the Svalbard coast and fjords that mix with the warmer, salty NAW contribute to cooling and freshening of the WSC as it flows north (Koenig et al., 2018). Dense water formation from heat loss to the atmosphere, sea ice formation, and related brine rejection can overflow the shelf edge (Quadfasel et al., 1988, 1992; Schauer, 1995; Bensi et al., 2019). Some of this overflow includes sediment-rich gravity plumes (sensu Fohrmann et al., 1998) that cascade downslope, transporting terrigenous sediment, oxygen, and nutrients offshore. Conversely, WSC warm waters can intrude into the shelf waters and in fjords (some 200–400 m water depth; Nilsen et al., 2016). The shoreward propagation of Atlantic waters from the WSC occurs both from wind-driven upwelling and from seasonal storms (Koenig et al., 2018). The addition of oceanic heat can increase the melt rate of ocean-terminated glaciers (especially ice shelves) and has been identified as a contributing mechanism leading to accelerating ice flow, thinning, and retreat (Nilsen et al., 2016 and references therein).

Decades of oceanographic monitoring indicate that core temperatures of the WSC are rising. For example, the decadal average temperatures of the WSC between 20 and 200 m water depth rose from 4.4°C in 1963 to 5.3°C in 2021 at monitoring stations at ~79°N (Norwegian Polar Institute, 2022). The influx of warm North Atlantic waters to the Arctic via the WSC flow through the Fram Strait is a primary contributor to modern Arctic sea ice loss. This "Atlantification" of the Nordic Seas and Arctic (Årthun et al., 2012; Tsubouchi et al., 2018; Tesi et al., 2021) in turn furthers heat transfer from the ocean to the atmosphere, as well as reduces regional albedo, resulting in disproportionate air and surface warming of the Arctic region (an "Arctic Amplification"), such that the Arctic has warmed 2–4 times faster than the global average since 1979 (Intergovernmental Panel on Climate Change, 2014; Rantanen et al., 2022) and may be transitioning to a new climate state.

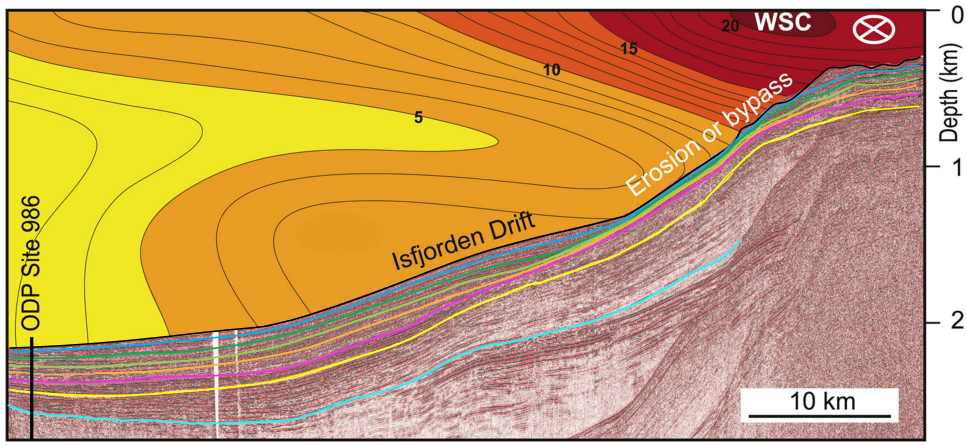

Figure F3. Seismic profile across Isfjorden drift plotted below the WSC velocity (cm/s) pattern (see Figure F1). Velocity profile of WSC presents two cores: strong shallow core of WSC transporting warm NAW (30–40 cm/s) causes sediment erosion and/or bypass in upper continental slope and shelf, whereas low-velocity deep core of the current (~1500 m water depth; 5–10 cm/s), transporting NSDW, promotes deposition with growth of Isfjorden drift. White cross symbol (arrow's tail) in top right corner indicates WSC northward flowing direction (modified after Rebesco et al., 2013).

As the WSC flows north of Svalbard it splits into two currents (Figure **F2B**). One branch (the North Spitsbergen Current) flows northeast along the Eurasian continental margin, ultimately contributing to the counterclockwise current system that encircles the entire Arctic Basin and returns to the Nordic Sea via the EGC. The other branch (the Yermak Slope Current) flows more directly north at intermediate depths along the western margin of the Yermak Plateau, transporting relatively warm North Atlantic waters into the Arctic Ocean interior.

Additionally, branches of the WSC recirculate west within the Fram Strait (Figure **F2B**; Bourke et al. 1988; Carmack et al., 2015). It is estimated that approximately half of the North Atlantic waters transported in the WSC recirculate westward between 76° and 81°N (Marnela et al., 2013) feeding the southward flowing EGC, and thereby ultimately contributing to the AMOC (Hattermann et al., 2016 and references therein). However, changes in the proportion transported north to the Arctic or west (recirculating) are influenced by seasonal climatic and hydrographic cycles (von Appen et al., 2016), as well as longer term regional and global changes, such as the dynamics of the North Atlantic Oscillation (Weijer et al., 2022), weakening of the Atlantic subpolar gyre associated with freshening of waters south of Greenland (Tesi et al., 2021), and anthropogenic global warming. Thus, the WSC is part of a complex oceanographic system that influences—and is influenced by—atmospheric, sea ice, and shelf-water interactions; its connections to regional gyres; and global ocean thermohaline circulation. Therefore, it is important to understand the behavior of the WSC under a range of climate states, transitions, and timescales.

3.2. Geologic setting

The timing and modality of the opening of the Fram Strait are still largely debated (Thiede and Myhre, 1996; Jokat et al., 2008; Knies and Gaina, 2008; Backman and Moran., 2009; Poirier and Hillaire-Marcel, 2011; Ehlers and Jokat, 2013; among others). Strike-slip movement and oblique ultraslow spreading in this region linked the active ocean ridge systems in the Norwegian-Greenland Sea (to the south) and the Arctic Eurasian Basin (to the north; Gruetzner et al., 2022). The continental areas were well separated by the early Miocene, but subsidence histories of different parts of strait are poorly known. However, much evidence indicates a deep ocean circulation was established between the Norwegian-Greenland Sea and the Arctic Ocean since about 6 Ma, during the Late Miocene (Jakobsson et al., 2007; Mattingsdal et al., 2014; Knies et al., 2014; Stärz et al., 2017).

The bathymetry of the eastern Fram Strait is related to its tectonic history, as well as its depositional history. Eiken and Hinz (1993) describe several bathymetric regions in this area; three of which are most relevant to the Expedition 403 sites (Figure **F1**):

- The region between the active spreading Knipovich Ridge and the western Svalbard continental slope. Ocean Drilling Program (ODP) Site 986 (Leg 162) and the southernmost Expedition 403 sites are in this region, with the Expedition 403 sites situated on plastered sediment drifts deposited along the continental slope.
- The region north of the Molloy transform fault (MTF) between the active spreading Molloy Ridge and the western Svalbard continental slope. The northernmost Expedition 403 sites are in this region at the west and east ends of an elongate sediment drift deposit that overlies relatively young oceanic crust (<19 Ma).
- The region south of the MTF between the Hovgaard Ridge and the northernmost extension of the Knipovich Ridge. The Hovgaard Ridge is an aseismic (i.e., nonspreading) ridge of uncertain origin (Myhre et al., 1982; Engen et al., 2008; Gruetzner et al., 2022). ODP Leg 151 Site 908 is located on that ridge, and ODP Site 909 is located in the Molloy Basin just north of it. One Expedition 403 site is located on a sediment drift deposit that extends off the western flank of the Knipovich Ridge and overlies very young (<10 Ma) oceanic crust.

The depositional history along the eastern Fram Strait is influenced by changes in strength of the WSC, as well as the onshore geology, including post-break-up regional tectonic uplift, and the dynamics of the Svalbard-Barents Sea Ice Sheet (SBSIS) complex. The archipelago of Svalbard is

the northwest emergent part of the Barents Sea Shelf. Western Svalbard is a mountainous terrain of faulted and folded Devonian to Paleogene sedimentary units partially overlying older crystalline basement rocks. Additionally, Quaternary volcanic units occur in the northwest. Western Svalbard experienced multiple episodes of uplift and erosion that occurred both pre- and postrifting (Lasabuda et al., 2021). Uplift events are associated with a range of tectonic (e.g., rift-flank uplift, crustal flexure, and transpressive movement), mantle, and glacio-isostatic processes (Minakov, 2018; Lasabuda et al., 2021). The creation of elevated topography may have been one of the necessary preconditions for glaciation at the Miocene–Pliocene transition and for the growth of ice sheets in Svalbard and across the broader Barents Sea Shelf in the late Pliocene and Pleistocene (Knies et al., 2014; Gruetzner et al. 2022).

The Barents Sea covers one of the Earth's most extensive continental shelves. It is characterized by a complex morphology of shallow banks (50–100 m water depth) and deep troughs (200–400 m water depth) cutting across the shelf (Nilsen et al., 2016) and was shaped by multiple advancements and retreats of the SBSIS in the Pliocene–Pleistocene (Alexandropoulou et al., 2021). Similar to the Antarctic margins, ice sheet basal ablation and ice mass weight caused deepening of the substrate and differential isostatic subsidence generating retrograde profiles along the main glacial troughs (e.g., Bjørnøyrenna, Storfjorden Trough). In the Pleistocene, the SBSIS complex became marine based (Laberg et al., 2010; Alexandropoulou et al., 2021), and this change potentially subjected the SBSIS to marine-ice sheet instabilities under warm oceanic conditions like those observed at the margin of the modern WAIS, as outlined by Petrini et al. (2018, 2020). To these extents, the paleo marine-based SBSIS can be considered the best analog to the modern marine-based WAIS, for which the loss of stability is a major concern for future global sea level projections in response to the present global warming. The record of the paleo-SBSIS is more easily accessible compared to Antarctica, making it an ideal laboratory to further investigate the effects of ice–atmosphere–ocean interactions under fast warm climatic oscillations, as well as the Late Miocene and Pliocene–Quaternary transitions that remain poorly constrained.

Recent bathymetric analysis of submarine glacial landforms in the Norwegian Sea provides further evidence that Nordic paleo-ice sheets records can inform scientific understanding about modern WAIS processes and future risks. Batchelor et al. (2023) identified submarine grounding lines along the mid-Norwegian shelf which indicate rapid (55–610 m/day) buoyancy-driven ice sheet retreat during the late Pleistocene deglaciation. These values exceed previously reported rates of glacial retreat from modern (satellite) and paleo (marine-geologic) records and suggest the possibility for rapid retreat of currently vulnerable glaciers, including those of the WAIS.

3.3. Depositional setting and processes

The sedimentary records that are the focus of Expedition 403 are contained within the contourite drifts that were built and shaped by the WSC flowing along the western margin of Svalbard into the Arctic Ocean (Figure **F3**). Contourite drifts are mounded depocenters generated by persistent (over millions of years) bottom currents that transport and deposit sediments delivered to the depositional system through other processes such as marine biological activity, downslope moving turbidity currents, and glaciogenic processes. They cover large areas of the European North Atlantic margin including the Norwegian Sea, Barents Sea, and western Svalbard along the eastern side of the Fram Strait (Laberg et al., 2005). Their development has been related to tectonically influenced intensification of the paleocirculation system transporting warm NAW to the North Atlantic and Nordic Seas. These influences include the closing of the Central American Gateway in the Pliocene (Coates and Obando, 1996; O'Dea et al., 2016), the subsidence of the Greenland-Scotland Ridge during the middle Miocene (Bohrmann et al., 1990; Wright, 1998), and the opening of the Fram Strait sometime between the late Eocene and late Miocene (20 and 5 Ma; Jakobsson et al., 2007; Knies and Gaina, 2008; Zachos et al., 2008; Geissler et al., 2011; Thompson et al., 2012; Hegewald and Jokat, 2013; Stärz et al., 2017; Stevenson et al., 2015; Tripati and Darby, 2018; among many others).

During times of glacial ice expansion and retreat (Figure **F4A, F4B, F4D**), terrigenous sediment has been delivered to the western Svalbard continental slope through two main glacigenic processes: (1) mass transport deposition, indicating shelf-edge glaciations, forming several tens of meters thick deposits of highly consolidated glacigenic diamicton (upper slope; Figure **F4**, Facies 1) and normally consolidated glacigenic debris flows (middle and low slope) (Solheim et al., 1996; Vorren and Laberg, 1997; Butt et al., 2000; Vanneste et al., 2007); and (2) sediment laden meltwater plumes associated with ice sheet melting and retreat during glacial terminations and responsible for the deposition of plumites (sensu Hesse et al., 1997) (Figure **F4**, Facies 3), having an aerial distribution confined within a few tens of kilometers from the source area (Lucchi et al., 2002, 2013; Shackleton et al., 2020). The thickness of plumites can vary from a few centimeters to several meters in the area proximal to the efflux point. Ice-rafted debris (IRD) (Figure **F4**, Facies 2) can be associated with meltwater deposition (ice sheet decay) or with a highly dynamic growing ice sheet

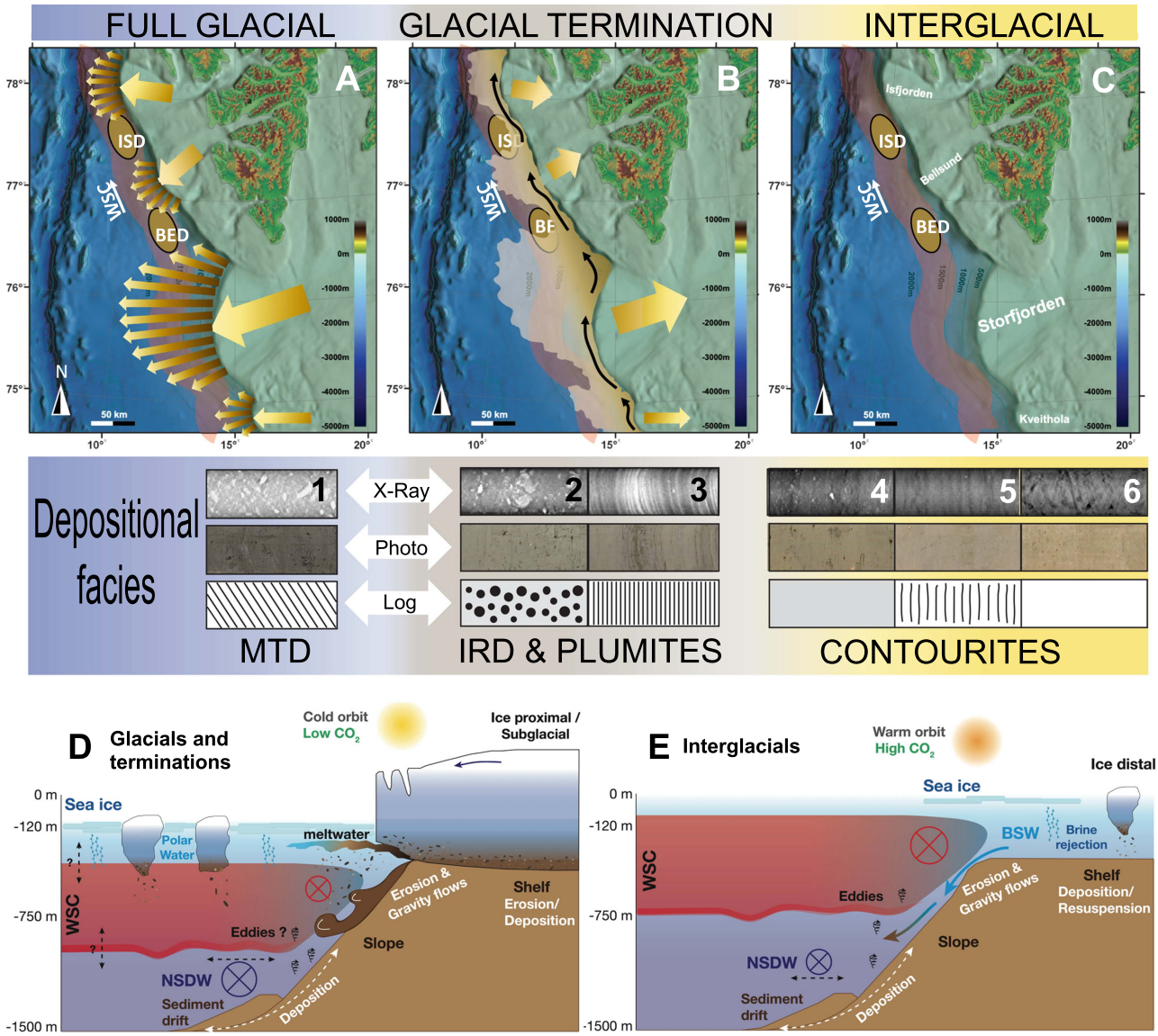

Figure F4. Depositional facies associated with climatic conditions after onset of shelf-edge glaciations on western margin of Svalbard (1.3 Ma). (A, B, C) Plan view and (D, E) cross section view give overview of depositional processes contributing sediments to contourite depositional system. Sediment facies analysis according to Lucchi et al. (2013): 1 = glacigenic diamicton, 2 = massive or layered IRD, 3 = plumites, 4 = bioturbated IRD-rich contourites, 5 = crudely layered contourites, 6 = heavily bioturbated contourites. MTD = mass transport deposit, BED = Bellsund drift, ISD = Isfjorden drift, WSC = West Spitsbergen Current, NSDW = Norwegian Sea Deep Water (includes deep branch of WSC), BSW = brine-enriched shelf waters.

(high calving rates). All these sediment types provide direct information on the ice sheet dynamics that is complementary to the paleoceanographic information and contribute to the reconstruction of the climate history of the area.

During warm interglacials (Figure **F4C, F4E**), the sedimentation is dominated by bottom currents generating condensed sequences in the upper slope where the current speed is higher (Figure **F4**, facies 4) and expanded sequences in the lower slope where sediment drifts build, formed by fine-grained crudely layered (Figure **F4**, Facies 5) or highly bioturbated sediments (Figure **F4**, Facies 6). Presently, and possibly during past interglacials, sediment input from near shore settings is delivered by downslope cascading of brine-enriched shelf waters (BSW) (Figure **F4E**) which form during winter through persistent freezing and brine rejection (Quadfasel et al., 1988; Schauer, 1995; Skogseth et al., 2005). Dense BSW, moving across the shelf, resuspend seafloor sediments that are transported to the shelf break and delivered to the deeper environments entering the NSDW and transported northward or deposited in sediment drifts. This process is thought to be the present principal mechanism responsible for initiation of slope convection in the Arctic Ocean contributing significantly to the overall heat and salt balance of the deep Arctic Ocean basins, providing ventilation to the deeper environments (Fer et al., 2003; Schauer, et al., 2004).

Given these sediment input processes, contourites provide records of marine biogenic and terrestrial/cryospheric variability through time, as well as changes in current intensity. Contourite drifts on the slope close to the outlet troughs of marine ice sheets can contain detailed information on ice sheet dynamics through time. Additionally, contourite drifts that develop on the slope between trough mouth fan systems can be especially useful for paleoceanographic reconstructions, as these interfan-slope depocenters are mainly under the influence of along slope currents and hemipelagic deposition, yet less directly in the path of debris flows (Figure **F4A**). These settings are characterized by relatively high and continuous accumulation rates. The sediments forming contourite drifts are typically bioturbated and very rich in biogenic fraction thanks to the continuous supply of oxygen and nutrients through the bottom currents, making these areas a suitable environment for the benthic biological community. In addition, high sedimentation rates allow fast burial of the biological remains facilitating good preservation in the stratigraphic sequences, making these sediments optimal for paleoreconstructions (Laberg and Vorren, 2004; Knutz, 2008; Rørvik et al., 2010; Rebesco et al., 2014a). The depositional sequences of the contourite drifts that developed along the western margin of Svalbard and eastern side of the Fram Strait, therefore, preserved a high-resolution, mostly continuous sedimentary record since the Late Miocene (Eiken and Hinz, 1993; Howe et al., 2008; Rebesco et al., 2013; Waghorn et al., 2018), with regionally consistent paleoceanographic and paleoclimatic records at least since 1.6–1.3 Ma (Butt et al., 2000; Rebesco et al., 2014b).

3.4. Paleoceanographic and paleoclimatic context

The establishment of the modern NAW circulation has been indicated as one of the main forcing mechanisms for the late Pliocene–Pleistocene onset of the North Hemisphere glaciation (NHG) (Haug et al., 2005; Schmidt, 2007; Lunt et al., 2008), in contrast with the warming effects of the mid-late Pliocene high concentration of atmospheric CO_2. The NAW flux and properties (salinity and temperature) exerted a strong control on the extent and dynamics of circum-Arctic and circum-North Atlantic ice sheets, sea ice formation and distribution, modulating brine production, deep water mass characteristics, and hence climate.

Expedition 403 is designed to target the continuous and expanded (>300 m/My) paleoceanographic records preserved in the contourite drifts developed on the western margin of Svalbard and eastern side of the Fram Strait (Bellsund and Isfjorden drifts and Svyatogor and Vestnesa Ridges; Figure **F1**) since the onset of the NAW circulation in the northern Atlantic and Arctic Ocean (Howe et al., 2008; Rebesco et al., 2013; Waghorn et al., 2018). The regional record of the following key paleoclimatic transitions and events are expected to be present in the Expedition 403 cored sedimentary sequence (Figure **F5**).

3.4.1. Late Miocene–Early Pliocene transition

The Late Miocene–Early Pliocene transition (7–3.6 Ma; Holbourn et al., 2018) marked the transition between the Late Miocene cooling (LMC; 7–5.5 Ma), signing the end of a period of gradual temperature decrease initiated at around 13 Ma after the Mid Miocene Climatic Optimum (17–14.8 Ma), and the Early Pliocene (5.5–3.6 Ma), characterized by temperatures warmer than today. The LMC was characterized by a substantial drop in atmospheric CO_2 (≤300 ppm; Zhang et al., 2013; Mejía et al., 2017). Proxy-based global sea-surface temperature (SST) reconstructions, showed that a sustained cooling occurred synchronously in both hemispheres culminating with ocean surface temperatures dipping to near-modern values and with a steepening of the pole-to-equator gradient between about 7 and 5.4 Ma (Herbert et al., 2016). The period of maximum cooling coincides with evidence for transient glaciations in southern Greenland (Wolf and Thiede, 1991; Jansen and Sjøholm, 1991; Larsen et al., 1994; Wolf-Welling et al., 1995; Bierman et al., 2016; St. John and Krissek, 2002), the Arctic (St. John, 2008), and southern Alaska (Krissek et al., 1995).

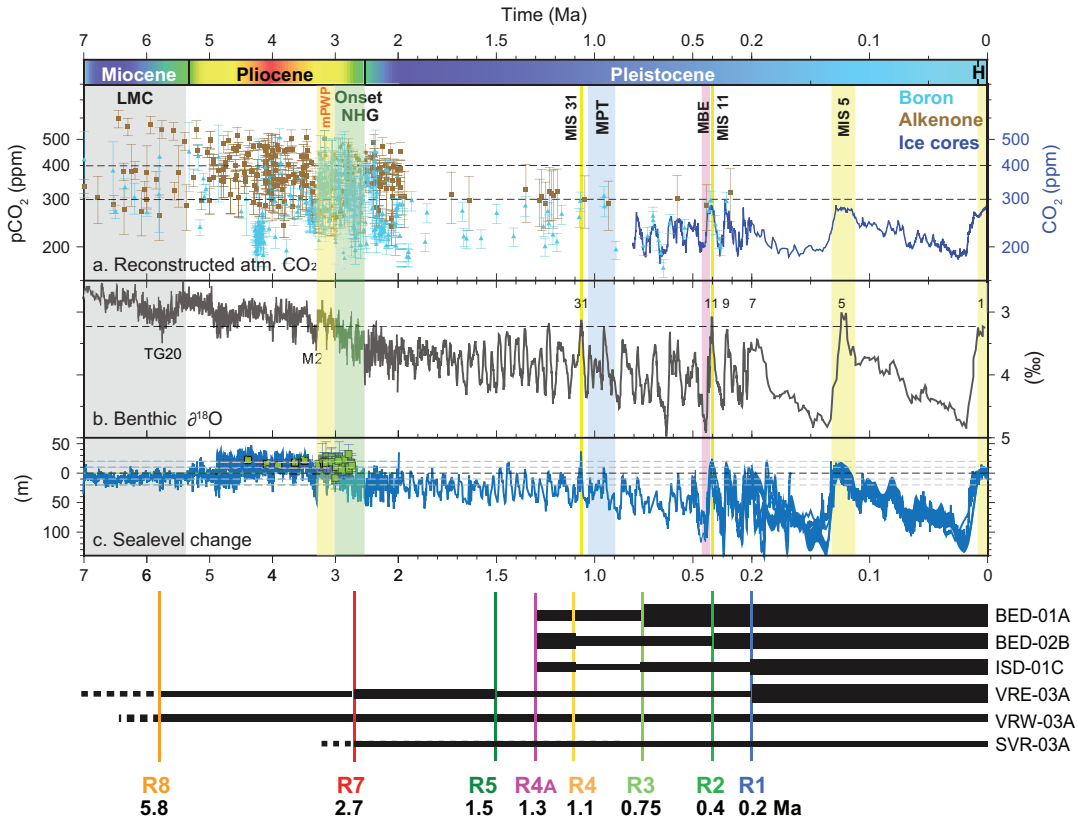

Figure F5. Composite record of major climatic transitions and events in last 7 My. Stratigraphic coverage of Expedition 403 primary sites is represented with black bars indicating stratigraphic resolution (thick lines = high resolution) and interpreted ages of main seismic reflectors (R1–R8). A. Reconstructed atmospheric pCO_2 levels are based on alkenone (Badger et al., 2013a, 2013b; Pagani et al., 2005, 2010, 2011; Seki et al., 2010; Super et al., 2018; Zhang et al., 2013) and boron measurements (Bartoli et al., 2011; Foster et al., 2012; Greenop et al., 2014; Hönisch et al., 2009). Late Pleistocene atmospheric CO_2 levels are based on Antarctic ice core composite record from Bereiter et al. (2015). B. Deep sea benthic $\delta^{18}O$ record from Zachos et al. (2001, 2008). Marine isotope stages (MIS; glacials and interglacials) are based on Miller et al. (1991) for Miocene, on Haywood et al. (2016) for Pliocene, and on Lisiecki and Raymo (2005) for Pleistocene. C. Proxy-based reconstructed global mean sea level changes (GMSL): benthic $\delta^{18}O$ (Miller et al., 2020), backstripped sequence stratigraphy from New Jersey (Kominz et al., 2008; Miller et al., 2005). For Pliocene, converted benthic $\delta^{18}O$ record from Dumitru et al. (2019) until Pliocene–Pleistocene Transition (PPT). Green squares = reconstructed Pliocene highstands (Dumitru et al., 2019; Dwyer and Chandler, 2009; Kulpecz et al., 2009; Miller et al., 2012; Naish and Wilson, 2009; Sosdian and Rosenthal, 2009; Wardlaw and Quinn, 1991; Winnick and Caves, 2015) and M2 glaciation (Dwyer and Chandler, 2009; Miller et al., 2005; Naish and Wilson, 2009). For last 400 ky, reconstructed curves of sea level changes are from Waelbroeck et al. (2002) and from Rohling et al. (2009). Yellow mask or line = warm periods of interest: mid-Pliocene Warm Period (mPWP), MIS 31, MIS 11, and MIS 5. Other transitions considered: Late Miocene cooling (LMC), onset of North Hemisphere glaciation (NHG), mid-Pleistocene transition (MPT), and mid-Brunhes event (MBE).

The Early Pliocene period is, instead, characterized by an increase in atmospheric CO_2 >400 ppm (Seki et al., 2010), global mean temperature higher by 2°–3°C relative to present with a culminating warmth at around 4.4 Ma (Fedorov et al., 2013), and a weaker meridional temperature gradient compared to present (Ford et al., 2015). Episodic seasonal Arctic sea ice was found through the Late Miocene (Stein et al., 2016) and was also recorded during the Early Pliocene on the Yermak Plateau at ca. 4.5 Ma with a substantial expansion observed from ca. 4 Ma (Clotten et al., 2019). A hypothesis relates this expansion with an increased northward transport of heat and moisture to the North Atlantic (Figure **F6**), likely leading to a fresher Arctic Ocean favoring sea ice formation (Clotten et al., 2019). The paucity of field information on this transition hampered the constraint of the possible forcing mechanisms.

3.4.2. Mid-Pliocene Warm Period

The mid-Pliocene Warm Period (mPWP; 3.3–3.0 Ma). Many scientists look at this period as the best analog to modern climatic conditions and its study can give important information to predict future scenarios. The Pliocene was characterized by a progressive rise of atmospheric CO_2 (>450 ppm) and temperatures, with values compatible with modern ones at about 4 Ma. This trend was suddenly interrupted at the beginning of the mPWP by a short cold period, the M2 glaciation (3.312–3.264 Ma; Lisiecki and Raymo, 2005), which is of particular interest because of its short duration (50 ka only) compared to the Pleistocene glaciations, its global character (20–60 m of global sea level drop), and its sharp termination (De Schepper et al., 2014), with a particularly intense interglacial (warm isotopic Stage KM5c) reaching temperature comparable to present day in a similar-to-present orbital context (Haywood et al., 2016). It is not yet understood what triggered the M2 glaciation (e.g., Tan et al., 2017) and what caused the following Stage KM5c warm conditions; however, such climatic events appear approximately coeval with transitory tectonic shallowing and deepening of the Central American Seaway preceding its final close (Schmidt, 2007).

The final closure of the Central American Seaway with formation of the Panama Isthmus at ca. 2.8 Ma (Coates and Obando, 1996; Burton et al., 1997; O'Dea et al., 2016) is postulated for the onset of the modern NAW configuration and intensification of NHG occurred since ca. 2.7 Ma (Figure **F6**).

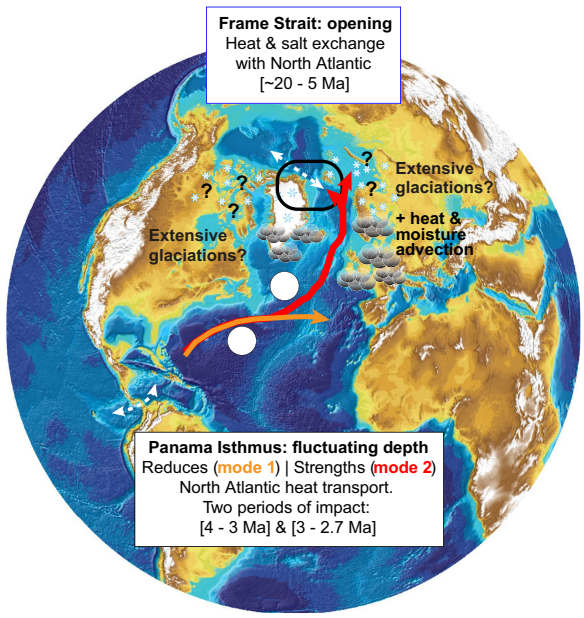

Figure F6. Effects of closure of Central American Gateway on north Atlantic oceanic circulation. Mode 1 = oceanic circulation with the open isthmus: weak north Atlantic circulation limited to low-mid latitudes, Mode 2 = oceanic circulation with presence of a shallow passage (4–3 Ma) or closed conditions (3–2.7 Ma): strong north Atlantic circulation with effective heat transport.

This also marks the first large-scale glaciation of western Svalbard (ca. 2.7 Ma) prograding onto the southernmost Yermak Plateau (Mattingsdal et al., 2014). Yet uncertainties remain about the timing of the Central American Seaway closure (Montes et al., 2015; Bacon et al., 2015), and numerical studies estimated that the heat provided by NAW strengthening, hindered hemispheric glaciations (e.g., Haug et al., 2005, Schmidt, 2007; Lunt et al., 2008; Tan et al., 2017), making the identification of possible forcing mechanisms still unsolved.

3.4.3. Onset of shelf-edge glaciations

Although based on poor age control, the SBSIS is interpreted to have reached the shelf break at different ages along the western Barents Sea/Svalbard margin. According to Alexandropoulou et al. (2021) an early, transient phase of shelf-edge glaciation occurred soon after 2.58 Ma and a second phase occurred between 1.95 and 1.78 Ma. Wide-spread shelf edge glaciation started at only ca. 1.5 Ma, reaching the shelf edge at the mouth of Bjørnøyrenna (Andreassen et al., 2007), and subsequently (ca. 1.2 Ma) on the Storfjorden/southern Spitsbergen margin (Rebesco et al., 2014b). The reasons for such diachronic onset, prograding from south to north under similar forcing mechanisms (Forsberg et al., 1999; Butt et al., 2000; Knies et al., 2009; Rebesco et al., 2014b), is still unclear.

3.4.4. Mid-Pleistocene transition

There is a general lack of consensus on the forcing mechanisms to explain the mid-Pleistocene transition (MPT; 1.2–0.7 Ma; Pisias and Moore, 1981), also known in the literature as the "100,000-year problem" (Shackleton, 2000; Raymo and Nisancioglu, 2003; Clark et al., 2006; Rial et al., 2013; Nyman and Ditlevsen, 2019). Recent studies indicated the interplay between atmospheric CO_2 concentration, orbital forcing, ocean circulation, and ice sheet dynamics to explain the shifts in glacial cyclicity from ca. 41 to 100 ky during the mid-Pleistocene (Holbourn et al., 2013; Levy et al., 2019), but robust constraints and definition of the main forcing mechanism are still missing.

3.4.5. Mid-Brunhes event

The causes of the mid-Brunhes event (MBE; ca. 400 ka), which marked the transition from cooler to warmer interglacials (Tzedakis et al., 2009; Cronin et al., 2017) characterized by larger amplitude stable oxygen isotope cycles and CO_2 cycles, with CO_2 overshooting 300 ppm (Tzedakis et al., 2009), and marked sea level highstands sometimes above present-day global mean sea level (e.g., Dutton et al., 2015), remain largely unclear.

3.4.6. Millennial-scale isotopic oscillations

Millennial-scale isotopic oscillations that occurred during the last 100 ky are the most similar past events to forecast future rapid climatic transition due to ice sheets melting. Those events were observed in ice core and sediment records, and they are referred to as Dansgaard-Oeschger (D-O) oscillations (warming abrupt event; Dansgaard et al., 1993) and Heinrich events (cooling events during cold stadials). In particular, 25 D-O oscillations (ca. each 2000 y to a few centuries in duration) have been identified in the North Greenland Ice Core Project ice core record over the last 125 ky (North Greenland Ice Core Project Members, 2004) and at least 6 Heinrich events (marked IRD layers) have been found in the North Atlantic sediment records (Bond et al., 1992), likely caused by massive iceberg discharge because of Laurentide Ice Sheet instabilities (Broecker et al., 1992). D-O and Heinrich events are not unrelated, and their alternation could be caused by the "bipolar seesaw" (Stocker and Johnsen, 2003) (i.e., oceanic heat and salt transfer from one hemisphere to another to balance freshwater input). This concept is also supported by the numerical simulations conducted by Golledge et al. (2019) and Turney et al. (2020) that clearly indicate the close tie existing between the antipodes polar areas.

3.5. Seismic studies/site survey data

The supporting site survey data for Expedition 403 are archived at the IODP Site Survey Data Bank (**https://ssdb.iodp.org/SSDBquery/SSDBquery.php**; select P985 for Proposal Number).

3.5.1. Site survey data

The geophysical data set includes multichannel seismic lines (2-D seismic), high-resolution P-Cable 3-D seismic, subbottom profiles, and multibeam bathymetry that were collected during several campaigns of acquisition from collaborating groups (2007–2021). The profiles were recorded with different sources and streamers and were merged into a homogeneous data set used to identify the six primary sites for Expedition 403.

To perform the depth conversion of the interpreted seismic horizons in the Bellsund-Isfjorden area including the water bottom, Seismic Reflectors R1 (0.2 Ma), R2 (0.4 Ma), R3 (0.75 Ma), R4 (1.1 Ma), and R4A (1.3 Ma) at the proposed sites, velocity functions derived from trace stacking were applied. For proposed primary Site BED-01A, the velocity analyses made at Shotpoint (SP) 2125 on Seismic Line EG-04 were used where Site BED-01A is projected (about 1 km distance), and the same velocity function of the proposed alternate Site ISD-03A at SP 3295 on Line EG-01A was used where proposed alternate Site ISD-04B is projected.

Different studies explored seismic velocity variations along and across Vestnesa Ridge (Singhroha et al., 2019; Goswami et al., 2015; Hustoft et al., 2009; Petersen et al., 2010). Seismic velocities were estimated for different intervals (~20–30 m layer interval thickness) through traveltime inversion. These data exist from stations at or close to the crest of the Vestnesa Ridge. This area however shows a gas-hydrate related bottom-simulating reflector (BSR), hence, the presence of hydrates and free gas beneath the BSR affects velocities, evident in the velocity inversion at about 180 meters below seafloor (mbsf).

Interval seismic velocities in different studies show an increase in *P*-wave velocity from ~1.5 km/s near the seafloor to ~1.8 km/s above the BSR. The highest interval seismic velocities (>1.8 km/s) are observed above the BSR and indicate the presence of gas hydrates. Seismic velocities below the BSR show variations from ~1.3 to 1.6 km/s and can be linked to variations in free gas concentrations. Uncertainty in seismic velocity estimates from different studies lies in between ~0.03 and 0.06 km/s. This will create uncertainty of ~4–8 m in depth estimates derived from these seismic velocity models.

All drill sites are exclusively chosen away from the BSR and any hydrocarbon indicators in seismic data.

Velocity estimates for the Svyatogor Ridge area are scarce. One ocean-bottom seismometer station exists slightly west of the ridge axis but still within an area with indications for a BSR and hydrocarbons in subsurface sediments. Nonetheless, the sedimentary section at the Svyatogor Ridge has very similar characteristics as Vestnesa Ridge with mostly drift sediments deposited over the relatively young basement. Hence, it has been assumed that velocity distribution with depth is not significantly different from Vestnesa Ridge.

3.5.2. Geologic record

Shallow sediment cores at or close to the drill sites provide initial sediment properties and paleoceanographic interpretations (Caricchi et al., 2019, 2020; Carbonara et al., 2016; Jessen et al., 2010; Lucchi et al., 2013, 2014, 2015, 2018; Melis et al., 2018; Rigual Hernández et al., 2017; Rasmussen et al., 2007, 2014; Ślubowska et al., 2005; Ślubowska-Woldengen et al., 2007, 2008; Torricella et al., 2022; among others). The existing geologic data set includes multicores, box cores, gravity cores, piston cores (including long Calypso piston cores), and MeBo drilling. The shallow sedimentation in this area consists of fine-grained, bioturbated, contour current sedimentation mainly associated with interglacial periods, coarser grained intervals of interlaminated mud and silty layers corresponding with meltwater deposition (plumites), and intervals with sparse or massive IRD deposition mainly associated to the SBSIS decay and retreat (Figure **F4**). The correlation of shallow sediment cores (Figure **F7**) outlined the almost synchronous onset of climatic related conditions along the western margin of Spitsbergen, with prominent meltwater events (e.g., MWP-1A) associated with the decay of the paleo-SBSIS.

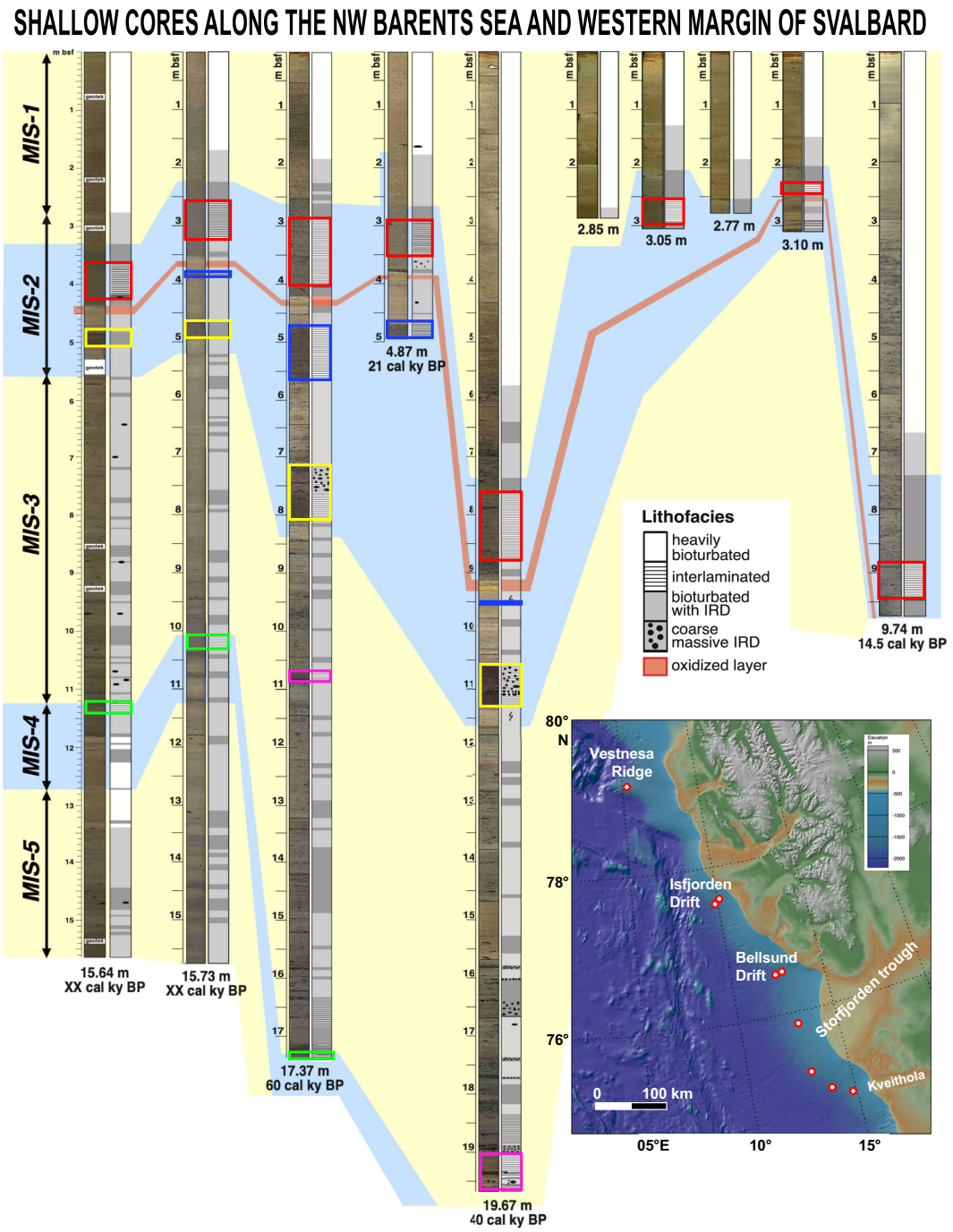

Figure F7. Correlation of shallow cores collected along northeastern margin of Barents Sea and west margin of Svalbard (location in inset map). Colored frames relate to stratigraphic marker beds (e.g., Meltwater pulses, Heinrich-like events) that were correlated all along margin, giving information on paleo-SBSIS dynamics.

4. Scientific objectives, hypotheses, and expected contributions

4.1. Relationships to the 2013–2023 IODP Science Plan and the 2050 Science Framework

Expedition 403 operates under the guidance of the 2013–2023 IODP Science Plan (Bickle et al., 2011). Specifically, the expedition science will address challenges (i.e., program-wide guiding questions) posed by three IODP Science Plan research themes:

- Climate and Ocean Change Challenges 1 and 2: How does Earth's climate system respond to elevated levels of atmospheric CO_2? How do ice sheets and sea level respond to a warming climate?
- Biosphere Frontiers Challenge 7: How sensitive are ecosystems and biodiversity to environmental change?
- Earth in Motion, Challenge 13: What properties and processes govern the flow and storage of carbon in the subseafloor?

The science objectives of Expedition 403 are also convergent with several areas of scientific inquiry described in the 2050 Science Framework (Koppers and Coggon, 2020). In particular, the Expedition 403 primary objective described below directly supports 2050 Science Framework Strategic Objective 3 Earth's Climate System to examine variations in ice sheets, ocean and atmospheric dynamics, and sea level. Understanding the interconnections among ocean, atmosphere, cryosphere, and marine biosphere in the eastern Fram Strait is an overarching Expedition 403 goal. In addition, the Expedition 403 secondary objectives described below focus on tectonic and deep biosphere scientific inquiries. These foci directly support 2050 Science Framework Strategic Objective 2 The Oceanic Life Cycle of Tectonic Plates, which aims to investigate the genesis, aging, motion, and destruction of oceanic lithosphere, and 2050 Science Framework Strategic Objective 1 Habitability and Life on Earth, which aims to define the conditions for, and the role of, life in the marine realm. Because Expedition 403 strives to obtain high-resolution paleoarchive records of Late Miocene to Pleistocene climate system events and transitions (including rapid warming events and paleoice sheet destabilizations), the 2050 Science Framework Objective 5 Tipping Points in Earth's History, which aims to use Earth's geologic past to illuminate future environmental change, is also of direct relevance. Finally, the scientific outcomes of Expedition 403 are expected to contribute data that can enable more robust modeling of direct and indirect cause and effect relationships in the Earth system under a range of CO_2 conditions, both similar to today and at levels projected for the near future. Therefore, the expedition science also contributes to 2050 Science Framework Flagship Initiative 1 Ground Truthing Future Climate Change.

4.2. Scientific objectives and hypotheses

4.2.1. Paleoceanographic/paleoclimatic objective

The primary objective of Expedition 403 is the reconstruction of the WSC (NAW) variability, its influence on climate changes particularly during key climate transitions (late Miocene–Pliocene transition, late Pliocene–Pleistocene transition, MPT, mid-Brunhes transition, and suborbital Heinrich-like events), and its impact on the Arctic glaciations, ice shelves development and stability, and sea ice distribution. The following related hypotheses can be tested.

4.2.1.1. Hypothesis 1

The WSC was the main forcing mechanism for the onset of the NHG and is a main forcing mechanism for climatic variability in the Northern Hemisphere through the supply of heat and salt modulating the growth and decay of the Arctic ice sheets and sea ice.

The establishment of the modern NAW has been indicated as one of the main forcing mechanisms for the onset of the NHG (e.g., Haug et al., 2005, Schmidt, 2007; Lunt et al., 2008). North Atlantic water flux and properties (salinity and temperature) control the extent and dynamics of circum-Arctic and circum-North Atlantic ice sheets, sea ice formation and distribution modulating brine

production, deepwater mass characteristics, and, hence, climate. How the ocean system worked during past warmer intervals of either/both high-insolation and/or high-atmospheric CO_2 content is still unknown and debated. Another critical issue to be addressed is the timing and evolution of the transitions into such warm intervals as gradual transition or punctuated by tipping points (e.g., Lenton et al., 2019).

4.2.1.2. Hypothesis 2

Quaternary variations in sea ice cover in the central Arctic Ocean were influenced by changes in the properties of the NAW, which in turn were affected by hemispheric or global climate shifts.

Only few studies exist that directly target the role of sea ice during Pleistocene glacial–interglacial cycles. Gildor and Tziperman (2001) used a simple box model of the ocean-atmosphere-sea ice-land ice climate system to propose the so-called "sea ice climate switch" to explain Pleistocene transitions from ice sheet advance into ice sheet retreat phases. The mechanism is based on the impact of sea ice on both the evaporation from high-latitude ocean areas and atmospheric moisture transport, which are pivotal for the continental ice sheet dynamics.

Massive discharge of Arctic sea ice through the Fram Strait during the Younger Dryas is increasingly suggested to have caused the weakening of the AMOC during the Younger Dryas resulting in a significant cooling at the end of the last deglaciation and highlighting the importance of nonterrestrial freshwater sources (opposed to glacial meltwater) for abrupt climate shifts (e.g., Bradley and England, 2008; Condron et al., 2020; Müller and Stein, 2014; Not and Hillaire-Marcel, 2012). Extended sea ice cover in the subpolar North Atlantic since 1 Ma has further been linked to lower primary productivity and elevated input of IRD during glacials (Stein and Fahl, 2013), but highly resolved records are missing to better constrain the role of sea ice during climate transitions.

4.2.1.3. Hypothesis 3

During the Quaternary, the variations of WSC pathway and characteristics triggered past SBSIS instabilities.

Reconstructions of the Barents Sea paleobathymetry suggest a similar evolution as for West Antarctica. The Barents Sea was much shallower and partly emerged until the Late Pliocene (Butt et al., 2002; Laberg et al., 2012; Zieba et al., 2017) and gradually deepened because of substrate erosion during past glaciations until most of the SBSIS became marine based with alternation of glaciations (Laberg et al., 2010). In analogy with West Antarctica during the Miocene (Colleoni et al., 2018), the SBSIS could have become more vulnerable to WSC intrusion on the continental shallow shelf.

We hypothesized that at some point in the Pleistocene the SBSIS became subject to more frequent instabilities of its grounding line, with rapid inland retreat and large IRD delivery and freshwater discharges along the Svalbard margin during warm intervals (e.g., interglacials, D-O events, and meltwater pulses). Those instabilities, combined with those of the Laurentide Ice Sheet, could have paced and shaped the glacial–interglacial cycles and their evolution throughout the Pleistocene (e.g., Clark et al., 1998).

4.2.1.4. Specific paleoceanographic/paleoclimatic objectives

The specific supporting objectives to be addressed that will fulfill the paleoceanographic and paleoclimatic goals include the following:

- The development of a high-resolution, Late Miocene–Quaternary chronostratigraphic record based on a suite of independent chronostratigraphic methods (Table **T1**) to temporally constrain paleoceanographic and paleoclimatic events and the paleo-SBSIS dynamics.
- The generation of multiproxy data sets to better constrain the potential concurrent forcing mechanisms responsible for Late Miocene to Quaternary climatic transitions.
- The identification of orbital-, suborbital-, and millennial-scale climate variations such as Heinrich events and possible associated prominent meltwater events (i.e., pulses of water discharge from ice sheet margins).

Table T1. Chronostratigraphic methods that may be applied to Expedition 403 sedimentary record. OM = organic matter, FMAZ = Faroe Marine Ash Zone, NAAZ = North Atlantic Ash Zone.

Method	Valid Time Range	Uncertainty	Requirements / Notes
Paleomagnetism and rock magnetism			
Geomagnetic Polarity reversals	>5My	$\pm10^3$ – 10^4 y	Fine-grained indisturbes sediments, stratigraphic continuity, well define component of magnetization. Note: dating is based on analysis of the stratigraphic trends. Problems: magnetic overprints acquired during later events in the sediment history, post-detrital remanent magnetization (pDRM) uncertainties, smearing and smoothing of the magnetic signal.
Relative paleointensity	<2My		
Geomagnetic polarity excursions	<2My	$\pm10^2$ – 10^3 y	
Paleosecular variation	<14ky		
Biostratigraphy			
Planktic and benthic Foraminifera	>5My	$\pm10^2$ – 10^4 y	Presence of microfossils. Note: biogenic carbonate abundance and preservation best during interglacials. Problems: microfossils preservation, sediment reworking.
Diatoms			
Dinoflagellate cysts			
Radiolaria			
Calcareous nannofossils			
Ostracods ecostratigraphy			
Others			
∂^{18}O stratigraphy	>5My	$\pm10^2$ – 10^3 y	Availability of not reworked planktic and benthic Foraminifera
Radiocarbon dating	<50ky	±10 – 10^3 y	Presence of biogenic carbonate and OM. Constraints on surface/bottom carbon reservoir during the last *ca.* 10ky
Orbital tuning	>5My	$\pm10^4$ y	Stratigraphic continuity
Tephrachronology	up to 780ky	±0.1 – 0.8 ky	Benchmark ages from well-documented ash layers e.g. Vedde Ash, FMAZ II-1, NAAZ II (II-RHY-1), 5e-Eem/Rhy I, etc.
Amino acid racemization	<1My	$\pm10^5$ y	Presence of Foraminifera
Be, Sr, Nd isotopes	>5My	$\pm10^2$ – 10^4 y	Carbonate preservation, stratigraphic correlation to orbital cycles
Extraterrestrial ^{3}He	>5My	$\pm10^4$ – 10^5 y	Used for vertical mass accumulation rates and/or timestamping of Late Miocene + Late Eocene solar system
^{230}Th/U dating	<500ky	±100 – 104 y	*In situ* deep-sea coral remains
^{210}Pb, ^{137}Cs	<100y	±10 y	Core-top sediment (anchoring with modern conditions)
eDNA chronology	This method is still at pioneering stage (e.g. Ellegaard et al., 2020). Samples will be collected to define / improve a eDNA chronostratigraphy.		

- The evaluation of the impact of past prominent sediment laden meltwater events on the paleoceanography, paleoenvironment, and paleoclimate.
- The reconstruction of the paleo-SBSIS dynamic history in relation to changes in the WSC pathways and characteristics as mechanisms inducing ice sheet instability and fast retreat.

In addition to the primary paleoceanographic/paleoclimatic set of objectives, the expedition will also address other two secondary, yet complementary objectives.

4.2.2. Tectonic objective

Expedition 403 will aim to constrain the spatial location of the Miocene–Pliocene transition (ca. 5.3 Ma) north and south of the MTF, at the Vestnesa Ridge and the Svyatogor Ridge, respectively (relevant connection to the canceled IODP Expedition 404), reducing the existing uncertainties about the spreading rate of the Molloy and north Knipovich Ridges inferred from magnetic anomalies Chrons 2A (2.8 Ma) and 5 (9.8 Ma) (e.g., Engen et al., 2008; Johnson et al., 2015). In addition, geomechanical and petrophysical data from these key regions will help constrain spatial variations in the effect of glacial and tectonic stresses on subseabed sediment deformation and carbon transport associated with paleoclimatic changes. In support of this objective, the following hypothesis can be tested.

4.2.2.1. Hypothesis 4

Glacial rebound has imposed significant forcing to the already complex tectonic stress field since the opening of the Fram Strait, enhancing sediment fracturing, fault reactivation, and associated carbon transport during key glacial–interglacial transitions.

4.2.3. Microbiological objective

The expedition will investigate the influence of the WSC variability, ice coverage, and climate on the microbial populations through time and to what extent this is still affecting contemporary geochemical fluxes. In support of this objective, the following hypotheses can be tested.

4.2.3.1. Hypothesis 5

Differences in organic carbon input between glacial and interglacial periods will affect microbial community abundance, diversity, and activity.

It is anticipated that glacial deposits will be enriched in microbial groups specialized in degrading organic matter of terrestrial origin and reflected in a higher frequency in metabolic pathways facilitating the degradation of more recalcitrant carbon as observed in the equatorial Atlantic and Baltic Sea (Freitas et al., 2020).

The sedimentary deep biosphere extends thousands of meters below the surface and hosts a vast and ecological significant microbial population that continues to be active even after millions of years of burial (Røy et al., 2012; Orsi, 2018; Zhao et al., 2019; Morono et al., 2020). Through their activity, they regulate the fluxes of dissolved geochemical species in and out of the seafloor and exert primary control on the long-term fate of sequestered organic carbon (Hoehler and Jørgensen, 2013). To this end, the microbial activity and population size are tightly coupled to the input of organic carbon to the seafloor (Kallmeyer et al., 2012). This in turn is a function of a number of parameters where key variables, such as primary productivity, are strongly influenced by ocean currents and sea ice coverage. However, to what extent past ocean circulation patterns and sea ice cover are preserved in the contemporary sedimentary microbial population in the form of abundances, diversity, and activity and if this continues to influence modern geochemical fluxes is very limited (Orsi et al., 2017).

4.2.3.2. Hypothesis 6

Microbial communities will have changed in response to freshwater input during glacial termination events.

The proposed drill sites are located in an area where profound changes in Earth's climate history are stored in the sedimentary record. Sampling of these relevant sedimentary sequences would couple the effect of changing climate, including changes in ice sheet dynamics (e.g., freshwater input) and sea ice cover to potential variability in microbial populations. The possibility to sample identical climatic periods at different geographical locations along the WSC provides an exceptional opportunity to study if specific oceanographic/climatic periods translate into specific microbial communities or if regional variables are more important. By extension, such information would allow more precise prediction of potential future scenarios caused by changing climate.

4.3. Contributions to other international actions

In addition to addressing expedition specific scientific objectives, sediment cores and data from Expedition 403 will contribute to other international scientific actions. In particular, the expedition will contribute data to refine the climate reference curve Cenozoic global reference benthic foraminifera carbon and oxygen isotope dataset (CENOGRID) (Westerhold et al., 2020), provide a unique marine paleoclimatic archive complementary to the Ice Memory archives (**https://www.ice-memory.org**), and contribute to the PlioVAR action (McClymont et al., 2020) aiming to coordinate a synthesis of terrestrial and marine data to characterize the spatial and temporal variability of Pliocene climate.

4.4. Connections with previous, ongoing, and future drilling expeditions

By meeting the above described scientific objectives, Expedition 403 will build upon the success of previous ODP Legs 151 and 162 in the Fram Strait and Integrated Ocean Drilling Program Expedition 302 in the Arctic Ocean. The primary objectives of Legs 151 and 162 were reconstructing the paleoceanography of the Fram Strait and glacial evolution in the circum-Nordic Seas during the Neogene (Jansen and Raymo, 1996; Thiede and Myhre, 1996). Integrated Ocean Drilling Program Expedition 302 (Arctic Coring Expedition [ACEX]) focused on the long-term Cenozoic paleoenvironmental history of the central Arctic Ocean (Backman and Moran, 2009). These previous expeditions mainly focused on recovery of condensed sequences, having the aim to reach the older units to reconstruct the dynamic history of the Arctic and Subarctic Oceans. In contrast, Expedition 403 will specifically focus on recovery of expanded sequences to increase the resolution of paleoclimatic reconstruction and complex feedbacks among the atmosphere–ocean–cryosphere.

The objectives of Expedition 403 are also synergistic and complementary with ongoing expeditions that are occurring in the IODP phase of scientific ocean drilling and with future drilling expeditions that may be scheduled in the next phase of the program. These include the following:

- Expedition 404 (the opening of the Arctic-Atlantic gateway: tectonic, oceanographic, and climatic dynamics; presently postponed) by dealing with the stratigraphic reconstruction of the sequences on the Svyatogor Ridge that over the past 2 Ma was possibly offset from the western Svalbard margin by the MTF, belonging to the rift system responsible for the opening of the Fram Strait.
- IODP Expedition 377 (Central Arctic Paleoceanography; presently postponed) and previous Expedition 302 by providing an opportunity to study the depositional architecture across the Arctic and motivating future seismic surveys to connect these regions. Additionally, three of the Expedition 377 science objectives share important elements with Expedition 403 objectives and/or hypotheses; a more complete reconstruction of Arctic Ocean paleocirculation, sea ice history, and characterization of the Pliocene warm interval will be accomplished through the results of both expeditions.
- Expedition 400 (Cenozoic evolution of the northern Greenland Ice Sheet; scheduled for August–September 2023), although dealing with different paleoceanographic/paleoclimatic systems of the Northern Hemisphere, the combination of the results obtained from all the Arctic-North Atlantic proposals can help our understanding of the pan-Arctic climatic system.

5. Expedition drilling locations

Three key areas were identified on the basis of their location with respect to the warm core of the WSC, the presence of undisturbed, high-resolution depositional sequences, and temporal extension to meet the objectives of Expedition 403 (Figure **F1**; Tables **T2**, **T3**, **T4**, **T5**, **T6**):

- The Bellsund and Isfjorden sediment drifts located on the western side of Svalbard, aside the respective glacial troughs and trough mouth fans depositional systems;
- The Vestnesa Ridge, a 100 km long submarine sediment drift developed over relatively young (<19 Ma) oceanic crust, extending in a northwest to west direction from the continental margin off western Svalbard; and
- The Svyatogor Ridge, a smaller but distinct sediment drift that lies on the western flank of the Knipovich Ridge valley and south of the Molloy transform on an even younger oceanic crust (<10 Ma).

5.1. Bellsund and Isfjorden sediment drifts

The Bellsund and Isfjorden drifts are two sedimentary depocenters that developed on the western margin of Svalbard between trough mouth fan depositional systems in areas that were mostly protected from direct glacigenic input from the SBSIS (Figure **F1**). The two drifts were interpreted to be plastered sediment drift (Figure **F3**) that formed under the persistent effect of the deep core of the WSC located within the NSDW, located at 1300–1800 m water depth and flowing with average velocities of 8.5±0.2 cm/s, at 10 m above seafloor, with seasonal intensification up to 30 cm/s during late winter/early spring. The NSDW is colder (less than –0.9°C) and slightly more saline (>34.91‰) with respect to the overlying NAW (Aagaard et al., 1985; Rudels et al., 2000; Langehaug and Falck, 2012), and it is periodically refilled by suspended sediments transported by BSW cascading from the shelf area (Figure **F3**).

Two long Calypso piston cores retrieved from both sediment drifts (Eurofleets2-PREPARED project; Lucchi et al., 2014) contain a continuous, very expanded paleoclimatic record spanning the last 60 ky with a submillennial to subcentennial resolution. A robust age model was defined through paleomagnetic and biostratigraphic analyses, identification of tephras, and radiocarbon dating of the abundant biogenic carbonate fraction (Caricchi et al., 2019, 2020). The sedimentologic analyses indicated the consistent presence of contouritic deposition and the existence of short-lived, abrupt depositional events associated to prominent meltwater events, like the MWP-1A (Lucchi et al., 2013, 2015), and Heinrich-like events indicating a highly dynamic SBSIS during last 60 ky (Lucchi et al., 2018; Caricchi et al., 2019). The drill sites on the Bellsund and Isfjorden drifts are designed to recover the most expanded sequence down to Seismic Reflector R4A to specifically address suborbital oscillations, MBE, MPT, and the onset of shelf edge glaciation in this area.

Proposed primary Sites BED-01A and BED-02B on the Bellsund drift are located between 1700 and 1800 m water depth (Figure **F8**), and therefore appear to be ideal sites for paleoceanographic studies characterized by a remarkably high sedimentation rate (>300 m/Ma; Table **T2**). To meet the necessity of retrieving expanded sequences with reduced disturbance, Site BED-01A will be drilled to Seismic Reflector R3 (most expanded sequence), whereas Site BED-02B will be drilled for the entire length to Seismic Reflector R4A (Figure **F8**).

Proposed primary Site ISD-01C and the proposed alternate Sites ISD-02A, ISD-03A, and ISD-04B on the Isfjorden drift cross less expanded sedimentary sequences (submillennial resolution) with respect to the Bellsund drift. The sequences contain glacial debris flows testifying to shelf-edge glaciations and a higher record of plumites indicating ice sheet melting thanks to the more proximal location with respect to the shelf edge (Figure **F8**; Table **T3**). These sites are therefore more suitable for the reconstruction of SBSIS history (like proposed alternate Site BED-03A closer to the shelf break). Although located in close proximity to the Bellsund drift, the Isfjorden drift sites will give additional information on the SBSIS dynamics and complementary information on the WSC characteristics and variability allowing us to discriminate between climate-driven events related to local or regional effects.

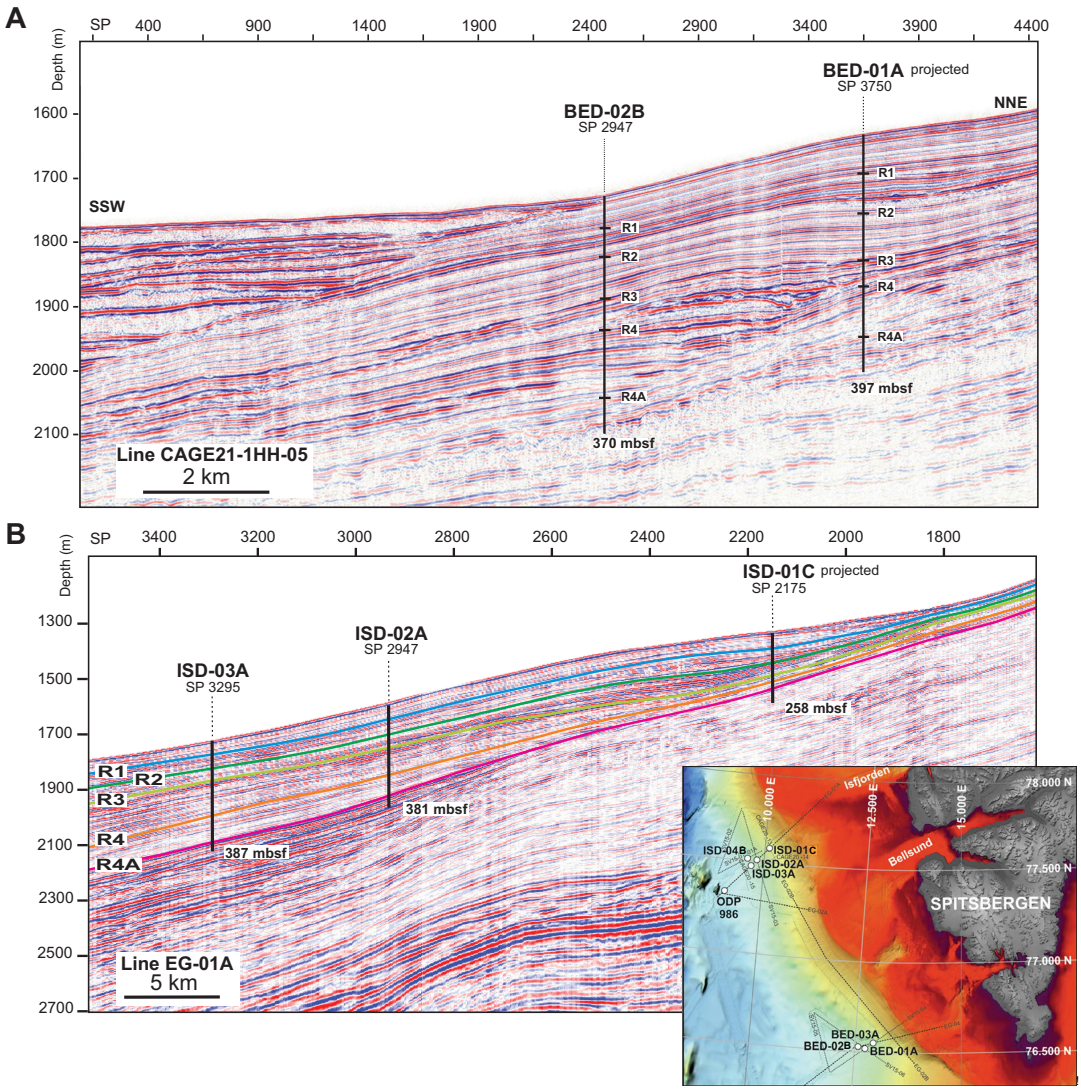

Figure F8. A. Multichannel seismic (MCS) In-Line CAGE21-1HH-05 along Bellsund drift with location of proposed primary drill sites BED-01A and BED-02B and alternate Site BED-03A. B. MCS In-Line EG-01A along Isfjorden drift with location of primary Site ISD-01C (projected) and alternate Sites ISD-02A and ISD-03A (Note that alternate Site ISD-04B is located on another line crossing sequence similar to Site ISD-03A).

Table T2. Summary of Bellsund drift drill sites depth, stratigraphic boundaries, and site survey information. SP = shotpoint, TWT = two-way traveltime, TD = total depth.

Site Name alternate	Lat N	Lon E	water depth (m)	Inline	SP	Crossline	SP
BED-01A	76.52160	12.73867	1647	SV15_04	1837	SV15_06	1800

Stratigraphy	TWT (s) below sea surface	TWT (s) interval	Interval thckness (m)	Depth below seafloor (m)	Interval velocity (m/s) (2)	Age (Ma)	Sed. rate (m/Ma)
Seafloor	2.225	0	1647	0	1480	0.00	0.00
R1	2.310	0.085	71	71	1678	0.20	356.6
R2	2.400	0.090	79	151	1761	0.40	396.2
R3	2.483	0.083	75	225	1800	0.75	213.4
R4	2.541	0.058	53	279	1840	1.10	152.5
R4A	2.615	0.074	68	**347**	1846	1.30	341.5
TD	2.667	0.052	50	**397**	1940		

Site Name primary	Lat N	Long E	water depth (m)	Inline	SP	Crossline	Projected SP
BED-02B	76.457500	12.554722	1665	CAGE21-1HH-05	2465	CAGE21-1HH-03	2890

Stratigraphy	TWT (s) below sea surface	TWT (s) interval	Interval thckness (m)	Depth below seafloor (m)	Interval velocity (m/s) (3)	Age (Ma)	Sed. rate (m/Ma)
Seafloor	2.350	0	1739	0	1480	0.00	0.00
R1	2.418	0.068	53	53	1562	0.20	265.5
R2	2.488	0.070	59	112	1673	0.40	292.8
R3	2.561	0.073	64	175	1744	0.75	181.9
R4	2.610	0.049	44	220	1812	1.10	126.8
R4A	2.709	0.099	95	**320**	1920	1.30	501.4
TD	2.759	0.050	50	**370**	2000		

Site Name alternate	Lat N	Long E	water depth (m)	Inline	SP	Crossline	SP
BED-03A	76.555	12.930	1502	SV15_04	2265	CAGE21-1HH-05	5560

Stratigraphy	TWT (s) below sea surface	TWT (s) interval	Interval thckness (m)	Depth below seafloor (m)	Interval velocity (m/s) (3)	Age (Ma)	Sed. rate (m/Ma)
Seafloor	2.030	0	1502	0	1480	0.00	0.00
R1	2.100	0.070	55	55	1562	0.20	273.4
R2	2.160	0.060	50	105	1673	0.40	251.0
R3	2.220	0.060	52	157	1744	0.75	149.5
R4	2.280	0.060	54	212	1812	1.10	155.3
R4A	2.395	0.115	110	**322**	1920	1.30	552.0
TD	2.445	0.050	50	**372**	2000		

Table T3. Summary of Isfjorden drift drill sites depth, stratigraphic boundaries, and site survey information. SP = shotpoint, TWT = two-way traveltime, TD = total depth.

Site Name primary	Lat N	Long E	water depth (m)	inline (projected)	SP	Crossline	SP
ISD-01C	77.58771	10.09379	1330	EG_01A	2177	CAGE20_5HH-13	3420

Stratigraphy	TWT (s) below sea surface	TWT (s) interval	Interval thckness (m)	Depth below seafloor (m)	Interval velocity (m/s) (4)	Age (Ma)	Sed. rate (m/Ma)
Seafloor	1.790	0	1330	0	14.8	0.00	0.00
R1	1.860	0.070	55	55	1585	0.20	277.4
R2	1.940	0.080	64	120	1611	0.40	322.2
R3	1.990	0.050	42	162	1686	0.75	120.4
R4	2.010	0.020	17	179	1705	1.10	48.7
R4A	2.040	0.030	29	**208**	1946	1.30	146.0
TD	2.090	0.050	50	**258**	2003		

Site Name alternate	Lat N	Long E	water depth (m)	Inline	SP	Crossline	SP
ISD-02A	77.52639	9.82167	1587.3	EG_01A	2947	SV15_03	1797

Stratigraphy	TWT (s) below sea surface	TWT (s) interval	Interval thckness (m)	Depth below seafloor (m)	Interval velocity (m/s) (5)	Age (Ma)	Sed. rate (m/Ma)
Seafloor	2.145	0	1587	0	1480	0.00	0.00
R1	2.210	0.065	48	48	1490	0.20	242.1
R2	2.280	0.070	53	102	1517	0.40	265.5
R3	2.360	0.080	63	165	1583	0.75	180.9
R4	2.430	0.070	65	230	1860	1.10	186.0
R4A	2.535	0.105	101	**331**	1932	1.30	507.2
TD	2.586	0.051	50	**381**	1969		

Site Name alternate	Lat N	Long E	water depth (m)	Inline	SP	Crossline	SP
ISD-03A	77.49732	9.70293	1733.8	EG_01A	3295	CAGE20_5HH-15	3254

Stratigraphy	TWT (s) below sea surface	TWT (s) interval	Interval thckness (m)	Depth below seafloor (m)	Interval velocity (m/s) (2)	Age (Ma)	Sed. rate (m/Ma)
Seafloor	2.343	0	1734	0	1480	0.00	0.00
R1	2.395	0.052	39	39	1490	0.20	193.7
R2	2.467	0.072	55	93	1517	0.40	273.1
R3	2.530	0.063	50	143	1583	0.75	142.5
R4	2.617	0.087	81	224	1860	1.10	231.2
R4A	2.734	0.117	113	**337**	1932	1.30	565.1
TD	2.785	0.051	50	**387**	1969		

Site Name alternate	Lat N	Long E	water depth (m)	Inline (projected)	SP	Crossline	SP
ISD-04B	77.52897	9.61072	1720	SV15_01	1491	CAGE20_5HH-15	4590

Stratigraphy	TWT (s) below sea surface	TWT (s) interval	Interval thckness (m)	Depth below seafloor (m)	Interval velocity (m/s) (2)	Age (Ma)	Sed. rate (m/Ma)
Seafloor	2.316	0	1714	0	1480	0.00	0.00
R1	2.365	0.049	37	37	1490	0.20	182.5
R2	2.453	0.088	67	103	1517	0.40	333.7
R3	2.517	0.064	51	154	1583	0.75	144.7
R4	2.608	0.091	85	239	1860	1.10	241.8
R4A	2.725	0.117	113	**352**	1932	1.30	565.1
TD	2.776	0.051	50	**402**	1969		

5.2. Vestnesa Ridge

The Vestnesa Ridge is a 100 km long submarine sediment drift developed over <19 Ma oceanic crust. The ridge extends in a northwest to west direction from the continental margin off western Svalbard with its crest lying in 1200–1600 m (east to west) water depth. The sedimentation and geologic development in this area has been heavily influenced by the Pliocene–Pleistocene glaciations and the ice sheet extent over Svalbard and the Arctic Ocean (Jakobsson et al., 2014). The upper succession of sediments on the Vestnesa Ridge is dominated by muddy–silty turbidites and contourites intercalated with abundant IRD (Eiken and Hinz, 1993; Howe et al., 2008). Sedimentation rates varied between ~10 and 130 cm/ky on glacial–interglacial timescales (Sztybor and Rasmussen, 2017b). Paleoceanographic records show an almost constant presence of NAW at Vestnesa Ridge since 43 ka (Sztybor and Rasmussen, 2017a). The Pleistocene succession occurs all along the Vestnesa Ridge and is thickest (~500 m) in the east, thinning westward.

Proposed Site VRE-03A is the primary site at the eastern termination of Vestnesa Ridge (Figure F9A; Table T4), where the major objective is to recover an expanded, complete sequence of the Pleistocene and the Pliocene–Pleistocene transition. This site will extend records obtained at the Bellsund and Isfjorden drifts to investigate the onset of NHG, glacial cyclicity, Brunhes events, the MPT, and the enigmatic Late Pliocene Glacial Event (M2). The targeted penetration at this site

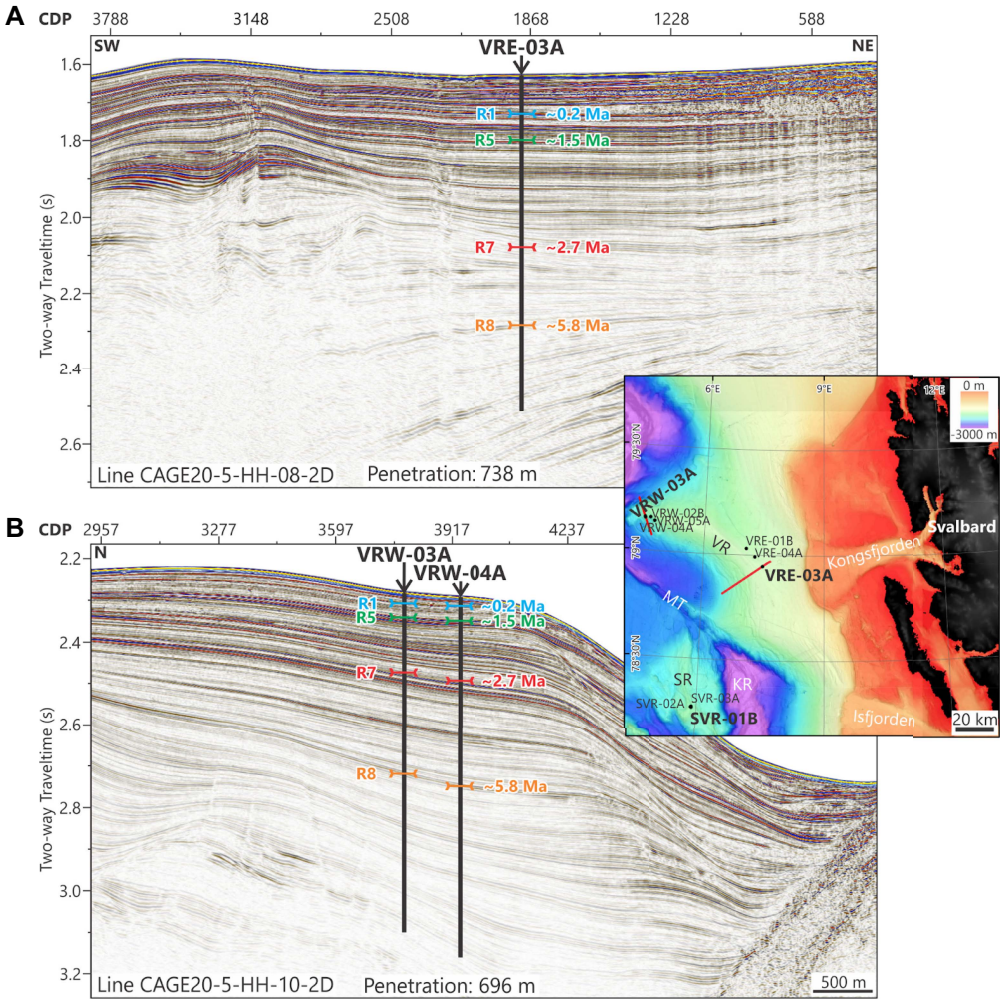

Figure F9. In-line multichannel seismic (MCS) lines indicating location of proposed primary Sites (A) VRE-03A and (B) VRW-03A on Vestnesa Ridge (VR) eastern and western termination, respectively. Inset map shows site location along Vestnesa Ridge. Stratigraphic markers are indicated by age and correlated from ODP Site 912 further north on Yermak Plateau (Mattingsdal et al., 2014). SR = Svyatogor Ridge, MT = Molloy transform, KR = Knipovich Ridge.

would also allow recovery of older sediments of Late Miocene to Pliocene age, although this would likely rely on the quality of sediment recovery using the extended core barrel (XCB) system.

Proposed Site VRW-03A is the primary site at the western termination of the Vestnesa Ridge (Figure **F9B**), where a major objective would be to extend the stratigraphic and paleoclimate record into the Miocene–Pliocene transition and possibly LMC. The Pleistocene occurs as a relatively condensed sedimentary succession at the end of Vestnesa Ridge and is approximately 200 m thick (Table **T5**). Deeper stratigraphic horizons are tentatively constrained by correlation from ODP sites on the Yermak Plateau (Mattingsdal et al., 2014). The basement crust at this location lies between magnetic Chrons 5 (9.8 Ma) and 2A (2.8 Ma) (Johnson et al., 2015) (i.e., an age between Late Miocene and Late Pliocene). This site provides the opportunity to study the main Pliocene–Quaternary climatic transitions and to recover the Late Miocene sequence to fill the knowledge

Table T4. Summary of Vestnesa Ridge (east) drill sites depth, stratigraphic boundaries, and site survey information. SP = shotpoint, TWT = two-way traveltime, TD = total depth.

Site Name alternate	Lat N	Lon E	water depth (m) (6)	Inline	CDP	Crossline	CDP
VRE-01B	79.03208	7.05774	1293	CAGE19-1-HH-051-2D	1529	CAGE19-1HH-052-2D	1655

Stratigraphy	TWT (s) below sea surface	TWT (s) interval	Interval thckness (m)	Depth below seafloor (m)	Interval velocity (m/s) (7)	Age (Ma)	Sed. rate (m/Ma)
Seafloor	1.753	0	1293	0	1475	0.00	0.00
R1	1.851	0.098	76	76	1550	0.20	379.8
R5	1.939	0.088	70	146	1600	1.50	54.2
R7	2.228	0.289	238	385	1650	2.70	198.7
R8	2.500	0.272	231	616	1700	5.80	74.6
TD	2.502	0.002	2	**618**	1750		

Site Name primary	Lat N	Lon E	water depth (m) (6)	Inline	CDP	Crossline	CDP
VRE-03A	78.94845	7.47311	1201	CAGE20-5-HH-08-2D	1903	CAGE20-5HH-02-2D	4563

Stratigraphy	TWT (s) below sea surface	TWT (s) interval	Interval thckness (m)	Depth below seafloor (m)	Interval velocity (m/s) (7)	Age (Ma)	Sed. rate (m/Ma)
Seafloor	1.630	0	1200	0	1473	0.00	0.00
R1	1.730	0.100	78	78	1550	0.20	387.5
R5	1.805	0.075	60	138	1600	1.50	46.2
R7	2.087	0.282	233	370	1650	2.70	193.9
R8	2.284	0.197	167	538	1700	5.80	54.0
TD	2.513	0.229	200	**738**	1750		

Site Name alternate	Lat N	Lon E	water depth (m) (6)	Inline	CDP	Crossline	CDP
VRE-04B	78.99940	7.31070	1257	CAGE20-5-HH-01-2D	7604	CAGE21-3HH-VST-06	5385

Stratigraphy	TWT (s) below sea surface	TWT (s) interval	Interval thckness (m)	Depth below seafloor (m)	Interval velocity (m/s) (7)	Age (Ma)	Sed. rate (m/Ma)
Seafloor	1.703	0	1252	0	1470	0.00	0.00
R1	1.800	0.097	75	75	1550	0.20	375.9
R5	1.884	0.084	67	142	1600	1.50	51.7
R7	2.169	0.285	235	378	1650	2.70	195.9
R8	2.380	0.211	179	557	1700	5.80	57.9
TD	2.578	0.198	173	**730**	1750		

Table T5. Summary of Vestnesa Ridge (west) drill sites depth, stratigraphic boundaries, and site survey information. SP = shotpoint, TWT = two-way traveltime, TD = total depth.

Site Name alternate	Lat N	Lon E	water depth (m) (6)	Inline	CDP	Crossline	CDP
VRW-02B	79.15870	4.62165	1607	CAGE18-4_08	1986	CAGE20-5HH-09-2D	4765

Stratigraphy	TWT (s) below sea surface	TWT (s) interval	Interval thckness (m)	Depth below seafloor (m)	Interval velocity (m/s) (7)	Age (Ma)	Sed. rate (m/Ma)
Seafloor	2.178	0	1607	0	1476	0.00	0.00
R1	2.205	0.027	21	21	1550	0.20	104.6
R5	2.258	0.053	42	63	1600	1.50	32.6
R7	2.531	0.273	225	289	1650	2.70	187.7
R8	2.816	0.285	242	531	1700	5.80	78.1
TD	2.983	0.167	146	**677**	1750		

Site Name primary	Lat N	Lon E	water depth (m) (6)	Inline	CDP	Crossline	CDP
VRW-03A	79.15985	4.48874	1681	CAGE20-5-HH-11-2D	7217	CAGE20-5HH-10-2D	3788

Stratigraphy	TWT (s) below sea surface	TWT (s) interval	Interval thckness (m)	Depth below seafloor (m)	Interval velocity (m/s) (7)	Age (Ma)	Sed. rate (m/Ma)
Seafloor	2.284	0	1681	0	1472	0.00	0.00
R1	2.307	0.023	18	18	1550	0.20	89.1
R5	2.340	0.033	26	44	1600	1.50	20.3
R7	2.480	0.140	116	160	1650	2.70	96.3
R8	2.720	0.240	204	364	1700	5.80	65.8
TD	3.100	0.380	333	**696**	1750		

Site Name alternate	Lat N	Lon E	water depth (m) (6)	Inline	CDP	Crossline	CDP
VRW-04A	79.15593	4.49753	1690	CAGE18-4_08	1145	CAGE20-5HH-10-2D	3940

Stratigraphy	TWT (s) below sea surface	TWT (s) interval	Interval thckness (m)	Depth below seafloor (m)	Interval velocity (m/s) (7)	Age (Ma)	Sed. rate (m/Ma)
Seafloor	2.293	0	1690	0	1474	0.00	0.00
R1	2.315	0.022	17	17	1550	0.20	85.2
R5	2.348	0.033	26	43	1600	1.50	20.3
R7	2.499	0.151	125	168	1650	2.70	103.8
R8	2.742	0.243	207	375	1700	5.80	66.6
TD	3.160	0.418	366	**740**	1750		

Site Name alternate	Lat N	Lon E	water depth (m) (6)	Inline	CDP	Crossline	CDP
VRW-05A	79.14327	4.73000	1621	CAGE20-5-HH-11-2D	5489	CAGE18-4_01	4210

Stratigraphy	TWT (s) below sea surface	TWT (s) interval	Interval thckness (m)	Depth below seafloor (m)	Interval velocity (m/s) (7)	Age (Ma)	Sed. rate (m/Ma)
Seafloor	2.197	0	1621	0	1476	0.00	0.00
R1	2.226	0.029	22	22	1550	0.20	112.4
R5	2.292	0.066	53	75	1600	1.50	40.6
R7	2.651	0.359	296	371	1650	2.70	246.8
R8	2.949	0.298	253	625	1700	5.80	81.7
TD	3.000	0.051	45	**669**	1750		

gap between LMC and the warm Early Pliocene. Successfully constraining the location of the Miocene/Pliocene boundary in the west termination of the Vestnesa Ridge drilling sites with respect to the Molloy spreading ridge will have important implications for reducing uncertainties on reported spreading rates and tectonic evolution of the Fram Strait.

Sites VRE-03A and VRW-03A are, furthermore, ideal sites to study spatial stress field variations (present and paleo) along the west Svalbard margin. Such study is necessary for understanding how the SBSIS, the Molloy and Knipovich ridge spreading, and the WSC have affected the architecture of the sedimentary drifts, near-surface deformation and fluid flow system dynamics.

5.3. Svyatogor Ridge

The Svyatogor Ridge is a smaller sediment drift deposit that lies to the west of the northern end of the Knipovich Ridge and south of the MTF on an even younger oceanic crust (<10 Ma) (Figure **F10**; Table **T6**). It has been hypothesized to have once been a part of Vestnesa Ridge before being offset along the MTF over the past 2 My (Johnson et al., 2015). Compared to Vestnesa Ridge, the sediment cover across Svyatogor Ridge is limited because displacement along the MTF has moved the ridge further away from the path of the WSC, which is controlling the sedimentation today. However, sediments are similar to those at Vestnesa Ridge. The chronostratigraphy at this site is largely unknown because correlation across the MTF is impossible and Site 909 further west is far outside the west Spitsbergen contourite drifts. However, based on interpretations by Waghorn et al. (2018), the base of the Pleistocene occurs at approximately 108 mbsf at the location of proposed primary Site SVR-03A. Similar to the western end of Vestnesa Ridge, the Svyatogor Ridge also resides on the basement crust between magnetic Chrons 5 and 2A (Johnson et al., 2015) (i.e., an age between Late Miocene and Late Pliocene).

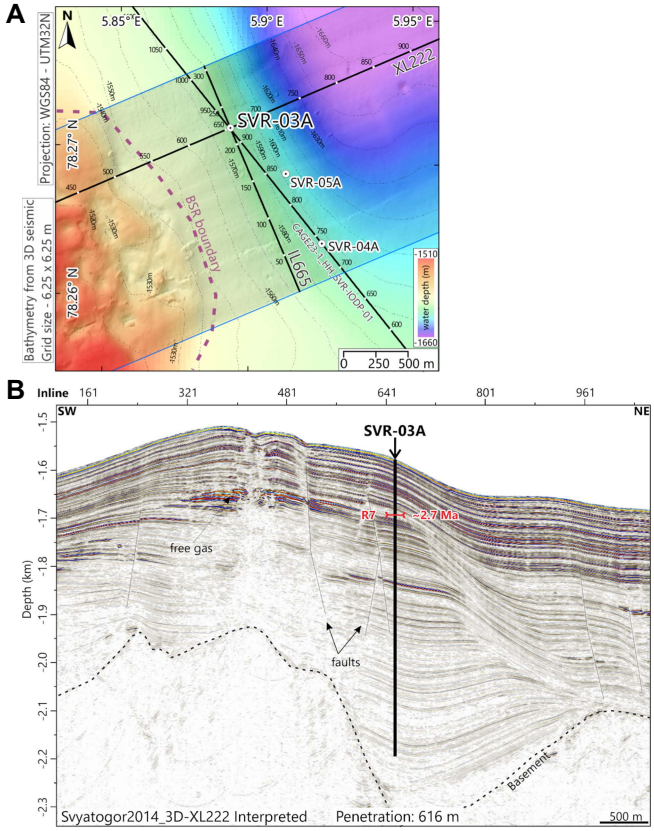

Figure F10. A. Location of primary Site SVR-03A along with outlines of intersecting in-line and cross-line in Svyatogor 2014 3-D seismic data. Location of other proposed drill sites in vicinity are also shown. Indications for hydrates occur only at crest of the Svyatogor Ridge. Contour interval = 10 m. B. Interpreted images of Cross-Line 222 from Svyatogor 2014 3-D seismic data containing stratigraphic section across primary Site SVR-03A. Stratigraphic marker from Waghorn et al. (2018).

Table T6. Summary of Svyatogor Ridge drill sites depth, stratigraphic boundaries, and site survey information. SP = shotpoint, TWT = two-way traveltime, TD = total depth.

Site Name primary	Lat N	Lon E	water depth (m) (6)	Inline	CDP	Crossline	CDP
SVR-03A	78.2718209	5.889665	1581	Svyatogor2014-3D-XL222	665	CAGE21-3HH_SVR-IODP-01	921

Stratigraphy	TWT (s) below sea surface	TWT (s) interval	Interval thckness (m)	Depth below seafloor (m)	Interval velocity (m/s) (7)	Age (Ma)	Sed. rate (m/Ma)
Seafloor	2.152	0	1581	0	1469	0.00	0.00
R7	2.283	0.131	108	108	1650	2.70	40.0
TD	2.864	0.581	508	**616**	1750		

Site Name alternate	Lat N	Lon E	water depth (m) (6)	Inline	CDP	Crossline	CDP
SVR-04A	78.2641	5.9231	1594	Svyatogor2014-3D-XL46	665	CAGE21-3HH_SVR-IODP-01	737

Stratigraphy	TWT (s) below sea surface	TWT (s) interval	Interval thckness (m)	Depth below seafloor (m)	Interval velocity (m/s) (7)	Age (Ma)	Sed. rate (m/Ma)
Seafloor	2.170	0	1594	0	1469	0.00	0.00
R7	2.319	0.149	123	123	1650	2.70	40.0
TD	3.03	0.711	622	**745**	1750		

Site Name alternate	Lat N	Lon E	water depth (m) (6)	Inline	CDP	Crossline	CDP
SVR-05A	78.2688	5.9095	1600	Svyatogor2014-3D-XL143	707	Svyatogor2014-3D-IL707	143

Stratigraphy	TWT (s) below sea surface	TWT (s) interval	Interval thckness (m)	Depth below seafloor (m)	Interval velocity (m/s) (7)	Age (Ma)	Sed. rate (m/Ma)
Seafloor	2.178	0	1600	0	1469	0.00	0.00
R7	2.309	0.131	108	108	1650	2.70	40.0
TD	3.029	0.720	630	**738**	1750		

6. Operations plan and coring strategy

6.1. Operations plan

As the pathway between the North Atlantic and the Arctic Ocean, the Fram Strait is a key region in the global climate system (Overland et al., 2011; Mahajan et al., 2011), and, as such, it has been the focus of several past and current research projects. The presented expedition is motivated by the necessity of retrieving continuous, high-resolution, and datable depositional sequences that can be used to reconstruct and understand the paleoceanographic characteristics and cryosphere evolution throughout past key transitions of the climate system following the opening of Fram Strait.

Answering the fundamental questions outlined in the scientific objectives requires extensive sampling of sediment drifts along the north–south axis of the eastern Fram Strait (Figure **F1**). Collection of sedimentary records reaching back to the Late Miocene transition (about 5.8 Ma) allows for the use of numerous proxies to understand the Arctic, Northern Hemisphere, and global climate system and ice-ocean-atmosphere connections.

Geochemical, geochronological, structural, and petrologic analyses of drilled sediments and IRD will provide constraints on the variability of the WSC (North Atlantic Current), its influence on the climate particularly during key climate transitions, its role during the Arctic glaciation, ice shelves development and stability, and sea ice distribution.

Ocean drilling provides the only means of obtaining these samples and is therefore essential for meeting these objectives.

Five primary sites were selected for the initial proposal (985-FULL), but some sites were later slightly added/shifted to address the IODP Science Evaluation Panel and Environmental Protection and Safety Panel (EPSP) review comments. In addition, 12 alternate sites were also identified, normally in close vicinity to the primary sites. In total, 17 sites are proposed (see **Site summaries**), of which 6 primary sites are proposed for drilling during Expedition 403 and the additional 11 alternate sitess are considered contingency sites.

The expedition is scheduled to operate for 60 days (Table T7), which includes 5 days of port call in Reykjavík, Iceland. Coring operations will amount to 36.2 days, with an additional 6.4 days envi-

Table T7. Operations plan and time estimates for primary sites, Expedition 403. mbrf = meters below rig floor, mbsf = meters below seafloor, EPSP = Environmental Protection and Safety Panel, VSP = vertical seismic profile.

Site	Location (latitude, longitude)	Seafloor depth (mbrf)	Operations description	Transit (days)	Drilling Coring (days)	Logging (days)
Reykjavik			Begin expedition 5.0	Port call days		
			Transit ~1095 nmi to BED-01A @ 10.5 kt	4.4		
BED-01A	76° 31.2958'N	1658	Hole A - APC/HLAPC/XCB to 397 mbsf - 4 APCT-3 measurements	0.0	2.3	0.0
EPSP	12° 44.3204'E		Hole B - APC/HLAPC/XCB to 397 mbsf	0.0	1.7	0.0
to 397 mbsf						
			Subtotal days on site: 4.1			
			Transit ~5 nmi to BED-02B @ 1.5 kt	0.1		
BED-02B	76° 27.4500'N	1676	Hole A - APC/HLAPC/XCB to 370 mbsf - 4 APCT-3 measurements	0.0	1.7	0.0
EPSP	12° 33.2833'E		Hole B - APC/HLAPC/XCB to 370 mbsf - Log with triple combo, FMS-sonic, and VSP	0.0	1.6	1.1
to 370 mbsf						
			Subtotal days on site: 4.4			
			Transit ~75 nmi to ISD-01C @ 10.5 kt	0.3		
ISD-01C	77° 35.2627'N	1336	Hole A - APC/HLAPC/XCB to 258 mbsf - 4 APCT-3 measurements	0.0	1.4	0.0
EPSP	10° 5.6277'E		Hole B - APC/HLAPC/XCB to 258 mbsf	0.0	1.0	0.0
to 258 mbsf			Hole C - APC/HLAPC/XCB to 258 mbsf	0.0	1.0	0.0
			Hole D - APC/HLAPC/XCB to 258 mbsf - Log with triple combo, FMS-sonic, and VSP	0.0	1.2	0.9
			Subtotal days on site: 5.6			
			Transit ~67 nmi to SVR-03A @ 10.5 kt	0.3		
SVR-03A	78° 16.3093'N	1592	Hole A - APC/HLAPC to 400 mbsf - 4 APCT-3 measurements	0.0	2.1	0.0
EPSP	5° 53.3799'E		Hole B - APC/HLAPC to 400 mbsf	0.0	1.7	0.0
to 616 mbsf			Hole C - APC/HLAPC/XCB to 616 mbsf - Log with triple combo, FMS-sonic, and VSP	0.0	3.0	1.3
			Subtotal days on site: 8.2			
			Transit ~45 nmi to VRE-03A @ 10.5 kt	0.2		
VRE-03A	78° 56.9069'N	1212	Hole A - APC/HLAPC to 400 mbsf - 4 APCT-3 measurements	0.0	1.8	0.0
EPSP	7° 28.3863'E		Hole B - APC/HLAPC to 400 mbsf	0.0	1.5	0.0
to 738 mbsf			Hole C - APC/HLAPC to 400 mbsf	0.0	1.5	0.0
			Hole D - APC/HLAPC/XCB to 738 mbsf - Log with triple combo, FMS-sonic, and VSP	0.0	3.4	1.5
			Subtotal days on site: 9.9			
			Transit ~36 nmi to VRW-03A @ 10.5 kt	0.1		
VRW-03A	79° 9.5910'N	1692	Hole A - APC/HLAPC to 400 mbsf - 4 APCT-3 measurements	0.0	2.1	0.0
EPSP	4° 29.3243'E		Hole B - APC/HLAPC to 400 mbsf	0.0	1.7	0.0
to 696 mbsf			Hole C - APC/HLAPC to 400 mbsf	0.0	1.7	0.0
			Hole D - APC/HLAPC/XCB to 696 mbsf - Log with triple combo, FMS-sonic, and VSP	0.0	3.5	1.5
			Subtotal days on site: 10.6			
			Transit ~1616 nmi to Amsterdam @ 10.2 kt	6.6		
Amsterdam			End expedition	12.0	36.2	6.4

Port call days:	5.0	Total operating days:	54.5
Subtotal days on site:	42.6	Total expedition days:	59.6

sioned for downhole wireline logging. Time spent for transit will amount to 4.4 days from Reykjavík to Site BED-01A and 6.6 days from Site VRW-03A to Amsterdam. In between sites, transit times range from 0.1 to 0.3 days. Thus, the proximity of all sites will allow us for greater operational flexibility in case of adverse weather or ice conditions.

6.2. Drilling strategy

The drilling strategy for the proposed boreholes is summarized in Figure **F11** and Tables **T7** and **T8**. The coring and logging tools available on *JOIDES Resolution* are described at **http://iodp.tamu.edu/tools** and **http://iodp.tamu.edu/tools/logging**. The drilling plan will provide a south-to-north transect along the eastern Fram Strait.

Standard *JOIDES Resolution* drilling and logging procedures will be followed. For three sites (BED-01A, BED-02B, and ISD-01C), advanced piston coring (APC) and half-length APC (HLAPC) will be used until refusal, followed by XCB drilling until the target depth. The targets for these sites are as follows:

- 397 mbsf for Site BED-01A,
- 370 mbsf for Site BED-02B,
- 258 mbsf for Site ISD-01C,
- Reflector R4A (Figure **F8**),
- Going back to about 1.3 Ma, and
- Understanding Quaternary climatic transitions and paleo-SBSIS dynamics.

The three northern sites (SVR-03A, VRE-03A, and VRW-03A) will drill three or four holes until APC/HLAPC refusal and extend one hole until the target depth via XCB coring.

The drilling targets for Site SVR-03A are as follows:

- 616 mbsf,
- Reflector R7 (Figure **F10**),
- Reaching about 2.7 Ma, and
- Understanding the Late Pliocene onset of the NHG, Quaternary climatic transitions, sediment tectonic stress, and evolution of the MTF.

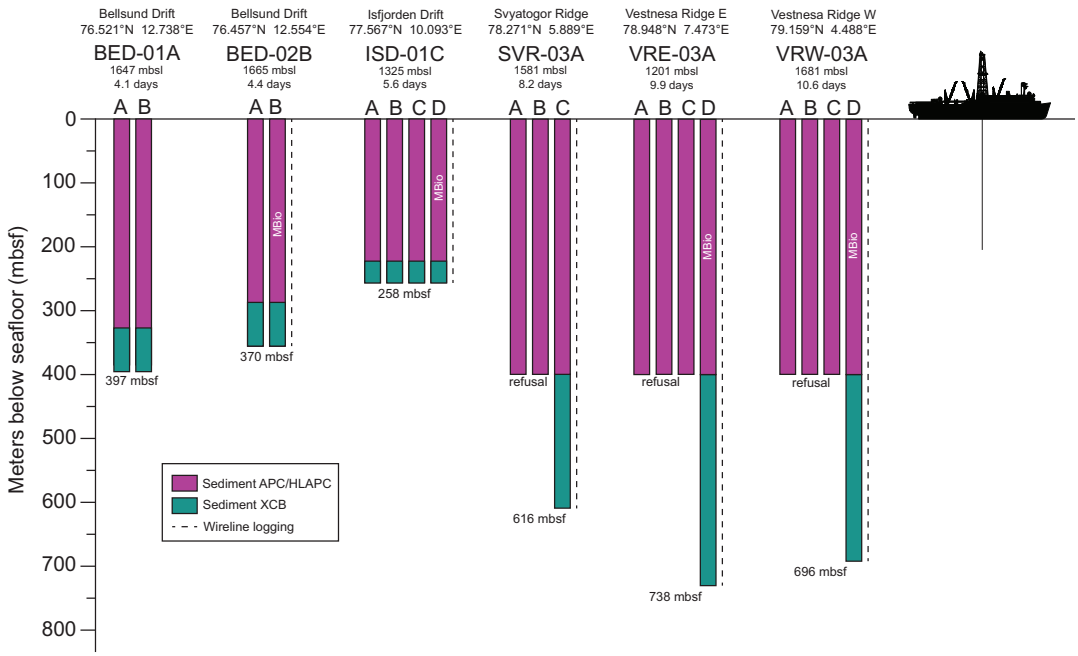

Figure F11. Operations schematics for primary sites, Expedition 403.

Table T8. Operations and time estimates for alternate sites, Expedition 403. mbrf = meters below rig floor, mbsf = meters below seafloor, EPSP = Environmental Protection and Safety Panel, VSP = vertical seismic profile.

Site	Location (latitude, longitude)	Seafloor depth (mbrf)	Operations description	Drilling/ Coring (days)	Logging (days)
BED-03A	76.555122°N	1513	Hole A - APC/HLAPC/XCB to 372 mbsf - 4 APCT-3 measurements	2.1	0.0
EPSP	12.930062°E		Hole B - APC/HLAPC/XCB to 372 mbsf - Log with triple combo, FMS-sonic, and VSP	1.6	1.1
to 372 mbsf					
			Subtotal days on site: 4.8		
ISD-02A	77.526390°N	1676	Hole A - APC/HLAPC/XCB to 381 mbsf - 4 APCT-3 measurements	2.2	0.0
EPSP	9.821670°E		Hole B - APC/HLAPC/XCB to 381 mbsf	1.8	0.0
to 381 mbsf			Hole C - APC/HLAPC/XCB to 381 mbsf	1.8	0.0
			Hole D - APC/HLAPC/XCB to 381 mbsf - Log with triple combo, FMS-sonic, and VSP	1.9	1.1
			Subtotal days on site: 8.8		
ISD-03A	77.497322°N	1745	Hole A - APC/HLAPC/XCB to 387 mbsf - 4 APCT-3 measurements	2.3	0.0
EPSP	9.702931°E		Hole B - APC/HLAPC/XCB to 387 mbsf	2.0	0.0
to 387 mbsf			Hole C - APC/HLAPC/XCB to 387 mbsf	2.0	0.0
			Hole D - APC/HLAPC/XCB to 387 mbsf - Log with triple combo, FMS-sonic, and VSP	2.1	1.1
			Subtotal days on site: 9.6		
ISD-04B	77.528969°N	1725	Hole A - APC/HLAPC/XCB to 402 mbsf - 4 APCT-3 measurements	2.4	0.0
EPSP	9.610717°E		Hole B - APC/HLAPC/XCB to 402 mbsf	2.1	0.0
to 402 mbsf			Hole C - APC/HLAPC/XCB to 402 mbsf	2.1	0.0
			Hole D - APC/HLAPC/XCB to 402 mbsf - Log with triple combo, FMS-sonic, and VSP	2.2	1.2
			Subtotal days on site: 9.9		
SVR-04A	78.264113°N	1601	Hole A - APC/HLAPC to 400 mbsf - 4 APCT-3 measurements	2.1	0.0
EPSP	5.923096°E		Hole B - APC/HLAPC to 400 mbsf	1.7	0.0
to 745 mbsf			Hole C - APC/HLAPC/XCB to 745 mbsf - Log with triple combo, FMS-sonic, and VSP	4.0	1.5
			Subtotal days on site: 9.2		
SVR-05A	78.268848°N	1611	Hole A - APC/HLAPC to 400 mbsf - 4 APCT-3 measurements	2.1	0.0
EPSP	5.909515°E		Hole B - APC/HLAPC to 400 mbsf	1.7	0.0
to 738 mbsf			Hole C - APC/HLAPC/XCB to 738 mbsf - Log with triple combo, FMS-sonic, and VSP	3.9	1.4
			Subtotal days on site: 9.2		
VRE-01B	79.032083°N	1304	Hole A - APC/HLAPC to 400 mbsf - 4 APCT-3 measurements	2.0	0.0
EPSP	7.057735°E		Hole B - APC/HLAPC to 400 mbsf	1.7	0.0
to 618 mbsf			Hole C - APC/HLAPC to 400 mbsf	1.7	0.0
			Hole D - APC/HLAPC/XCB to 618 mbsf - Log with triple combo, FMS-sonic, and VSP	2.9	1.4
			Subtotal days on site: 9.8		
VRE-04B	78.999400°N	1268	Hole A - APC/HLAPC to 400 mbsf - 4 APCT-3 measurements	1.9	0.0
EPSP	7.310700°E		Hole B - APC/HLAPC to 400 mbsf	1.6	0.0
to 730 mbsf			Hole C - APC/HLAPC to 400 mbsf	1.6	0.0
			Hole D - APC/HLAPC/XCB to 730 mbsf - Log with triple combo, FMS-sonic, and VSP	3.3	1.5
			Subtotal days on site: 9.9		
VRW-02B	79.158704°N	1618	Hole A - APC/HLAPC to 400 mbsf - 4 APCT-3 measurements	2.1	0.0
EPSP	4.621648°E		Hole B - APC/HLAPC to 400 mbsf	1.7	0.0
to 677 mbsf			Hole C - APC/HLAPC to 400 mbsf	1.7	0.0
			Hole D - APC/HLAPC/XCB to 677 mbsf - Log with triple combo, FMS-sonic, and VSP	3.3	1.5
			Subtotal days on site: 10.4		
VRW-04A	79.155928°N	1701	Hole A - APC/HLAPC to 400 mbsf - 4 APCT-3 measurements	2.1	0.0
EPSP	4.497530°E		Hole B - APC/HLAPC to 400 mbsf	1.7	0.0
to 740 mbsf			Hole C - APC/HLAPC to 400 mbsf	1.7	0.0
			Hole D - APC/HLAPC/XCB to 740 mbsf - Log with triple combo, FMS-sonic, and VSP	3.8	1.6
			Subtotal days on site: 10.9		
VRW-05A	79.143266°N	1632	Hole A - APC/HLAPC to 400 mbsf - 4 APCT-3 measurements	2.1	0.0
EPSP	4.729997°E		Hole B - APC/HLAPC to 400 mbsf	1.7	0.0
to 669 mbsf			Hole C - APC/HLAPC to 400 mbsf	1.7	0.0
			Hole D - APC/HLAPC/XCB to 669 mbsf - Log with triple combo, FMS-sonic, and VSP	3.3	1.5
			Subtotal days on site: 10.3		

The targets for Sites VRE-03A and VRW-03A are as follows:

- 738 mbsf for Site VRE-03A,
- 696 mbsf for Site VRW-03A,
- Reflector R8 (Figure **F9**),
- 5.8 Ma, and
- Understanding the Late Miocene transition, Pliocene–Quaternary climatic transitions, sediment tectonic stress, and evolution of the MTF.

The second hole of Site BED-02B as well as the fourth hole of Sites ISD-01C, VRE-03A, and VRW-03A will be dedicated to microbiological sampling. At all times the protocol for continuous assessment of potential contamination will be applied. Sites BED-01A and SVR-03A will not have a dedicated microbiology program.

In case of adverse hole conditions, weather, ice, or other difficulties, 11 alternate sites (Table **T8**) are available to achieve the objectives of Expedition 403. Every working area has multiple alternate sites in the vicinity, thus switching drilling targets and sites will result in a minimal time penalty.

7. Wireline logging/Downhole measurements strategy

A comprehensive wireline logging program with the triple combo (Figure **F12**) and the Formation MicroScanner (FMS)-sonic in combination with the General Purpose Inclinometry Tool (GPIT) is planned for all sites. Checkout surveys with the Versatile Seismic Imager (VSI) are planned for two sites, where core-log-seismic integration is important. The wireline logs are also very useful for core-log integration and the establishment of a high-resolution stratigraphy in both volcanic and sedimentary sequences.

The drilling plan is to start downhole logging at the second site (BED-02B) at the Bellsund drift (76°45800′N, 12°5547′E) and then continue northwest along the Fram Strait toward western Vestnesa Ridge Site VRW-03A (79°1599′N, 4°48873′E). We do expect some downtime because of weather and/or ice, and technical problems may cause us to skip some of the sites or reduce the logging program. In this case, the highest priority sites for wireline logging are Sites BED-02B and

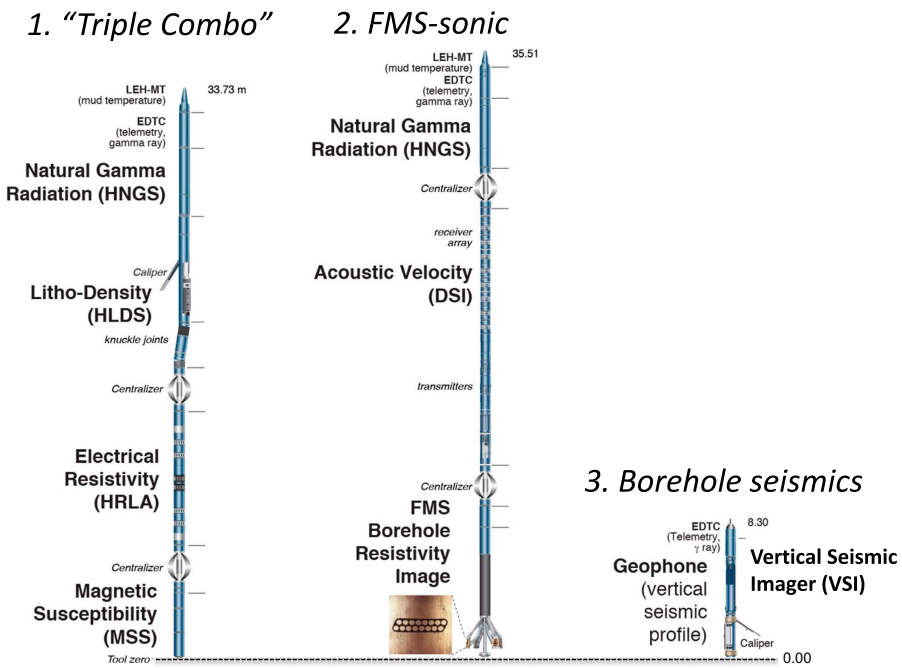

Figure F12. Triple combo, FMS-sonic, and VSI downhole logging tool strings (see **http://iodp.tamu.edu/tools/logging**) intended for use during Expedition 403 wireline logging.

VRE-03A. Thus, if the logging program has to be reduced because of time, weather, or ice, it is our intention to keep these two sites and abandon downhole logging at one or several of the remaining sites.

For all sites, we aim to deploy the advanced piston corer temperature (APCT-3) probe in at least one hole. The deployment interval might vary, but we aim to deploy it every third APC core (e.g., Cores 4H, 7H, 10H, and 13H).

8. Risks and contingency

The proposed sites are located in the eastern Fram Strait, a region that enables us to better understand the geologic evolution of the Arctic, as well as past, present, and future polar and global climate and thus has been studied extensively. Comprehensive seismic survey data are available for all sites. All proposed locations have been reviewed and approved by the EPSP. However, a number of key factors pose risks or potential hazards for this expedition, including the possible presence of gas hydrates (5/8 km upslope of Sites VRE-03A and VRW-03A), weather, freezing, sea ice, and icebergs. A detailed safety report was prepared for the EPSP and is available from the JRSO.

This expedition will sail in the later part of the Northern Hemisphere summer, and sea-surface conditions can be rough in the Fram Strait. Therefore, adverse weather conditions, sea state, and the resulting heave can have adverse effects on drilling operations and can significantly affect core quality and recovery. It may also cause a significant loss of time.

Based on the record of the last 10 y, drill sites at Bellsund (BED), Isfjorden (ISD), and Svyatogor (SVR) are ice-free all year round. Drill sites on the eastern Vestnesa Ridge (VRE) are ice-free in the June–October weather window. Drill sites at the western Vestnesa Ridge (VRW) may have a 50% chance of patches of sea-ice in June and July. Thus, we will start our drilling program in the southern part of our research area and progress toward the north throughout the expedition. Because ice might be a risk, two ice observers will sail during Expedition 403.

Bottom current speeds at depths of ~1000 meters below sea level (mbsl) have an average speed of 30 cm/s with local jets exceeding 40 cm/s (Bensi et al., 2019). In the deeper environment (1250–2000 mbsl), bottom current velocities range 10–5 cm/s (Beszczynska-Möller et al., 2012).

No geophysical indication of gas-related features exists at the Bellsund and Isfjorden drifts. In addition, the quantity of free hydrocarbons from rock-eval data at nearby Leg 162 Site 986 is generally low throughout the site. On the Vestnesa and Svyatogor Ridges, indications for hydrocarbons and gas hydrate are limited at the crests of the sediment drifts and in the greater vicinity of the proposed site (at least >2 and >1 km away, respectively) but not directly at the proposed locations.

Two different coring systems (APC and XCB) will be primarily used to ensure we meet the scientific objectives. All sites will be drilled/cored using the piston coring (APC/HLAPC) and XCB systems to attempt to recover high-quality sequences suitable for high-resolution paleoceanographic studies. If conditions are not suitable for XCB coring (e.g., drilling progress is too slow or intense biscuitting) some holes might require the use of the rotary core barrel (RCB) system.

It should be noted that drilled holes on the Norwegian continental margin normally may not be deeper than 200 m because of government safety regulations. However, there is precedent of scientific drilling of deep holes at the Norwegian margin (IODP Expedition 396; Planke et al., 2022), and we believe that the Norwegian authorities will allow deeper drilling in our case along the western Svalbard margin.

Other risks to the successful completion of the program include operational problems caused by lower than predicted penetration rates or unstable borehole conditions. Hole stability is always a risk during coring operations, and the risk is higher when there are longer sections of open (not cased) hole. Unconsolidated sediments may create unstable borehole conditions, particularly for reaching deep targets. Poor hole conditions, such as loose unconsolidated material or collapsing holes, can prevent our ability to penetrate deeply or successfully conduct logging. They can also

lead to a stuck drill pipe. A stuck drill string is always a risk during coring operations, and expedition time can be consumed while attempting to free the stuck drill string or, in the worst case, severing the stuck drill string. This can result in the complete loss of the hole and loss of equipment. *JOIDES Resolution* carries sufficient spare drilling equipment to enable the continuation of coring, but the time lost for the expedition can be significant. Hiatuses in the recovered sediments or incomplete sections may prevent the recovery of key sedimentary sections and result in not achieving all the scientific objectives.

The ideal drill scenario—six sites starting in the south, progressing toward the north—is shown in Figure **F11** and Table **T7**. However, if time is a limiting factor (e.g., because of lost time while waiting on weather), we anticipate possibly reducing one or more of our quadruple-hole sites (ISD-01C, VRE-03A, and VRW-03A) by one hole. In addition, the logging program might be reduced as described in the paragraph above. Furthermore, the microbiology program might be reduced, keeping the highest priority sites in the south (BED) and north (VRE).

The highest risk for sea ice will be encountered at our northernmost Site VRW-03A. Thus, if ice conditions prevent the vessel from drilling at the western Vestnesa Ridge, we will drill one of the two alternate VRE sites (VRE-01B or VRE-04B). If ice conditions improve during this time, a reduced drilling program with fewer holes will be conducted at Site VRW-03A.

In case gas hydrates become a safety concern at the SVR, VRE, or VRW sites, the hole and ultimately the site might be abandoned, and the vessel will drill one of the alternate sites. However, if hydrates still remain of concern, we will move toward the southern sites, where gas hydrates are of lower or no concern.

9. Sampling and data sharing strategy

Shipboard and shore-based researchers should refer to the IODP Sample, Data, and Obligations Policy and Implementation Guidelines posted on the Web at **http://www.iodp.org/top-resources/program-documents/policies-and-guidelines**. This document outlines the policy for distributing IODP samples and data to research scientists, curators, and educators. The document also defines the obligations that sample and data recipients incur. The Sample Allocation Committee (SAC; composed of the Co-Chief Scientists, Staff Scientist, and IODP Curator on shore and curatorial representative on board the ship) will work with the entire scientific party to formulate a formal expedition-specific sampling plan for shipboard and postexpedition sampling.

Shipboard scientists are expected to submit sample requests (at **http://iodp.tamu.edu/curation/samples.html**) ~6 months before the beginning of the expedition. Based on sample requests (shore based and shipboard) submitted by this deadline, the SAC will prepare a tentative sampling plan, which will be revised on the ship as dictated by core recovery and cruise objectives. The sampling plan will be subject to modification depending upon the actual material recovered and collaborations that may evolve between scientists during the expedition. Modification of the strategy during the expedition must be approved by the Co-Chief Scientists, Staff Scientist, and curatorial representative on board the ship.

The minimum permanent archive will be the standard archive half of each core. All sample frequencies and sizes must be justified on a scientific basis and will depend on core recovery, the full spectrum of other requests, and the cruise objectives. Some redundancy of measurement is unavoidable, but minimizing the duplication of measurements among the shipboard party and identified shore-based collaborators will be a factor in evaluating sample requests.

If some critical intervals are recovered, there may be considerable demand for samples from a limited amount of cored material. These intervals may require special handling, a higher sampling density, reduced sample size, or continuous core sampling by a single investigator. A sampling plan coordinated by the SAC may be required before critical intervals are sampled.

Following Expedition 403, cores will be delivered to the Bremen Core Repository (BCR) in Germany. However, the archive halves may be shipped to the IODP Gulf Coast Repository in Col-

lege Station, Texas (United States) for postcruise programmatic X-ray fluorescence (XRF) core scanning. Upon completion of these measurements, cores will be sent to the BCR for permanent storage.

All collected data and samples will be protected by a 1 y moratorium period following the completion of the postexpedition sampling party. During this time, data and samples will be available only to the Expedition 403 shipboard scientists and approved shore-based participants.

10. Expedition scientists and scientific participants

The current list of participants for Expedition 403 can be found at **http://iodp.tamu.edu/scienceops/expeditions/eastern_fram_strait_paleo_archive.html**.

11. Acknowledgments

The Expedition 403 *Scientific Prospectus* draws largely on the content of IODP Proposal 985-Full2 (Eastern Fram Strait Palaeo-archive). The proposal co-proponents provided an excellent scientific foundation for the expedition. Thank you to S. Bünz (data lead), M. Rebesco, F. Colleoni, R. Geletti, T.M. Cronin, K. Husum, A. Plaza-Faverola, S. Vadakkepuliyambatta, J.S. Laberg, A. de Vernal, C. Caricchi, J. Müller, J. Pike, H. Haflidason, S.L. Jørgensen, P. Grunert, C. Morigi, J. Knies, R. Stein, C. Hillaire-Marcel, and J. Grützner. Acknowledgments go to W. Gessler, N. Alexandropoulou, and the other participants of the EFRAM-ARC Magellan Plus Workshop (Trieste-Italy; January 2020) for contributing with critical discussion at the initial stage of the proposal. Special thanks to F. Colleoni, who compiled the data for Figure **F5**.

References

Aagaard, K., Swift, J.H., and Carmack, E.C., 1985. Thermohaline circulation in the Arctic Mediterranean Seas. Journal of Geophysical Research: Oceans, 90(C3):4833–4846. **https://doi.org/10.1029/JC090iC03p04833**

Agarwal, S., and Worster, M.G., 2021. Sea-ice distribution and mixed-Layer depths in Fram Strait. arXiv, 1712.07599vi. **https://doi.org/10.48550/arXiv.1712.07599**

Alexandropoulou, N., Winsborrow, M., Andreassen, K., Plaza-Faverola, A., Dessandier, P.-A., Mattingsdal, R., Baeten, N., and Knies, J., 2021. A continuous seismostratigraphic framework for the Western Svalbard-Barents Sea margin over the last 2.7 Ma: implications for the Late Cenozoic glacial history of the Svalbard-Barents Sea Ice Sheet. Frontiers in Earth Science, 9:656732. **https://doi.org/10.3389/feart.2021.656732**

Andreassen, K., Ødegaard, C.M., and Rafaelsen, B., 2007. Imprints of former ice streams, imaged and interpreted using industry three-dimensional seismic data from the south-western Barents Sea. In Davies, R.J., Posamentier, H.W., Wood, L.J., and Cartwright, J.A. (Eds.), Seismic Geomorphology: Applications to Hydrocarbon Exploration and Production. Special Publication - Geological Society of London, 277: 151–169. **https://doi.org/10.1144/GSL.SP.2007.277.01.09**

Årthun, M., Eldevik, T., Smedsrud, L.H., Skagseth, Ø., and Ingvaldsen, R.B., 2012. Quantifying the influence of Atlantic heat on Barents Sea ice variability and retreat. Journal of Climate, 25(13):4736–4743. **https://doi.org/10.1175/JCLI-D-11-00466.1**

Backman, J., and Moran, K., 2009. Expanding the Cenozoic paleoceanographic record in the Central Arctic Ocean: IODP Expedition 302 synthesis. Open Geosciences, 1(2):157–175. **https://doi.org/10.2478/v10085-009-0015-6**

Bacon, C.D., Silvestro, D., Jaramillo, C., Smith, B.T., Chakrabarty, P., and Antonelli, A., 2015. Biological evidence supports an early and complex emergence of the Isthmus of Panama. Proceedings of the National Academy of Sciences of the United States of America, 112(19):6110–6115. **https://doi.org/10.1073/pnas.1423853112**

Badger, M.P.S., Lear, C.H., Pancost, R.D., Foster, G.L., Bailey, T.R., Leng, M.J., and Abels, H.A., 2013a. CO_2 drawdown following the Middle Miocene expansion of the Antarctic Ice Sheet. Paleoceanography, 28(1):42–53. **https://doi.org/10.1002/palo.20015**

Badger, M.P.S., Schmidt, D.N., Mackensen, A., and Pancost, R.D., 2013b. High-resolution alkenone palaeobarometry indicates relatively stable pCO_2 during the Pliocene (3.3–2.8 Ma). Philosophical Transactions of the Royal Society A: Mathematical, Physical and Engineering Sciences, 371(2001):20130094. **https://doi.org/10.1098/rsta.2013.0094**

Bartoli, G., Hönisch, B., and Zeebe, R.E., 2011. Atmospheric CO_2 decline during the Pliocene intensification of Northern Hemisphere glaciations. Paleoceanography, 26(4):PA4213. **https://doi.org/10.1029/2010PA002055**

Batchelor, C.L., Christie, F.D.W., Ottesen, D., Montelli, A., Evans, J., Dowdeswell, E.K., Bjarnadóttir, L.R., and Dowdeswell, J.A., 2023. Rapid, buoyancy-driven ice-sheet retreat of hundreds of metres per day. Nature. **https://doi.org/10.1038/s41586-023-05876-1**

Bensi, M., Kovačević, V., Langone, L., Aliani, S., Ursella, L., Goszczko, I., Soltwedel, T., Skogseth, R., Nilsen, F., Deponte, D., Mansutti, P., Laterza, R., Rebesco, M., Rui, L., Lucchi, R.G., Wåhlin, A., Viola, A., Beszczynska-Möller, A., and Rubino, A., 2019. Deep flow variability offshore south-west Svalbard (Fram Strait). Water, 11(4):683. **https://doi.org/10.3390/w11040683**

Bereiter, B., Eggleston, S., Schmitt, J., Nehrbass-Ahles, C., Stocker, T.F., Fischer, H., Kipfstuhl, S., and Chappellaz, J., 2015. Revision of the EPICA Dome C CO_2 record from 800 to 600 kyr before present. Geophysical Research Letters, 42(2):542–549. **https://doi.org/10.1002/2014GL061957**

Beszczynska-Möller, A., Fahrbach, E., Schauer, U., and Hansen, E., 2012. Variability in Atlantic water temperature and transport at the entrance to the Arctic Ocean, 1997–2010. ICES Journal of Marine Science, 69(5):852–863. **https://doi.org/10.1093/icesjms/fss056**

Bickle, M., Arculus, R., Barrett, P., DeConto, R., Camoin, G., Edwards, K., Fisher, F., Inagaki, F., Kodaira, S., and Ohkouchi, N., 2011. Illuminating Earth's Past, Present and Future The Science Plan for the International Ocean Discovery Program 2013-2023: Washington, DC (Integrated Ocean Drilling Program). **http://www.iodp.org/about-iodp/iodp-science-plan-2013-2023**

Bierman, P.R., Shakun, J.D., Corbett, L.B., Zimmerman, S.R., and Rood, D.H., 2016. A persistent and dynamic East Greenland Ice Sheet over the past 7.5 million years. Nature, 540(7632):256–260. **https://doi.org/10.1038/nature20147**

Bohrmann, G., Henrich, R., and Thiede, J., 1990. Miocene to Quaternary paleoceanography in the northern North Atlantic: variability in carbonate and biogenic opal accumulation. In Bleil, U., and Thiede, J. (Eds.), Geological History of the Polar Oceans: Arctic versus Antarctic. NATO ASI Series, 308: 647-675. **https://doi.org/10.1007/978-94-009-2029-3_34**

Bond, G., Heinrich, H., Broecker, W., Labeyrie, L., McManus, J., Andrews, J., Huon, S., Jantschik, R., Clasen, S., Simet, C., Tedesco, K., Klas, M., Bonani, G., and Ivy, S., 1992. Evidence for massive discharges of icebergs into the North Atlantic ocean during the last glacial period. Nature, 360(6401):245–249. **https://doi.org/10.1038/360245a0**

Bourke, R.H., Weigel, A.M., and Paquette, R.G., 1988. The westward turning branch of the West Spitsbergen Current. Journal of Geophysical Research: Oceans, 93(C11):14065–14077. **https://doi.org/10.1029/JC093iC11p14065**

Bradley, R.S., and England, J.H., 2008. The Younger Dryas and the sea of ancient ice. Quaternary Research, 70(1):1–10. **https://doi.org/10.1016/j.yqres.2008.03.002**

Broecker, W., Bond, G., Klas, M., Clark, E., and McManus, J., 1992. Origin of the northern Atlantic's Heinrich events. Climate Dynamics, 6(3):265–273. **https://doi.org/10.1007/BF00193540**

Burton, K.W., Ling, H.-F., and O'Nions, R.K., 1997. Closure of the Central American Isthmus and its effect on deep-water formation in the North Atlantic. Nature, 386(6623):382–385. **https://doi.org/10.1038/386382a0**

Butt, F.A., Drange, H., Elverhøi, A., Otterå, O.H., and Solheim, A., 2002. Modelling Late Cenozoic isostatic elevation changes in the Barents Sea and their implications for oceanic and climatic regimes: preliminary results. Quaternary Science Reviews, 21(14–15):1643–1660. **https://doi.org/10.1016/S0277-3791(02)00018-5**

Butt, F.A., Elverhøi, A., Solheim, A., and Forsberg, C.F., 2000. Deciphering late Cenozoic development of the western Svalbard Margin from ODP Site 986 results. Marine Geology, 169(3):373–390. **https://doi.org/10.1016/S0025-3227(00)00088-8**

Carbonara, K., Mezgec, K., Varagona, G., Musco, M.E., Lucchi, R.G., Villa, G., Morigi, C., Melis, R., and Caffau, M., 2016. Palaeoclimatic changes in Kveithola, Svalbard, during the Late Pleistocene deglaciation and Holocene: evidences from microfossil and sedimentary records. Palaeogeography, Palaeoclimatology, Palaeoecology, 463:136–149. **https://doi.org/10.1016/j.palaeo.2016.10.003**

Caricchi, C., Lucchi, R.G., Sagnotti, L., Macrì, P., Di Roberto, A., Del Carlo, P., Husum, K., Laberg, J.S., and Morigi, C., 2019. A high-resolution geomagnetic relative paleointensity record from the Arctic Ocean deep-water gateway deposits during the last 60 kyr. Geochemistry, Geophysics, Geosystems, 20(5):2355–2377. **https://doi.org/10.1029/2018GC007955**

Caricchi, C., Sagnotti, L., Campuzano, S.A., Lucchi, R.G., Macrì, P., Rebesco, M., and Camerlenghi, A., 2020. A refined age calibrated paleosecular variation and relative paleointensity stack for the NW Barents Sea: implication for geomagnetic field behavior during the Holocene. Quaternary Science Reviews, 229:106133. **https://doi.org/10.1016/j.quascirev.2019.106133**

Carmack, E., Polyakov, I., Padman, L., Fer, I., Hunke, E., Hutchings, J., Jackson, J., Kelley, D., Kwok, R., Layton, C., Melling, H., Perovich, D., Persson, O., Ruddick, B., Timmermans, M.-L., Toole, J., Ross, T., Vavrus, S., and Winsor, P., 2015. Toward quantifying the increasing role of oceanic heat in sea ice loss in the new Arctic. Bulletin of the American Meteorological Society, 96(12):2079–2105. **https://doi.org/10.1175/BAMS-D-13-00177.1**

Clark, P.U., Archer, D., Pollard, D., Blum, J.D., Rial, J.A., Brovkin, V., Mix, A.C., Pisias, N.G., and Roy, M., 2006. The Middle Pleistocene transition: characteristics, mechanisms, and implications for long-term changes in atmospheric pCO_2. Quaternary Science Reviews, 25(23–24):3150–3184. **https://doi.org/10.1016/j.quascirev.2006.07.008**

Clark, P.U., and Pollard, D., 1998. Origin of the Middle Pleistocene transition by ice sheet erosion of regolith. Paleoceanography, 13(1):1–9. **https://doi.org/10.1029/97PA02660**

Clotten, C., Stein, R., Fahl, K., Schreck, M., Risebrobakken, B., and De Schepper, S., 2019. On the causes of Arctic sea ice in the warm Early Pliocene. Scientific Reports, 9(1):989. **https://doi.org/10.1038/s41598-018-37047-y**

Coates, A.G., and Obando, J.A., 1996. The geologic evolution of the central American isthmus. In Jackson, J.B.C., Budd, A.F., and Coates, A.G. (Eds.), Evolution and Environment in Tropical America. Chicago (University of Chicago Press).

Colleoni, F., De Santis, L., Montoli, E., Olivo, E., Sorlien, C.C., Bart, P.J., Gasson, E.G.W., Bergamasco, A., Sauli, C., Wardell, N., and Prato, S., 2018. Past continental shelf evolution increased Antarctic ice sheet sensitivity to climatic conditions. Scientific Reports, 8(1):11323. **https://doi.org/10.1038/s41598-018-29718-7**

Condron, A., Joyce, A.J., and Bradley, R.S., 2020. Arctic sea ice export as a driver of deglacial climate. Geology, 48(4):395–399. **https://doi.org/10.1130/G47016.1**

Cronin, T.M., Dwyer, G.S., Caverly, E.K., Farmer, J., DeNinno, L.H., Rodriguez-Lazaro, J., and Gemery, L., 2017. Enhanced Arctic amplification began at the Mid-Brunhes Event ~400,000 years ago. Scientific Reports, 7(1):14475. **https://doi.org/10.1038/s41598-017-13821-2**

Curry, R., 2010. Wikipedia File: OCP07 Fig-6.jpg. **https://editors.eol.org/eoearth/wiki/File:OCP07_Fig-6.jpg**

Dansgaard, W., Johnsen, S.J., Clausen, H.B., Dahl-Jensen, D., Gundestrup, N.S., Hammer, C.U., Hvidberg, C.S., Steffensen, J.P., Sveinbjörnsdottir, A.E., Jouzel, J., and Bond, G., 1993. Evidence for general instability of past climate from a 250-kyr ice-core record. Nature, 364(6434):218–220. **https://doi.org/10.1038/364218a0**

De Schepper, S., Gibbard, P.L., Salzmann, U., and Ehlers, J., 2014. A global synthesis of the marine and terrestrial evidence for glaciation during the Pliocene epoch. Earth-Science Reviews, 135:83–102. **https://doi.org/10.1016/j.earscirev.2014.04.003**

Dumitru, O.A., Austermann, J., Polyak, V.J., Fornós, J.J., Asmerom, Y., Ginés, J., Ginés, A., and Onac, B.P., 2019. Constraints on global mean sea level during Pliocene warmth. Nature, 574(7777):233–236. **https://doi.org/10.1038/s41586-019-1543-2**

Dutton, A., Carlson, A.E., Long, A.J., Milne, G.A., Clark, P.U., DeConto, R., Horton, B.P., Rahmstorf, S., and Raymo, M.E., 2015. Sea-level rise due to polar ice-sheet mass loss during past warm periods. Science, 349(6244):aaa4019. **https://doi.org/10.1126/science.aaa4019**

Dwyer, G.S., and Chandler, M.A., 2009. Mid-Pliocene sea level and continental ice volume based on coupled benthic Mg/Ca palaeotemperatures and oxygen isotopes. Philosophical Transactions of the Royal Society, A: Mathematical, Physical and Engineering Sciences, 367(1886):157–168. **https://doi.org/10.1098/rsta.2008.0222**

Ehlers, B.-M., and Jokat, W., 2013. Paleo-bathymetry of the northern North Atlantic and consequences for the opening of the Fram Strait. Marine Geophysical Research, 34(1):25–43. **https://doi.org/10.1007/s11001-013-9165-9**

Eiken, O., and Hinz, K., 1993. Contourites in the Fram Strait. Sedimentary Geology, 82(1–4):15–32. **https://doi.org/10.1016/0037-0738(93)90110-Q**

Ellegaard, M., Clokie, M.R.J., Czypionka, T., Frisch, D., Godhe, A., Kremp, A., Letarov, A., McGenity, T.J., Ribeiro, S., and Anderson, N.J., 2020. Dead or alive: sediment DNA archives as tools for tracking aquatic evolution and adaptation. Communications Biology, 3(1):169. **https://doi.org/10.1038/s42003-020-0899-z**

Engen, Ø., Faleide, J.I., and Dyreng, T.K., 2008. Opening of the Fram Strait gateway: a review of plate tectonic constraints. Tectonophysics, 450(1–4):51–69. **https://doi.org/10.1016/j.tecto.2008.01.002**

Fedorov, A.V., Brierley, C.M., Lawrence, K.T., Liu, Z., Dekens, P.S., and Ravelo, A.C., 2013. Patterns and mechanisms of early Pliocene warmth. Nature, 496(7443):43–49. **https://doi.org/10.1038/nature12003**

Fer, I., Skogseth, R., Haugan, P.M., and Jaccard, P., 2003. Observations of the Storfjorden overflow. Deep Sea Research, Part I: Oceanographic Research Papers, 50(10):1283–1303. **https://doi.org/10.1016/S0967-0637(03)00124-9**

Fohrmann, H., Backhaus, J.O., Blaume, F., and Rumohr, J., 1998. Sediments in bottom-arrested gravity plumes: numerical case studies. Journal of Physical Oceanography, 28(11):2250–2274. **https://doi.org/10.1175/1520-0485(1998)028%3C2250:SIBAGP%3E2.0.CO;2**

Ford, H.L., Ravelo, A.C., Dekens, P.S., LaRiviere, J.P., and Wara, M.W., 2015. The evolution of the equatorial thermocline and the early Pliocene El Padre mean state. Geophysical Research Letters, 42(12):4878–4887. **https://doi.org/10.1002/2015GL064215**

Forsberg, C.F., Solheim, A., Elverhoi, A., Jansen, E., Channell, J.E.T., and Andersen, E.S., 1999. The depositional environment of the western Svalbard margin during the late Pliocene and the Pleistocene; sedimentary facies changes at Site 986. In Raymo, M.E., Jansen, E., Blum, P., and Herbert, T.D. (Eds.), Proceedings of the Ocean Drilling Program, Scientific Results. 162: College Station, TX (Ocean Drilling Program). **https://doi.org/10.2973/odp.proc.sr.162.032.1999**

Foster, G.L., Lear, C.H., and Rae, J.W.B., 2012. The evolution of pCO_2, ice volume and climate during the middle Miocene. Earth and Planetary Science Letters, 341–344:243–254. **https://doi.org/10.1016/j.epsl.2012.06.007**

Freitas, L., Appolinario, L., Calegario, G., Campeão, M., Tschoeke, D., Garcia, G., Venancio, I.M., Cosenza, C.A.N., Leomil, L., Bernardes, M., Albuquerque, A.L., Thompson, C., and Thompson, F., 2020. Glacial-interglacial transitions in microbiomes recorded in deep-sea sediments from the western equatorial Atlantic. Science of The Total Environment, 746:140904. **https://doi.org/10.1016/j.scitotenv.2020.140904**

Geissler, W.H., Jokat, W., and Brekke, H., 2011. The Yermak Plateau in the Arctic Ocean in the light of reflection seismic data-implication for its tectonic and sedimentary evolution. Geophysical Journal International, 187(3):1334–1362. **https://doi.org/10.1111/j.1365-246X.2011.05197.x**

Gildor, H., and Tziperman, E., 2001. A sea ice climate switch mechanism for the 100-kyr glacial cycles. Journal of Geophysical Research: Oceans, 106(C5):9117–9133. **https://doi.org/10.1029/1999JC000120**

Golledge, N.R., Keller, E.D., Gomez, N., Naughten, K.A., Bernales, J., Trusel, L.D., and Edwards, T.L., 2019. Global environmental consequences of twenty-first-century ice-sheet melt. Nature, 566(7742):65–72. **https://doi.org/10.1038/s41586-019-0889-9**

Goswami, B.K., Weitemeyer, K.A., Minshull, T.A., Sinha, M.C., Westbrook, G.K., Chabert, A., Henstock, T.J., and Ker, S., 2015. A joint electromagnetic and seismic study of an active pockmark within the hydrate stability field at the Vestnesa Ridge, West Svalbard margin. Journal of Geophysical Research: Solid Earth, 120(10):6797–6822. **https://doi.org/10.1002/2015JB012344**

Greenop, R., Foster, G.L., Wilson, P.A., and Lear, C.H., 2014. Middle Miocene climate instability associated with high-amplitude CO_2 variability. Paleoceanography and Paleoclimatology, 29(9):845–853. **https://doi.org/10.1002/2014PA002653**

Gruetzner, J., Matthiessen, J., Geissler, W.H., Gebhardt, A.C., and Schreck, M., 2022. A revised core-seismic integration in the Molloy Basin (ODP Site 909): implications for the history of ice rafting and ocean circulation in the

Atlantic-Arctic gateway. Global and Planetary Change, 215:103876. **https://doi.org/10.1016/j.gloplacha.2022.103876**

Hattermann, T., Isachsen, P.E., von Appen, W.-J., Albretsen, J., and Sundfjord, A., 2016. Eddy-driven recirculation of Atlantic Water in Fram Strait. Geophysical Research Letters, 43(7):3406–3414. **https://doi.org/10.1002/2016GL068323**

Haug, G.H., Ganopolski, A., Sigman, D.M., Rosell-Mele, A., Swann, G.E.A., Tiedemann, R., Jaccard, S.L., Bollmann, J., Maslin, M.A., Leng, M.J., and Eglinton, G., 2005. North Pacific seasonality and the glaciation of North America 2.7 million years ago. Nature, 433(7028):821–825. **https://doi.org/10.1038/nature03332**

Haywood, A.M., Dowsett, H.J., and Dolan, A.M., 2016. Integrating geological archives and climate models for the mid-Pliocene warm period. Nature Communications, 7(1):10646. **https://doi.org/10.1038/ncomms10646**

Hegewald, A., and Jokat, W., 2013. Tectonic and sedimentary structures in the northern Chukchi region, Arctic Ocean. Journal of Geophysical Research: Solid Earth, 118(7):3285–3296. **https://doi.org/10.1002/jgrb.50282**

Herbert, T.D., Lawrence, K.T., Tzanova, A., Peterson, L.C., Caballero-Gill, R., and Kelly, C.S., 2016. Late Miocene global cooling and the rise of modern ecosystems. Nature Geoscience, 9(11):843–847. **https://doi.org/10.1038/ngeo2813**

Hesse, R., Khodabakhsh, S., Klaucke, I., and Ryan, W.B.F., 1997. Asymmetrical turbid surface-plume deposition near ice-outlets of the Pleistocene Laurentide ice sheet in the Labrador Sea. Geo-Marine Letters, 17(3):179-187. **https://doi.org/10.1007/s003670050024**

Hoehler, T.M., and Jørgensen, B.B., 2013. Microbial life under extreme energy limitation. Nature Reviews Microbiology, 11(2):83. **http://hdl.handle.net/10.1038/nrmicro2939**

Holbourn, A., Kuhnt, W., Clemens, S., Prell, W., and Andersen, N., 2013. Middle to Late Miocene stepwise climate cooling: evidence from a high-resolution deep water isotope curve spanning 8 million years. Paleoceanography, 28(4):688–699. **https://doi.org/10.1002/2013PA002538**

Holbourn, A.E., Kuhnt, W., Clemens, S.C., Kochhann, K.G.D., Jöhnck, J., Lübbers, J., and Andersen, N., 2018. Late Miocene climate cooling and intensification of southeast Asian winter monsoon. Nature Communications, 9(1):1584. **https://doi.org/10.1038/s41467-018-03950-1**

Hönisch, B., Hemming, N.G., Archer, D., Siddall, M., and McManus, J.F., 2009. Atmospheric carbon dioxide concentration across the mid-Pleistocene transition. Science, 324(5934):1551. **http://hdl.handle.net/10.1126/science.1171477**

Howe, J.A., Shimmield, T.M., Harland, R., and Eyles, N., 2008. Late Quaternary contourites and glaciomarine sedimentation in the Fram Strait. Sedimentology, 55(1):179–200. **https://doi.org/10.1111/j.1365-3091.2007.00897.x**

Hustoft, S., Bünz, S., Mienert, J., and Chand, S., 2009. Gas hydrate reservoir and active methane-venting province in sediments on <20 Ma young oceanic crust in the Fram Strait, offshore NW-Svalbard. Earth and Planetary Science Letters, 284(1–2):12–24. **https://doi.org/10.1016/j.epsl.2009.03.038**

Intergovernmental Panel on Climate Change, 2014. Climate Change 2013 – The Physical Science Basis: Cambridge, UK (Cambridge University Press). **https://doi.org/10.1017/CBO9781107415324.013**

Jakobsson, M., Backman, J., Rudels, B., Nycander, J., Frank, M., Mayer, L., Jokat, W., Sangiorgi, F., O'Regan, M., Brinkhuis, H., King, J., and Moran, K., 2007. The Early Miocene onset of ventilated circulation regime in the Arctic Ocean. Nature, 447(7147):986–990. **https://doi.org/10.1038/nature05924**

Jakobsson, M., Ingólfsson, Ó., Long, A.J., and Spielhagen, R.F., 2014. The dynamic Arctic. Quaternary Science Reviews, 92:1–8. **https://doi.org/10.1016/j.quascirev.2014.03.022**

Jakobsson, M., Mayer, L., Coakley, B., Dowdeswell, J.A., Forbes, S., Fridman, B., Hodnesdal, H., Noormets, R., Pedersen, R., Rebesco, M., Schenke, H.W., Zarayskaya, Y., Accettella, D., Armstrong, A., Anderson, R.M., Bienhoff, P., Camerlenghi, A., Church, I., Edwards, M., Gardner, J.V., Hall, J.K., Hell, B., Hestvik, O., Kristofferson, Y., Marcussen, C., Mohammad, R., Mosher, D., Nghiem, S.V., Pedrosa, M.T., Travaglini, P.G., and Weatherall, P., 2012. The International Bathymetric Chart of the Arctic Ocean (IBCAO) Version 3.0. Geophysical Research Letters, 39(12):L12609. **https://doi.org/10.1029/2012GL052219**

Jansen, E., and Raymo, M.E., 1996. Leg 162: new frontiers on past climates. In Jansen, E., Raymo, M.E., Blum, P., et al., Proceedings of the Ocean Drilling Program, Initial Reports. 162: College Station, TX (Ocean Drilling Program), 5–20. **https://doi.org/10.2973/odp.proc.ir.162.101.1996**

Jansen, E., and Sjøholm, J., 1991. Reconstruction of glaciation over the past 6 Myr from ice-borne deposits in the Norwegian Sea. Nature, 349(6310):600–603. **https://doi.org/10.1038/349600a0**

Jessen, S.P., Rasmussen, T.L., Nielsen, T., and Solheim, A., 2010. A new late Weichselian and Holocene marine chronology for the western Svalbard slope 30,000–0 cal years BP. Quaternary Science Reviews, 29(9–10):1301–1312. **https://doi.org/10.1016/j.quascirev.2010.02.020**

Johnson, J.E., Mienert, J., Plaza-Faverola, A., Vadakkepuliyambatta, S., Knies, J., Bünz, S., Andreassen, K., and Ferré, B., 2015. Abiotic methane from ultraslow-spreading ridges can charge Arctic gas hydrates. Geology, 43(5):371–374. **https://doi.org/10.1130/G36440.1**

Jokat, W., Geissler, W., and Voss, M., 2008. Basement structure of the north-western Yermak Plateau. Geophysical Research Letters, 35(5). **https://doi.org/10.1029/2007GL032892**

Kallmeyer, J., Pockalny, R., Adhikari, R.R., Smith, D.C., and D'Hondt, S., 2012. Global distribution of microbial abundance and biomass in subseafloor sediment. Proceedings of the National Academy of Sciences of the United States of America, 109(40):16213–16216. **https://doi.org/10.1073/pnas.1203849109**

Knies, J., and Gaina, C., 2008. Middle Miocene ice sheet expansion in the Arctic: views from the Barents Sea. Geochemistry, Geophysics, Geosystems, 9(2):Q02015. **https://doi.org/10.1029/2007GC001824**

Knies, J., Matthiessen, J., Vogt, C., Laberg, J.S., Hjelstuen, B.O., Smelror, M., Larsen, E., Andreassen, K., Eidvin, T., and Vorren, T.O., 2009. The Plio-Pleistocene glaciation of the Barents Sea–Svalbard region: a new model based on

revised chronostratigraphy. Quaternary Science Reviews, 28(9):812–829. **https://doi.org/10.1016/j.quascirev.2008.12.002**

Knies, J., Mattingsdal, R., Fabian, K., Grøsfjeld, K., Baranwal, S., Husum, K., De Schepper, S., Vogt, C., Andersen, N., Matthiessen, J., Andreassen, K., Jokat, W., Nam, S.-I., and Gaina, C., 2014. Effect of early Pliocene uplift on late Pliocene cooling in the Arctic–Atlantic gateway. Earth and Planetary Science Letters, 387:132–144. **https://doi.org/10.1016/j.epsl.2013.11.007**

Knutz, P.C., 2008. Palaeoceanographic significance of contourite drifts. In Rebesco, M., and Camerlenghi, A. (Eds.), Contourites. Developments in Sedimentology, 60: (Elsevier), 511–535. **https://doi.org/10.1016/S0070-4571(08)10024-3**

Koenig, Z., Meyer, A., Provost, C., Sennéchael, N., Sundfjord, A., Beguery, L., Athanase, M., and Gascard, J.-C., 2018. Cooling and freshening of the West Spitsbergen Current by shelf-origin cold core lenses. Journal of Geophysical Research: Oceans, 123(11):8299–8312. **https://doi.org/10.1029/2018JC014463**

Kominz, M.A., Browning, J.V., Miller, K.G., Sugarman, P.J., Mizintseva, S., and Scotese, C.R., 2008. Late Cretaceous to Miocene sea-level estimates from the New Jersey and Delaware coastal plain coreholes: an error analysis. Basin Research, 20(2):211–226. **https://doi.org/10.1111/j.1365-2117.2008.00354.x**

Koppers, A., and Coggon, R. (Eds.), 2020. Exploring Earth by Scientific Ocean Drilling: 2050 Science Framework: San Diego, CA (UC San Diego Library). **https://doi.org/10.6075/J0W66J9H**

Krissek, L.A., 1995. Late Cenozoic ice-rafting records from Leg 145 sites in the North Pacific; late Miocene onset, late Pliocene intensification, and Pliocene-Pleistocene events. In Rea, D.K., Basov, I.A., Scholl, D.W., and Allan, J.F. (Eds.), Proceedings of the Ocean Drilling Program, Scientific Results. 145: College Station, TX (Ocean Drilling Program), 179–194. **https://doi.org/10.2973/odp.proc.sr.145.118.1995**

Kulpecz, A.A., Miller, K.G., Browning, J.V., Edwards, L.E., Powars, D.S., McLaughlin, P.P., Jr., Harris, A.D., Feigenson, M.D., Gohn, G.S., Koeberl, C., Miller, K.G., and Reimold, W.U., 2009. Postimpact deposition in the Chesapeake Bay impact structure: variations in eustasy, compaction, sediment supply, and passive-aggressive tectonism. In Gohn, G.S., Koeberl, C., Miller, K.G., and Reimold, W.U. (Eds.), The ICDP-USGS Deep Drilling Project in the Chesapeake Bay impact structure: Results from the Eyreville Core Holes. 458: (Special Paper - Geological Society of America). **https://doi.org/10.1130/2009.2458(34)**

Laberg, J.S., Andreassen, K., Knies, J., Vorren, T.O., and Winsborrow, M., 2010. Late Pliocene–Pleistocene development of the Barents Sea Ice Sheet. Geology, 38(2):107–110. **https://doi.org/10.1130/G30193.1**

Laberg, J.S., Andreassen, K., and Vorren, T.O., 2012. Late Cenozoic erosion of the high-latitude southwestern Barents Sea shelf revisited. Geological Society of America Bulletin, 124(1–2):77–88. **https://doi.org/10.1130/B30340.1**

Laberg, J.S., Stoker, M.S., Dahlgren, K.I.T., Haas, H.d., Haflidason, H., Hjelstuen, B.O., Nielsen, T., Shannon, P.M., Vorren, T.O., van Weering, T.C.E., and Ceramicola, S., 2005. Cenozoic alongslope processes and sedimentation on the NW European Atlantic margin. Marine and Petroleum Geology, 22(9–10):1069–1088. **https://doi.org/10.1016/j.marpetgeo.2005.01.008**

Laberg, J.S., and Vorren, T.O., 2004. Weichselian and Holocene growth of the northern high-latitude Lofoten Contourite Drift on the continental slope of Norway. Sedimentary Geology, 164(1):1–17. **https://doi.org/10.1016/j.sedgeo.2003.07.004**

Langehaug, H.R., and Falck, E., 2012. Changes in the properties and distribution of the intermediate and deep waters in the Fram Strait. Progress in Oceanography, 96(1):57–76. **https://doi.org/10.1016/j.pocean.2011.10.002**

Larsen, H.C., Saunders, A.D., Clift, P.D., Beget, J., Wei, W., and Spezzaferri, S., 1994. Seven million years of glaciation in Greenland. Science, 264(5161):952–955. **https://doi.org/10.1126/science.264.5161.952**

Lasabuda, A.P.E., Johansen, N.S., Laberg, J.S., Faleide, J.I., Senger, K., Rydningen, T.A., Patton, H., Knutsen, S.-M., and Hanssen, A., 2021. Cenozoic uplift and erosion of the Norwegian Barents Shelf – a review. Earth-Science Reviews, 217:103609. **https://doi.org/10.1016/j.earscirev.2021.103609**

Lenton, T.M., Rockström, J., Gaffney, O., Rahmstorf, S., Richardson, K., Steffen, W., and Schellnhuber H.J., 2019. Climate tipping points — too risky to bet against. Nature, 575:592–595. **https://doi.org/10.1038/d41586-019-03595-0**

Levy, R.H., Meyers, S.R., Naish, T.R., Golledge, N.R., McKay, R.M., Crampton, J.S., DeConto, R.M., De Santis, L., Florindo, F., Gasson, E.G.W., Harwood, D.M., Luyendyk, B.P., Powell, R.D., Clowes, C., and Kulhanek, D.K., 2019. Antarctic ice-sheet sensitivity to obliquity forcing enhanced through ocean connections. Nature Geoscience, 12(2):132–137. **https://doi.org/10.1038/s41561-018-0284-4**

Lisiecki, L.E., and Raymo, M.E., 2005. A Pliocene-Pleistocene stack of 57 globally distributed benthic $\delta^{18}O$ records. Paleoceanography, 20(1):PA1003. **https://doi.org/10.1029/2004PA001071**

Lucchi, R., Kovacevic, V., Aliani, S., Caburlotto, A., Celussi, M., Corgnati, L., Cosoli, S., Ersdal, E.A., Fredriksson, S., Goszczko, I., Husum, K., G, I., Laberg, J., Łącka, M., Langone, L., P, M., K, M., Morigi, C., Realdon, G., and Tirelli, V., 2014. Prepared present and past flow regime. On contourite drifts west of Spitsbergen. EUROFLEETS-2 Cruise Summary Report R/V G.O. Sars, Cruise No. 191. **https://doi.org/10.13140/2.1.1975.3769**

Lucchi, R.G., Camerlenghi, A., Rebesco, M., Colmenero-Hidalgo, E., Sierro, F.J., Sagnotti, L., Urgeles, R., Melis, R., Morigi, C., Bárcena, M.A., Giorgetti, G., Villa, G., Persico, D., Flores, J.A., Rigual-Hernández, A.S., Pedrosa, M.T., Macri, P., and Caburlotto, A., 2013. Postglacial sedimentary processes on the Storfjorden and Kveithola trough mouth fans: significance of extreme glacimarine sedimentation. Global and Planetary Change, 111:309–326. **https://doi.org/10.1016/j.gloplacha.2013.10.008**

Lucchi, R.G., Morigi, C., Sverre Laberg, J., Husum, K., Gamboa Sojo, V., Musco, M.E., Caricchi, C., Caffau, M., Sagnotti, L., Macrì, P., Princivalle, F., Giorgetti, G., Caburlotto, A., and Rebesco, M., 2018. The climatic significance of laminated sediments from turbid meltwaters on the NW Barents Sea continental margin (Arctic). Geophysical Research Abstracts, 20:EGU2018-3115. **https://doi.org/10.1007/s41063-015-0008-6**

Lucchi, R.G., Rebesco, M., Camerlenghi, A., Busetti, M., Tomadin, L., Villa, G., Persico, D., Morigi, C., Bonci, M.C., and Giorgetti, G., 2002. Mid-Late Pleistocene glacimarine sedimentary processes of a high-latitude, deep-sea sediment drift (Antarctic Peninsula Pacific margin). Marine Geology, 189(3–4):343–370. **https://doi.org/10.1016/S0025-3227(02)00470-X**

Lucchi, R.G., Sagnotti, L., Camerlenghi, A., Macrì, P., Rebesco, M., Pedrosa, M.T., and Giorgetti, G., 2015. Marine sedimentary record of Meltwater Pulse 1a along the NW Barents Sea continental margin. arktos, 1(1):7. **https://doi.org/10.1007/s41063-015-0008-6**

Lunt, D.J., Valdes, P.J., Haywood, A., and Rutt, I.C., 2008. Closure of the Panama Seaway during the Pliocene: implications for climate and Northern Hemisphere glaciation. Climate Dynamics, 30(1):1–18. **https://doi.org/10.1007/s00382-007-0265-6**

Mahajan, S., Zhang, R., and Delworth, T.L., 2011. Impact of the Atlantic Meridional Overturning Circulation (AMOC) on Arctic surface air temperature and sea ice variability. Journal of Climate, 24(24):6573–6581. **https://doi.org/10.1175/2011JCLI4002.1**

Marnela, M., Rudels, B., Houssais, M.N., Beszczynska-Möller, A., and Eriksson, P.B., 2013. Recirculation in the Fram Strait and transports of water in and north of the Fram Strait derived from CTD data. Ocean Sci., 9(3):499–519. **https://doi.org/10.5194/os-9-499-2013**

Mattingsdal, R., Knies, J., Andreassen, K., Fabian, K., Husum, K., Grøsfjeld, K., and De Schepper, S., 2014. A new 6 Myr stratigraphic framework for the Atlantic–Arctic gateway. Quaternary Science Reviews, 92:170–178. **https://doi.org/10.1016/j.quascirev.2013.08.022**

McClymont, E.L., Ford, H.L., Ho, S.L., Tindall, J.C., Haywood, A.M., Alonso-Garcia, M., Bailey, I., Berke, M.A., Littler, K., Patterson, M.O., Petrick, B., Peterse, F., Ravelo, A.C., Risebrobakken, B., De Schepper, S., Swann, G.E.A., Thirumalai, K., Tierney, J.E., van der Weijst, C., White, S., Abe-Ouchi, A., Baatsen, M.L.J., Brady, E.C., Chan, W.L., Chandan, D., Feng, R., Guo, C., von der Heydt, A.S., Hunter, S., Li, X., Lohmann, G., Nisancioglu, K.H., Otto-Bliesner, B.L., Peltier, W.R., Stepanek, C., and Zhang, Z., 2020. Lessons from a high-CO_2 world: an ocean view from ~3 million years ago. Climate of the Past, 16(4):1599–1615. **https://doi.org/10.5194/cp-16-1599-2020**

Mejía, L.M., Méndez-Vicente, A., Abrevaya, L., Lawrence, K.T., Ladlow, C., Bolton, C., Cacho, I., and Stoll, H., 2017. A diatom record of CO_2 decline since the Late Miocene. Earth and Planetary Science Letters, 479:18–33. **https://doi.org/10.1016/j.epsl.2017.08.034**

Melis, R., Carbonara, K., Villa, G., Morigi, C., Bárcena, M.A., Giorgetti, G., Caburlotto, A., Rebesco, M., and Lucchi, R.G., 2018. A new multi-proxy investigation of Late Quaternary palaeoenvironments along the north-western Barents Sea (Storfjorden Trough Mouth Fan). Journal of Quaternary Science, 33(6):662–676. **https://doi.org/10.1002/jqs.3043**

Miller, K.G., Kominz, M.A., Browning, J.V., Wright, J.D., Mountain, G.S., Katz, M.E., Sugarman, P.J., Cramer, B.S., Christie-Blick, N., and Pekar, S.F., 2005. The Phanerozoic record of global sea-level change. Science, 310(5752):1293–1298. **https://doi.org/10.1126/science.1116412**

Miller, K.G., Schmelz, W.J., Browning, J.V., Kopp, R.E., Mountain, G.S., and Wright, J.D., 2020. Ancient sea level as key to the future. Oceanography, 33(2):32–41. **https://doi.org/10.5670/oceanog.2020.224**

Miller, K.G., Wright, J.D., Browning, J.V., Kulpecz, A., Kominz, M., Naish, T.R., Cramer, B.S., Rosenthal, Y., Peltier, W.R., and Sosdian, S., 2012. High tide of the warm Pliocene: implications of global sea level for Antarctic deglaciation. Geology, 40(5):407–410. **https://doi.org/10.1130/G32869.1**

Miller, K.G., Wright, J.D., and Fairbanks, R.G., 1991. Unlocking the Ice House: Oligocene-Miocene oxygen isotopes, eustasy, and margin erosion. Journal of Geophysical Research: Solid Earth, 96(B4):6829–6848. **https://doi.org/10.1029/90JB02015**

Minakov, A., 2018. Late Cenozoic lithosphere dynamics in Svalbard: interplay of glaciation, seafloor spreading and mantle convection. Journal of Geodynamics, 122:1–16. **https://doi.org/10.1016/j.jog.2018.09.009**

Montes, C., Cardona, A., Jaramillo, C., Pardo, A., Silva, J.C., Valencia, V., Ayala, C., Pérez-Angel, L.C., Rodriguez-Parra, L.A., Ramirez, V., and Niño, H., 2015. Middle Miocene closure of the Central American Seaway. Science, 348(6231):226–229. **https://doi.org/10.1126/science.aaa2815**

Morono, Y., Ito, M., Hoshino, T., Terada, T., Hori, T., Ikehara, M., D'Hondt, S., and Inagaki, F., 2020. Aerobic microbial life persists in oxic marine sediment as old as 101.5 million years. Nature Communications, 11(1):3626. **https://doi.org/10.1038/s41467-020-17330-1**

Müller, J., and Stein, R., 2014. High-resolution record of late glacial and deglacial sea ice changes in Fram Strait corroborates ice–ocean interactions during abrupt climate shifts. Earth and Planetary Science Letters, 403:446–455. **https://doi.org/10.1016/j.epsl.2014.07.016**

Myhre, A.M., Eldholm, O., and Sundvor, E., 1982. The margin between Senja and Spitsbergen fracture zones: implications from plate tectonics. Tectonophysics, 89(1–3):33–50. **https://doi.org/10.1016/0040-1951(82)90033-6**

Naish, T.R., and Wilson, G.S., 2009. Constraints on the amplitude of Mid-Pliocene (3.6–2.4 Ma) eustatic sea-level fluctuations from the New Zealand shallow-marine sediment record. Philosophical Transactions of the Royal Society, A: Mathematical, Physical and Engineering Sciences, 367(1886):169–187. **https://doi.org/10.1098/rsta.2008.0223**

Nilsen, F., Skogseth, R., Vaardal-Lunde, J., and Inall, M., 2016. A simple shelf circulation model: intrusion of Atlantic Water on the West Spitsbergen shelf. Journal of Physical Oceanography, 46(4):1209–1230. **https://doi.org/10.1175/JPO-D-15-0058.1**

North Greenland Ice Core Project Members, 2004. High-resolution record of Northern Hemisphere climate extending into the last interglacial period. Nature, 431(7005):147–151. **https://doi.org/10.1038/nature02805**

Norwegian Polar Institute, 2022. Temperature and salinity in the Fram Strait. MOSJ (Environmental Monitoring of Svalbard and Jan Mayen). **https://mosj.no/en/indikator/climate/ocean/temperature-and-salinity-in-the-fram-strait/**

Not, C., and Hillaire-Marcel, C., 2012. Enhanced sea-ice export from the Arctic during the Younger Dryas. Nature Communications, 3(1):647. **https://doi.org/10.1038/ncomms1658**

Nyman, K.H.M., and Ditlevsen, P.D., 2019. The middle Pleistocene transition by frequency locking and slow ramping of internal period. Climate Dynamics, 53(5):3023–3038. **https://doi.org/10.1007/s00382-019-04679-3**

O'Dea, A., Lessios, H.A., Coates, A.G., Eytan, R.I., Restrepo-Moreno, S.A., Cione, A.L., Collins, L.S., de Queiroz, A., Farris, D.W., Norris, R.D., Stallard, R.F., Woodburne, M.O., Aguilera, O., Aubry, M.-P., Berggren, W.A., Budd, A.F., Cozzuol, M.A., Coppard, S.E., Duque-Caro, H., Finnegan, S., Gasparini, G.M., Grossman, E.L., Johnson, K.G., Keigwin, L.D., Knowlton, N., Leigh, E.G., Leonard-Pingel, J.S., Marko, P.B., Pyenson, N.D., Rachello-Dolmen, P.G., Soibelzon, E., Soibelzon, L., Todd, J.A., Vermeij, G.J., and Jackson, J.B.C., 2016. Formation of the Isthmus of Panama. Science Advances, 2(8):e1600883. **https://doi.org/10.1126/sciadv.1600883**

Orsi, W.D., 2018. Ecology and evolution of seafloor and subseafloor microbial communities. Nature Reviews Microbiology, 16(11):671–683. **https://doi.org/10.1038/s41579-018-0046-8**

Orsi, W.D., Coolen, M.J.L., Wuchter, C., He, L., More, K.D., Irigoien, X., Chust, G., Johnson, C., Hemingway, J.D., Lee, M., Galy, V., and Giosan, L., 2017. Climate oscillations reflected within the microbiome of Arabian Sea sediments. Scientific Reports, 7(1):6040. **https://doi.org/10.1038/s41598-017-05590-9**

Overland, J.E., Wood, K.R., and Wang, M., 2011. Warm Arctic - cold continents: climate impacts of the newly open Arctic Sea. Polar Research. **https://doi.org/10.3402/polar.v30i0.15787**

Pagani, M., Huber, M., Liu, Z., Bohaty, S.M., Henderiks, J., Sijp, W., Krishnan, S., and DeConto, R.M., 2011. The role of carbon dioxide during the onset of Antarctic glaciation. Science, 334(6060):1261–1264. **https://doi.org/10.1126/science.1203909**

Pagani, M., Liu, Z., LaRiviere, J., and Ravelo, A.C., 2010. High Earth-system climate sensitivity determined from Pliocene carbon dioxide concentrations. Nature Geoscience, 3(1):27–30. **https://doi.org/10.1038/ngeo724**

Pagani, M., Zachos, J.C., Freeman, K.H., Tipple, B., and Bohaty, S., 2005. Marked decline in atmospheric carbon dioxide concentrations during the Paleogene. Science, 309(5734):600–603. **https://doi.org/10.1126/science.1110063**

Petersen, C.J., Bünz, S., Hustoft, S., Mienert, J., and Klaeschen, D., 2010. High-resolution P-Cable 3D seismic imaging of gas chimney structures in gas hydrated sediments of an Arctic sediment drift. Marine and Petroleum Geology, 27(9):1981–1994. **https://doi.org/10.1016/j.marpetgeo.2010.06.006**

Petrini, M., Colleoni, F., Kirchner, N., Hughes, A.L.C., Camerlenghi, A., Rebesco, M., Lucchi, R.G., Forte, E., Colucci, R.R., and Noormets, R., 2018. Interplay of grounding-line dynamics and sub-shelf melting during retreat of the Bjørnøyrenna Ice Stream. Scientific Reports, 8(1):7196. **https://doi.org/10.1038/s41598-018-25664-6**

Petrini, M., Colleoni, F., Kirchner, N., Hughes, A.L.C., Camerlenghi, A., Rebesco, M., Lucchi, R.G., Forte, E., Colucci, R.R., Noormets, R., and Mangerud, J., 2020. Simulated last deglaciation of the Barents Sea Ice Sheet primarily driven by oceanic conditions. Quaternary Science Reviews, 238:106314. **https://doi.org/10.1016/j.quascirev.2020.106314**

Pisias, N.G., and Moore, T.C., 1981. The evolution of Pleistocene climate: a time series approach. Earth and Planetary Science Letters, 52(2):450–458. **https://doi.org/10.1016/0012-821X(81)90197-7**

Planke, S., Berndt, C., Alvarez Zarikian, C.A., and the Expedition 396 Scientists, 2022. Expedition 396 Preliminary Report: Mid-Norwegian Margin Magmatism and Paleoclimate Implications. International Ocean Discovery Program. **https://doi.org/10.14379/iodp.pr.396.2022**

Poirier, A., and Hillaire-Marcel, C., 2011. Improved Os-isotope stratigraphy of the Arctic Ocean. Geophysical Research Letters, 38(14):L14607. **https://doi.org/10.1029/2011GL047953**

Quadfasel, D., Rudels, B., and Kurz, K., 1988. Outflow of dense water from a Svalbard fjord into the Fram Strait. Deep Sea Research, Part A. Oceanographic Research Papers, 35(7):1143–1150. **https://doi.org/10.1016/0198-0149(88)90006-4**

Quadfasel, D., Rudels, B., and Selchow, S., 1992. The Central Bank vortex in the Barents Sea: water mass transformation and circulation. ICES Marine Science Symposia, 195:40–51.

Rahmstorf, S., Box, J.E., Feulner, G., Mann, M.E., Robinson, A., Rutherford, S., and Schaffernicht, E.J., 2015. Exceptional twentieth-century slowdown in Atlantic Ocean overturning circulation. Nature Climate Change, 5(5):475–480. **https://doi.org/10.1038/nclimate2554**

Rantanen, M., Karpechko, A.Y., Lipponen, A., Nordling, K., Hyvärinen, O., Ruosteenoja, K., Vihma, T., and Laaksonen, A., 2022. The Arctic has warmed nearly four times faster than the globe since 1979. Communications Earth & Environment, 3(1):168. **https://doi.org/10.1038/s43247-022-00498-3**

Rasmussen, T.L., Thomsen, E., and Nielsen, T., 2014. Water mass exchange between the Nordic seas and the Arctic Ocean on millennial timescale during MIS 4–MIS 2. Geochemistry, Geophysics, Geosystems, 15(3):530–544. **https://doi.org/10.1002/2013GC005020**

Rasmussen, T.L., Thomsen, E., Ślubowska, M.A., Jessen, S., Solheim, A., and Koç, N., 2007. Paleoceanographic evolution of the SW Svalbard margin (76°N) since 20,000 14C yr BP. Quaternary Research, 67(1):100–114. **https://doi.org/10.1016/j.yqres.2006.07.002**

Raymo, M.E., and Nisancioglu, K.H., 2003. The 41 kyr world: Milankovitch's other unsolved mystery. Paleoceanography, 18(1):1011. **https://doi.org/10.1029/2002PA000791**

Rebesco, M., Hernández-Molina, F.J., Van Rooij, D., and Wåhlin, A., 2014a. Contourites and associated sediments controlled by deep-water circulation processes: state-of-the-art and future considerations. Marine Geology, 352:111–154. **https://doi.org/10.1016/j.margeo.2014.03.011**

Rebesco, M., Laberg, J.S., Pedrosa, M.T., Camerlenghi, A., Lucchi, R.G., Zgur, F., and Wardell, N., 2014b. Onset and growth of Trough-Mouth Fans on the North-Western Barents Sea margin – implications for the evolution of the Barents Sea/Svalbard Ice Sheet. Quaternary Science Reviews, 92:227–234. **https://doi.org/10.1016/j.quascirev.2013.08.015**

Rebesco, M., Wåhlin, A., Laberg, J.S., Schauer, U., Beszczynska-Möller, A., Lucchi, R.G., Noormets, R., Accettella, D., Zarayskaya, Y., and Diviacco, P., 2013. Quaternary contourite drifts of the Western Spitsbergen margin. Deep Sea Research, Part I: Oceanographic Research Papers, 79:156–168. **https://doi.org/10.1016/j.dsr.2013.05.013**

Rial, J.A., Oh, J., and Reischmann, E., 2013. Synchronization of the climate system to eccentricity forcing and the 100,000-year problem. Nature Geoscience, 6(4):289–293. **https://doi.org/10.1038/ngeo1756**

Rigual-Hernández, A.S., Colmenero-Hidalgo, E., Martrat, B., Bárcena, M.A., de Vernal, A., Sierro, F.J., Flores, J.A., Grimalt, J.O., Henry, M., and Lucchi, R.G., 2017. Svalbard ice-sheet decay after the Last Glacial Maximum: new insights from micropalaeontological and organic biomarker paleoceanographical reconstructions. Palaeogeography, Palaeoclimatology, Palaeoecology, 465:225–236. **https://doi.org/10.1016/j.palaeo.2016.10.034**

Rohling, E.J., Grant, K., Bolshaw, M., Roberts, A.P., Siddall, M., Hemleben, C., and Kucera, M., 2009. Antarctic temperature and global sea level closely coupled over the past five glacial cycles. Nature Geoscience, 2(7):500–504. **https://doi.org/10.1038/ngeo557**

Rørvik, K.L., Laberg, J.S., Hald, M., Ravna, E.K., and Vorren, T.O., 2010. Behavior of the northwestern part of the Fennoscandian Ice Sheet during the Last Glacial Maximum – a response to external forcing. Quaternary Science Reviews, 29(17):2224–2237. **https://doi.org/10.1016/j.quascirev.2010.05.022**

Røy, H., Kallmeyer, J., Adhikari, R.R., Pockalny, R., Jørgensen, B.B., and D'Hondt, S., 2012. Aerobic microbial respiration in 86-million-year-old deep-sea red clay. Science, 336(6083):922–925. **https://doi.org/10.1126/science.1219424**

Rudels, B., Meyer, R., Fahrbach, E., Ivanov, V.V., Østerhus, S., Quadfasel, D., Schauer, U., Tverberg, V., and Woodgate, R.A., 2000. Water mass distribution in Fram Strait and over the Yermak Plateau in summer 1997. Annales Geophysicae, 18(6):687–705. **https://angeo.copernicus.org/articles/18/687/2000/**

Saloranta, T.M., and Haugan, P.M., 2004. Northward cooling and freshening of the warm core of the West Spitsbergen Current. Polar Research, 23(1):79–88. **https://doi.org/10.3402/polar.v23i1.6268**

Schauer, U., 1995. The release of brine-enriched shelf water from Storfjord into the Norwegian Sea. Journal of Geophysical Research: Oceans, 100(C8):16015–16028. **https://doi.org/10.1029/95JC01184**

Schauer, U., Fahrbach, E., Osterhus, S., and Rohardt, G., 2004. Arctic warming through the Fram Strait: Oceanic heat transport from 3 years of measurements. Journal of Geophysical Research: Oceans, 109(C6):C06026. **https://doi.org/10.1029/2003JC001823**

Schmidt, D., 2007. The closure history of the Panama Isthmus: evidence from isotopes and fossils to models and molecules. In Williams, M., Haywood, A.M., Gregory, F.J., and Schmidt, D.N. (Eds.) Deep-Time Perspectives on Climate Change: Marrying the Signal from Computer Models and Biological Proxies. Special Publication - Geological Society of London: 429–444.

Seki, O., Foster, G.L., Schmidt, D.N., Mackensen, A., Kawamura, K., and Pancost, R.D., 2010. Alkenone and boron-based Pliocene pCO_2 records. Earth and Planetary Science Letters, 292(1–2):201–211. **https://doi.org/10.1016/j.epsl.2010.01.037**

Shackleton, C.S., Winsborrow, M.C.M., Andreassen, K., Lucchi, R.G., and Bjarnadóttir, L.R., 2020. Ice-margin retreat and grounding-zone dynamics during initial deglaciation of the Storfjordrenna Ice Stream, western Barents Sea. Boreas, 49(1):38–51. **https://doi.org/10.1111/bor.12420**

Shackleton, N.J., 2000. The 100,000-year ice-age cycle identified and found to lag temperature, carbon dioxide, and orbital eccentricity. Science, 289(5486):1897–1902. **https://doi.org/10.1126/science.289.5486.1897**

Singhroha, S., Chand, S., and Bünz, S., 2019. Constraints on gas hydrate distribution and morphology in Vestnesa Ridge, Western Svalbard margin, using multicomponent ocean-bottom seismic data. Journal of Geophysical Research: Solid Earth, 124(5):4343–4364. **https://doi.org/10.1029/2018JB016574**

Skogseth, R., Haugan, P.M., and Jakobsson, M., 2005. Watermass transformations in Storfjorden. Continental Shelf Research, 25(5–6):667–695. **https://doi.org/10.1016/j.csr.2004.10.005**

Ślubowska, M.A., Koç, N., Rasmussen, T.L., and Klitgaard-Kristensen, D., 2005. Changes in the flow of Atlantic water into the Arctic Ocean since the last deglaciation: evidence from the northern Svalbard continental margin, 80°N. Paleoceanography, 20(4):PA4014. **https://doi.org/10.1029/2005PA001141**

Ślubowska-Woldengen, M., Koç, N., Rasmussen, T.L., Klitgaard-Kristensen, D., Hald, M., and Jennings, A.E., 2008. Time-slice reconstructions of ocean circulation changes on the continental shelf in the Nordic and Barents Seas during the last 16,000 cal yr B.P. Quaternary Science Reviews, 27(15–16):1476–1492. **https://doi.org/10.1016/j.quascirev.2008.04.015**

Ślubowska-Woldengen, M., Rasmussen, T.L., Koç, N., Klitgaard-Kristensen, D., Nilsen, F., and Solheim, A., 2007. Advection of Atlantic Water to the western and northern Svalbard shelf since 17,500 calyr BP. Quaternary Science Reviews, 26(3–4):463–478. **https://doi.org/10.1016/j.quascirev.2006.09.009**

Solheim, A., Andersen, E.S., Elverhøi, A., and Fiedler, A., 1996. Late Cenozoic depositional history of the western Svalbard continental shelf, controlled by subsidence and climate. Global and Planetary Change, 12(1–4):135–148. **https://doi.org/10.1016/0921-8181(95)00016-X**

Sosdian, S., and Rosenthal, Y., 2009. Deep-sea temperature and ice volume changes across the Pliocene-Pleistocene climate transitions. Science, 325(5938):306–310. **https://doi.org/10.1126/science.1169938**

St. John, K., 2008. Cenozoic ice-rafting history of the central Arctic Ocean: terrigenous sands on the Lomonosov Ridge. Paleoceanography and Paleoclimatology, 23(1):PA1S05. **https://doi.org/10.1029/2007PA001483**

St. John, K.E.K., and Krissek, L.A., 2002. The Late Miocene to Pleistocene ice-rafting history of southeast Greenland. Boreas, 31(1):28–35. **https://doi.org/10.1111/j.1502-3885.2002.tb01053.x**

Stärz, M., Jokat, W., Knorr, G., and Lohmann, G., 2017. Threshold in North Atlantic-Arctic Ocean circulation controlled by the subsidence of the Greenland-Scotland Ridge. Nature Communications, 8(1):15681. **https://doi.org/10.1038/ncomms15681**

Stein, R., and Fahl, K., 2013. Biomarker proxy shows potential for studying the entire Quaternary Arctic sea ice history. Organic Geochemistry, 55:98–102. **https://doi.org/10.1016/j.orggeochem.2012.11.005**

Stein, R., Fahl, K., Schreck, M., Knorr, G., Niessen, F., Forwick, M., Gebhardt, C., Jensen, L., Kaminski, M., Kopf, A., Matthiessen, J., Jokat, W., and Lohmann, G., 2016. Evidence for ice-free summers in the late Miocene central Arctic Ocean. Nature Communications, 7(1):11148. **https://doi.org/10.1038/ncomms11148**

Stevenson, R., Poirier, A., Véron, A., Carignan, J., and Hillaire-Marcel, C., 2015. Late Eocene to present isotopic (Sr-Nd-Pb) and geochemical evolution of sediments from the Lomonosov Ridge, Arctic Ocean: implications for continental sources and linkage with the North Atlantic Ocean. Comptes Rendus Geoscience, 347(5–6):227–135. **https://doi.org/10.1016/j.crte.2015.02.008**

Stocker, T.F., and Johnsen, S.J., 2003. A minimum thermodynamic model for the bipolar seesaw. Paleoceanography and Paleoclimatology, 18(4):1087. **https://doi.org/10.1029/2003PA000920**

Super, J.R., Thomas, E., Pagani, M., Huber, M., O'Brien, C., and Hull, P.M., 2018. North Atlantic temperature and pCO_2 coupling in the early-middle Miocene. Geology, 46(6):519–522. **https://doi.org/10.1130/G40228.1**

Swift, J.H., and Koltermann, K.P., 1988. The origin of Norwegian Sea Deep Water. Journal of Geophysical Research: Oceans, 93(C4):3563–3569. **https://doi.org/10.1029/JC093iC04p03563**

Sztybor, K., and Rasmussen, T., 2017a. Late glacial and deglacial palaeoceanographic changes at Vestnesa Ridge, Fram Strait: methane seep versus non-seep environments. Palaeogeography, Palaeoclimatology, Palaeoecology, 476:77–89. **http://dx.doi.org/10.1016/j.palaeo.2017.04.001**

Sztybor, K., and Rasmussen, T.L., 2017b. Diagenetic disturbances of marine sedimentary records from methane-influenced environments in the Fram Strait as indications of variation in seep intensity during the last 35 000 years. Boreas, 46(2):212–228. **https://doi.org/10.1111/bor.12202**

Tan, N., Ramstein, G., Dumas, C., Contoux, C., Ladant, J.-B., Sepulchre, P., Zhang, Z., and De Schepper, S., 2017. Exploring the MIS M2 glaciation occurring during a warm and high atmospheric CO_2 Pliocene background climate. Earth and Planetary Science Letters, 472:266–276. **https://doi.org/10.1016/j.epsl.2017.04.050**

Teigen, S.H., Nilsen, F., and Gjevik, B., 2010. Barotropic instability in the West Spitsbergen Current. Journal of Geophysical Research: Oceans, 115(C7). **https://doi.org/10.1029/2009JC005996**

Tesi, T., Muschitiello, F., Mollenhauer, G., Miserocchi, S., Langone, L., Ceccarelli, C., Panieri, G., Chiggiato, J., Nogarotto, A., Hefter, J., Ingrosso, G., Giglio, F., Giordano, P., and Capotondi, L., 2021. Rapid Atlantification along the Fram Strait at the beginning of the 20th century. Science Advances, 7(48):eabj2946. **https://doi.org/10.1126/sciadv.abj2946**

Thiede, J., and Myhre, A.M., 1996. The paleoceanographic history of the North Atlantic-Arctic gateways: synthesis of the Leg 151 drilling results. In Thiede, J., Myhre, A.M., Firth, J.V., Johnson, G.L., and Ruddiman, W.F. (Eds.), Proceedings of the Ocean Drilling Program, Scientific Results. 151: College Station, TX (Ocean Drilling Program), 645–658. **https://doi.org/10.2973/odp.proc.sr.151.147.1996**

Thompson, B., Jakobsson, M., Nilsson, J., Nycander, J., and Döös, K., 2012. A model study of the first ventilated regime of the Arctic Ocean during the early Miocene. Polar Research, 31(0). **https://doi.org/10.3402/polar.v31i0.10859**

Torricella, F., Gamboa Sojo, V.M., Gariboldi, K., Douss, N., Musco, M.E., Caricchi, C., Lucchi, R.G., Carbonara, K., and Morigi, C., 2022. Multiproxy investigation of the last 2,000 years BP marine paleoenvironmental record along the western Spitsbergen margin. Arctic, Antarctic, and Alpine Research, 54(1):562–583. **https://doi.org/10.1080/15230430.2022.2123859**

Tripati, A., and Darby, D., 2018. Evidence for ephemeral middle Eocene to early Oligocene Greenland glacial ice and pan-Arctic sea ice. Nature Communications, 9(1):1038. **https://doi.org/10.1038/s41467-018-03180-5**

Tsubouchi, T., Bacon, S., Aksenov, Y., Naveira Garabato, A.C., Beszczynska-Möller, A., Hansen, E., de Steur, L., Curry, B., and Lee, C.M., 2018. The Arctic Ocean seasonal cycles of heat and freshwater fluxes: observation-based inverse estimates. Journal of Physical Oceanography, 48(9):2029–2055. **https://doi.org/10.1175/JPO-D-17-0239.1**

Turney, C.S.M., Fogwill, C.J., Golledge, N.R., McKay, N.P., van Sebille, E., Jones, R.T., Etheridge, D., Rubino, M., Thornton, D.P., Davies, S.M., Ramsey, C.B., Thomas, Z.A., Bird, M.I., Munksgaard, N.C., Kohno, M., Woodward, J., Winter, K., Weyrich, L.S., Rootes, C.M., Millman, H., Albert, P.G., Rivera, A., van Ommen, T., Curran, M., Moy, A., Rahmstorf, S., Kawamura, K., Hillenbrand, C.-D., Weber, M.E., Manning, C.J., Young, J., and Cooper, A., 2020. Early Last Interglacial ocean warming drove substantial ice mass loss from Antarctica. Proceedings of the National Academy of Sciences of the United States of America, 117(8):3996–4006. **https://doi.org/10.1073/pnas.1902469117**

Tzedakis, P.C., Raynaud, D., McManus, J.F., Berger, A., Brovkin, V., and Kiefer, T., 2009. Interglacial diversity. Nature Geoscience, 2(11):751–755. **https://doi.org/10.1038/ngeo660**

Vanneste, M., Berndt, C., Sverre Laberg, J., and Mienert, J., 2007. On the origin of large shelf embayments on glaciated margins—effects of lateral ice flux variations and glacio-dynamics west of Svalbard. Quaternary Science Reviews, 26(19):2406–2419. **https://doi.org/10.1016/j.quascirev.2007.05.005**

von Appen, W.-J., Schauer, U., Hattermann, T., and Beszczynska-Möller, A., 2016. Seasonal cycle of mesoscale instability of the West Spitsbergen Current. Journal of Physical Oceanography, 46(4):1231–1254. **https://doi.org/10.1175/JPO-D-15-0184.1**

Vorren, T.O., and Laberg, J.S., 1997. Trough mouth fans — palaeoclimate and ice-sheet monitors. Quaternary Science Reviews, 16(8):865–881. **https://doi.org/10.1016/S0277-3791(97)00003-6**

Waelbroeck, C., Labeyrie, L., Michel, E., Duplessy, J.C., McManus, J.F., Lambeck, K., Balbon, E., and Labracherie, M., 2002. Sea-level and deep water temperature changes derived from benthic foraminifera isotopic records. Quaternary Science Reviews, 21(1):295–305. **https://doi.org/10.1016/S0277-3791(01)00101-9**

Waghorn, K.A., Bünz, S., Plaza-Faverola, A., and Johnson, J.E., 2018. 3-D seismic investigation of a gas hydrate and fluid flow system on an active mid-ocean ridge; Svyatogor Ridge, Fram Strait. Geochemistry, Geophysics, Geosystems, 19(8):2325–2341. **https://doi.org/10.1029/2018GC007482**

Wardlaw, B.R., and Quinn, T.M., 1991. The record of Pliocene sea-level change at Enewetak Atoll. Quaternary Science Reviews, 10(2–3):247–258. **https://doi.org/10.1016/0277-3791(91)90023-N**

Weijer, W., Haine, W.N., Siddiqui, A.H., Cheng, W., Veneziani, M., and Kurtakoti, P., 2022. Interactions between the Arctic Mediterranean and the Atlantic Meridional Overturning Circulation: a review. Oceanography, 35(3–4):118–127. **https://doi.org/10.5670/oceanog.2022.130**

Westerhold, T., Marwan, N., Drury, A.J., Liebrand, D., Agnini, C., Anagnostou, E., Barnet, J.S.K., Bohaty, S.M., De Vleeschouwer, D., Florindo, F., Frederichs, T., Hodell, D.A., Holbourn, A.E., Kroon, D., Lauretano, V., Littler, K., Lourens, L.J., Lyle, M., Pälike, H., Röhl, U., Tian, J., Wilkens, R.H., Wilson, P.A., and Zachos, J.C., 2020. An astronomically dated record of Earth's climate and its predictability over the last 66 million years. Science, 369(6509):1383–1387. **https://doi.org/10.1126/science.aba6853**

Winnick, M.J., and Caves, J.K., 2015. Oxygen isotope mass-balance constraints on Pliocene sea level and East Antarctic Ice Sheet stability. Geology, 43(10):879–882. **https://doi.org/10.1130/G36999.1**

Wolf, T.C.W., and Thiede, J., 1991. History of terrigenous sedimentation during the past 10 m.y. in the North Atlantic (ODP Legs 104 and 105 and DSDP Leg 81). Marine Geology, 101(1–4):83–102. **https://doi.org/10.1016/0025-3227(91)90064-B**

Wolf-Welling, T.C.W., Thiede, J., Myhre, A.M., and Leg 151 Shipboard Scientific Party, 1995. Bulk sediment parameter and coarse fraction analysis: paleoceanographic implications of Fram Strait Sites 908 and 909, ODP Leg 151 (NAAG). Eos, Transactions of the American Geophysical Union, 76:166.

Wright, J.D., 1998. The role of the Greenland-Scotland ridge in Neogene climate changes. Oxford Monographs on Geology and Geophysics, 39:192–211.

Zachos, J., Pagani, M., Sloan, L., Thomas, E., and Billups, K., 2001. Trends, rhythms, and aberrations in global climate 65 Ma to Present. Science, 292(5517):686–693. **https://doi.org/10.1126/science.1059412**

Zachos, J.C., Dickens, G.R., and Zeebe, R.E., 2008. An early Cenozoic perspective on greenhouse warming and carbon-cycle dynamics. Nature, 451(7176):279–283. **https://doi.org/10.1038/nature06588**

Zhang, Z.S., Nisancioglu, K.H., Chandler, M.A., Haywood, A.M., Otto-Bliesner, B.L., Ramstein, G., Stepanek, C., Abe-Ouchi, A., Chan, W.L., Bragg, F.J., Contoux, C., Dolan, A.M., Hill, D.J., Jost, A., Kamae, Y., Lohmann, G., Lunt, D.J., Rosenbloom, N.A., Sohl, L.E., and Ueda, H., 2013. Mid-Pliocene Atlantic meridional overturning circulation not unlike modern. Climate of the Past, 9(4):1495–1504. **https://doi.org/10.5194/cp-9-1495-2013**

Zhao, R., Hannisdal, B., Mogollon, J.M., and Jørgensen, S.L., 2019. Nitrifier abundance and diversity peak at deep redox transition zones. Scientific Reports, 9(1):8633. **https://doi.org/10.1038/s41598-019-44585-6**

Zieba, K.J., Omosanya, K.d.O., and Knies, J., 2017. A flexural isostasy model for the Pleistocene evolution of the Barents Sea bathymetry. Norwegian Journal of Geology, 97(1):1–19. **http://dx.doi.org/10.17850/njg97-1-01**

Site summaries

Site BED-01A (Bellsund Drift)

Priority:	Primary
Position:	76.52160° N 12.73867° E
Water depth (m):	1646
Target drilling depth (mbsf):	347
Approved maximum penetration (mbsf):	397
Survey coverage (track map; seismic profile):	SV15-04.segy; SV15-06.segy
Objective(s):	Seismic reflector R4A (1.5 My), Quaternary climatic transitions, paleo SBSIS dynamic
Coring program:	Hole A: APC/HLAPC/XCB to 397 mbsf 4 APCT measurements Hole B: APC/HLAPC/XCB to 397 mbsf
Downhole measurements program:	n/a
Nature of rock anticipated:	Fine grained contourites and glaciomarine sediments

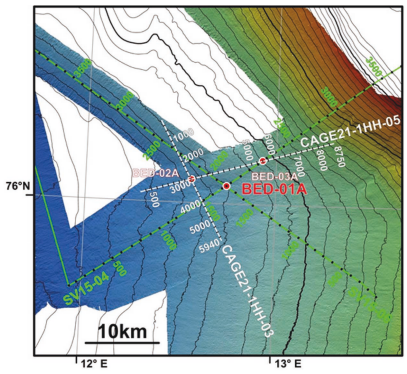

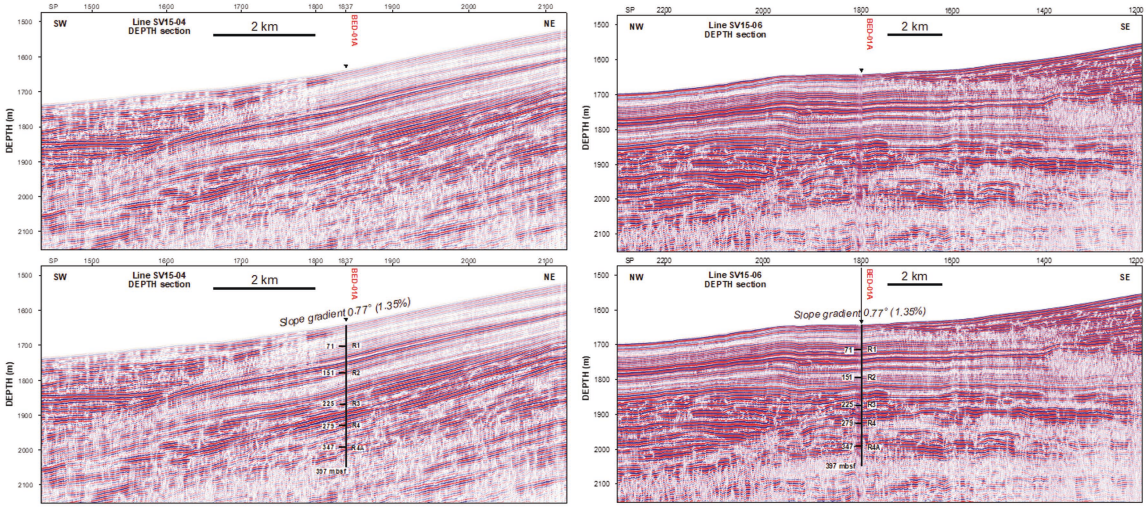

Figure AF1. Top: multibeam bathymetric map with location of primary Site BED-01A on Bellsund drift, west of Svalbard margin. Contour interval = 50 m (thick lines every 500 m). Bottom: Multichannel seismic (Left) Line SV15-04 and (Right) Cross-Line SV15-06 showing stratigraphic section (Top: clean; Bottom: interpreted). Ages of seismic reflectors: R1 = 0.2 Ma, R2 = 0.4 Ma, R3 = 0.75 Ma, R4 = 1.1 Ma, R4A = 1.3 Ma.

Site BED-02B (Bellsund Drift)

Priority:	Primary
Position:	76.457500°N 12.554722°E
Water depth (m):	1665
Target drilling depth (mbsf):	320
Approved maximum penetration (mbsf):	370
Survey coverage (track map; seismic profile):	CAGE21-1HH-05.segy; CAGE21-1HH-03.segy
Objective(s):	Seismic reflector R4A (1.5 My), Quaternary climatic transitions, paleo SBSIS dynamic
Coring program:	Hole A: APC/HLAPC/XCB to 370 mbsf - 4 APCT measurements Hole B: APC/HLAPC/XCB to 370 mbsf
Downhole measurements program:	Hole B: Wireline log with Triple Combo; FMS-sonic; VSI
Nature of rock anticipated:	Fine grained contourites and glaciomarine sediments

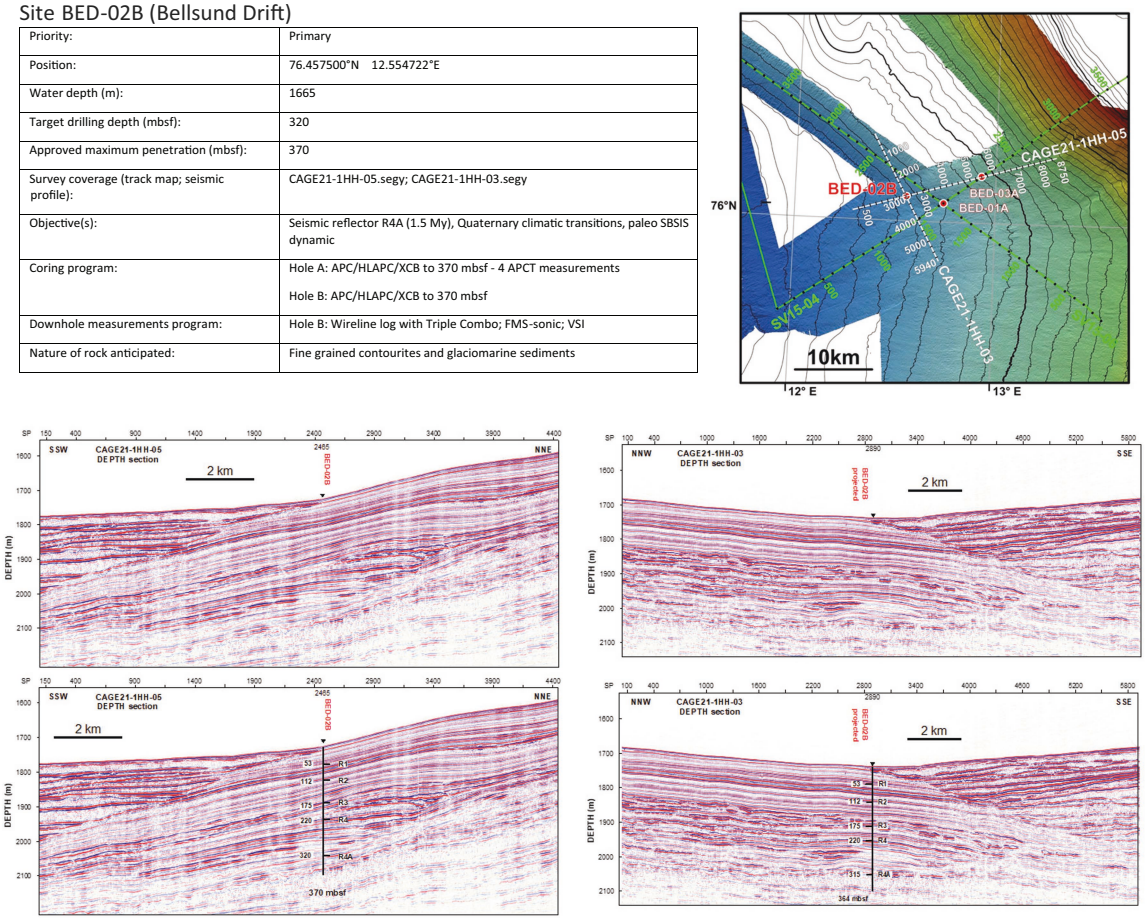

Figure AF2. Top: multibeam bathymetric map with location of primary Site BED-02B on Bellsund drift, west of Svalbard margin. Contour interval = 50 m (thick lines every 500 m). Bottom: Multichannel seismic (Left) In-Line CAGE21-1HH-05 and (Right) Cross-Line CAGE21-1HH-03 showing stratigraphic section (Top: clean; Bottom: interpreted). Ages of seismic reflectors: R1 = 0.2 Ma, R2 = 0.4 Ma, R3 = 0.75 Ma, R4 = 1.1 Ma, R4A = 1.3 Ma.

Site BED-03A (Bellsund Drift)

Priority:	Alternate
Position:	76.555122°N 12.930°E
Water depth (m):	1502
Target drilling depth (mbsf):	332
Approved maximum penetration (mbsf):	372
Survey coverage (track map; seismic profile):	SV15_04.segy; CAGE21-1HH-05.segy
Objective(s):	Seismic reflector R4A (1.5 My), Quaternary climatic transitions, paleo SBSIS dynamic
Coring program:	Hole A: APC/HLAPC/XCB to 372 mbsf - 4 APCT measurements Hole B: APC/HLAPC/XCB to 372 mbsf
Downhole measurements program:	Hole B: Wireline log with Triple Combo; FMS-sonic; VSI
Nature of rock anticipated:	Fine grained contourites and glaciomarine sediments

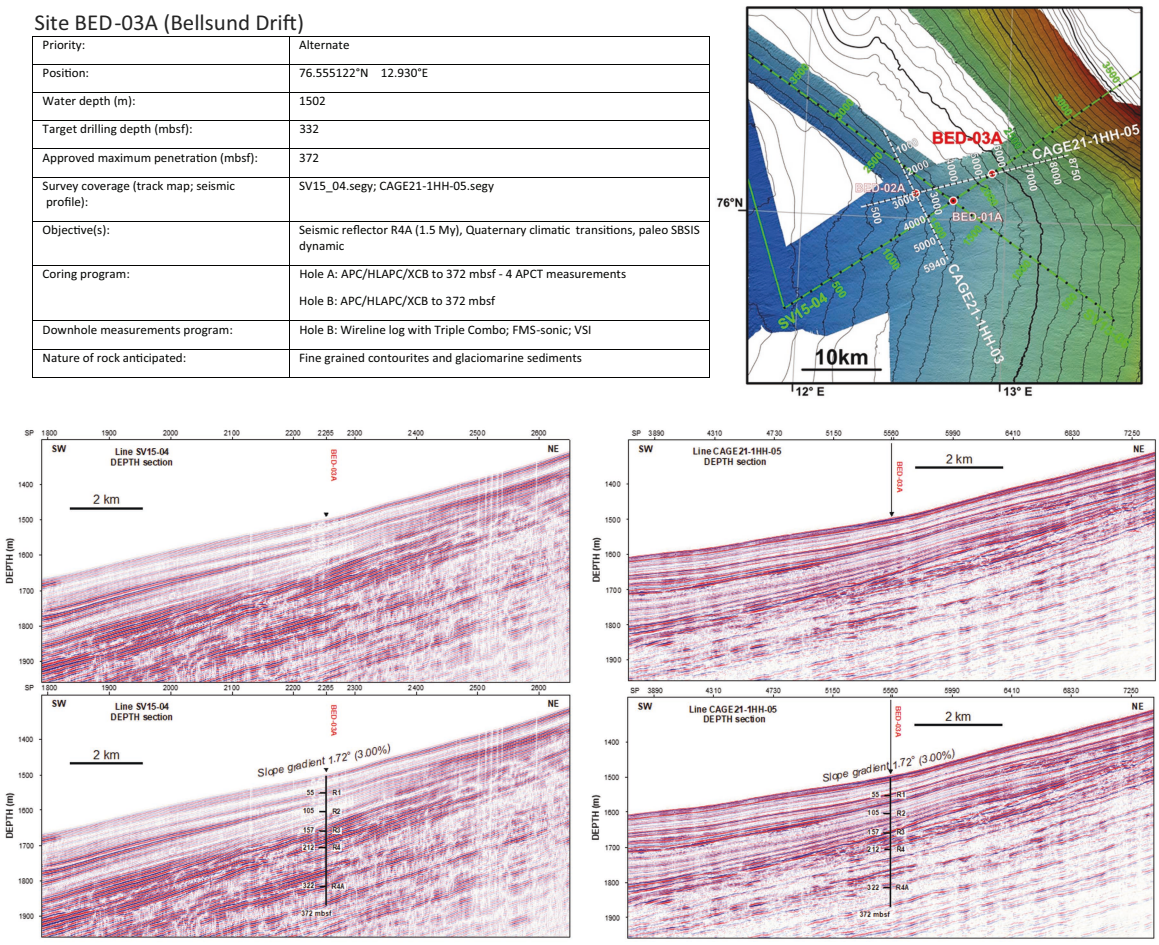

Figure AF3. Top: multibeam bathymetric map with location of alternate Site BED-03A on Bellsund drift, west of Svalbard margin. Contour interval = 50 m (thick lines every 500 m). Bottom: Multichannel seismic (Left) Line SV15-04 and (Right) Cross-Line CAGE21-1HH-05 showing stratigraphic section (Top: clean; Bottom: interpreted). Ages of seismic reflectors: R1 = 0.2 Ma, R2 = 0.4 Ma, R3 = 0.75 Ma, R4 = 1.1 Ma, R4A = 1.3 Ma.

Site ISD-01C (Isfjorden Drift)

Priority:	Primary
Position:	77.58771°N 10.09379°E
Water depth (m):	1330
Target drilling depth (mbsf):	208
Approved maximum penetration (mbsf):	258
Survey coverage (track map; seismic profile):	EG_01A.segy; CAGE21-5HH-13.segy
Objective(s):	Seismic reflector R4A (1.5 My), Quaternary climatic transitions, paleo SBSIS dynamic
Coring program:	Hole A: APC/HLAPC/XCB to 370 mbsf - 4 APCT measurements Hole B: APC/HLAPC/XCB to 370 mbsf Hole C: APC/HLAPC/XCB to 370 mbsf Hole D: APC/HLAPC/XCB to 370 mbsf
Downhole measurements program:	Hole D: Wireline log with Triple Combo; FMS-sonic; VSI
Nature of rock anticipated:	Fine grained contourites and glaciomarine sediments

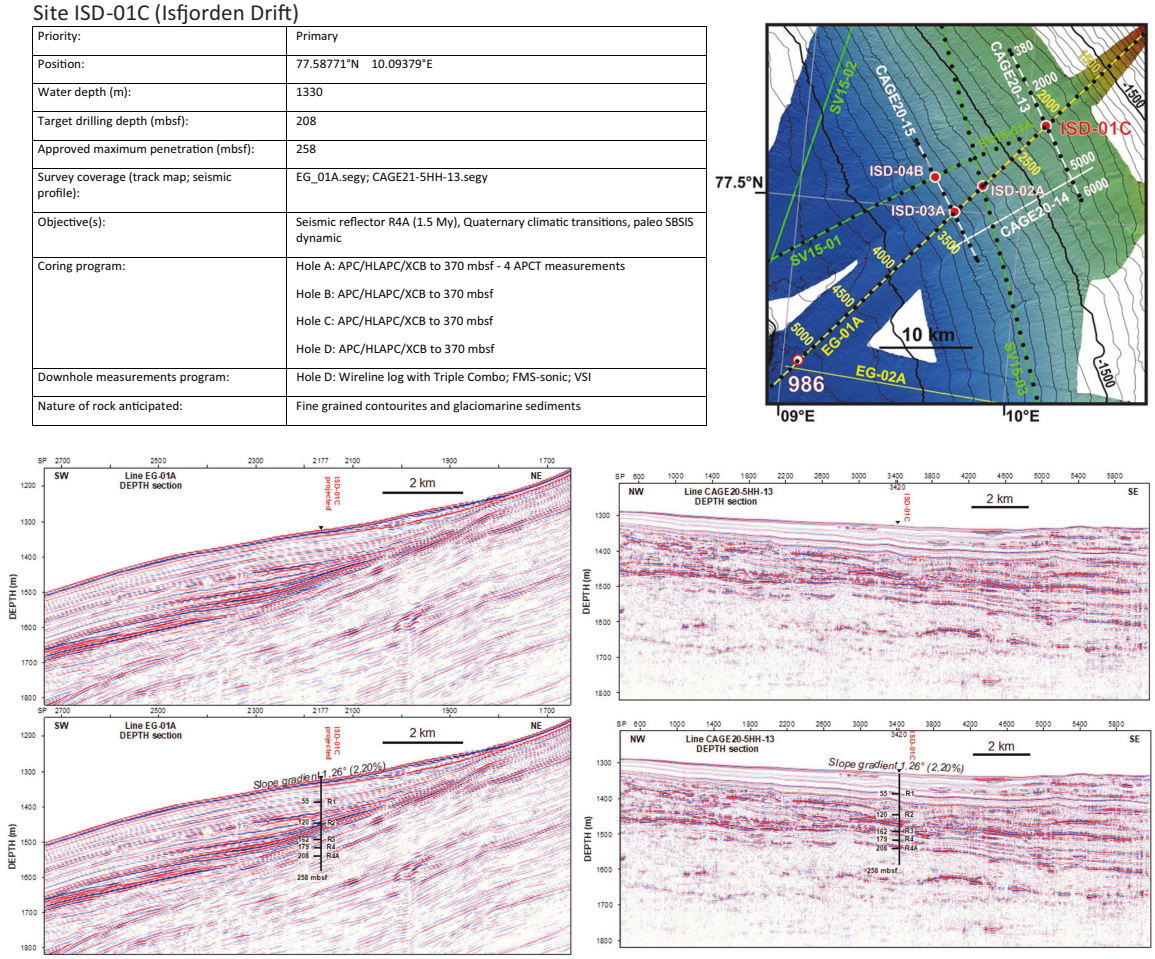

Figure AF4. Top: multibeam bathymetric map with location of primary Site ISD-01C on Isfjorden drift and crossing multichannel seismic (MCS) lines. Contour interval = 50 m (thick lines every 500 m). 986 = ODP Site 896. Bottom: MCS (Left) Cross-Line EG-01A and (Right) Cross-Line CAGE20-5HH-13 showing stratigraphic section (Top: clean; Bottom: interpreted). Ages of seismic reflectors: R1 = 0.2 Ma, R2 = 0.4 Ma, R3 = 0.75 Ma, R4 = 1.1 Ma, R4A = 1.3 Ma.

Site ISD-02A (Isfjorden Drift)

Priority:	Alternate
Position:	77.52639°N 9.82167°E
Water depth (m):	1587.3
Target drilling depth (mbsf):	331
Approved maximum penetration (mbsf):	381
Survey coverage (track map; seismic profile):	EG_01A.segy; SV15_03.segy
Objective(s):	Seismic reflector R4A (1.5 My), Quaternary climatic transitions, paleo SBSIS dynamic
Coring program:	Hole A: APC/HLAPC/XCB to 381 mbsf - 4 APCT measurements Hole B: APC/HLAPC/XCB to 381 mbsf Hole C: APC/HLAPC/XCB to 381 mbsf Hole D: APC/HLAPC/XCB to 381 mbsf
Downhole measurements program:	Hole D: Wireline log with Triple Combo; FMS-sonic; VSI
Nature of rock anticipated:	Fine grained contourites and glaciomarine sediments

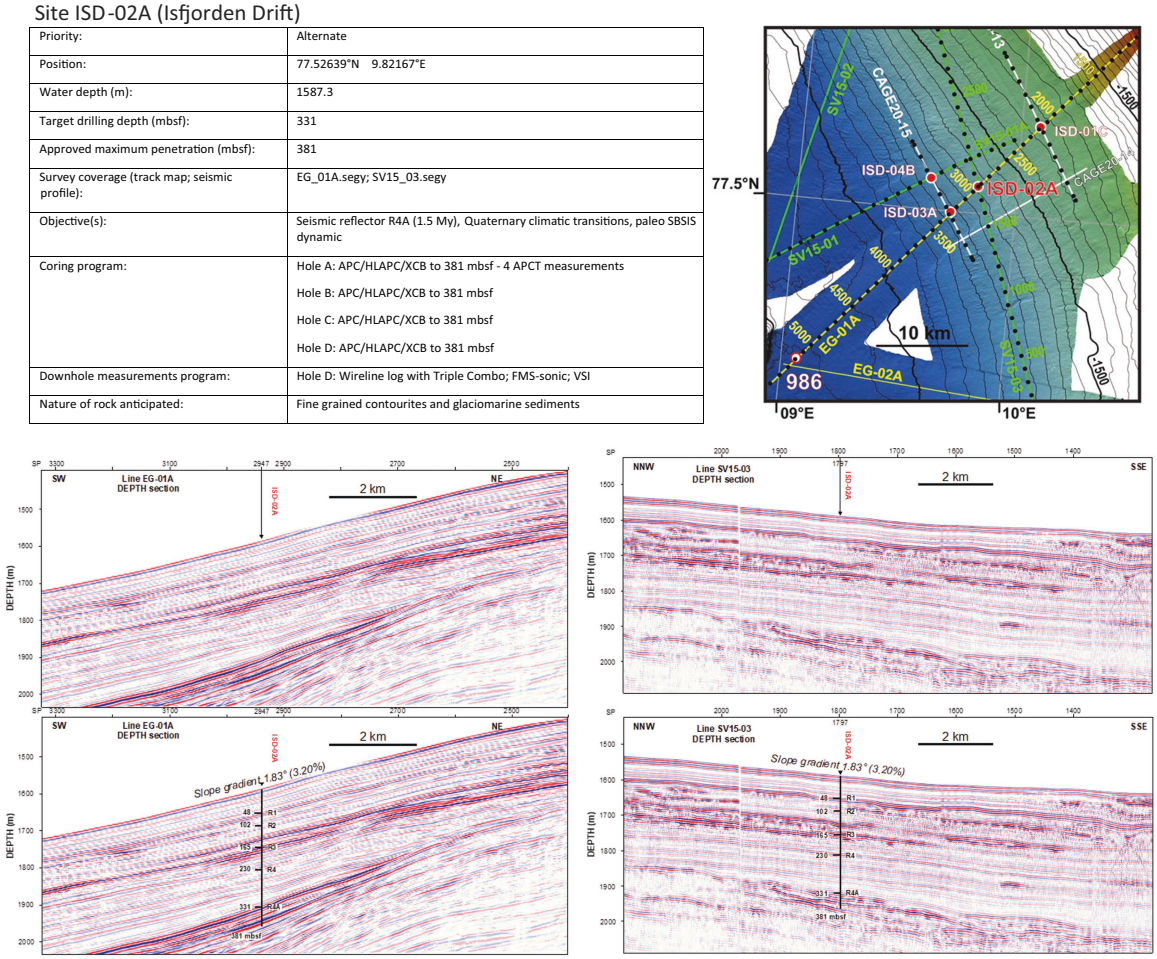

Figure AF5. Top: multibeam bathymetric map with location of alternate Site ISD-02A on Isfjorden drift and crossing multichannel seismic (MCS) lines. Contour interval = 50 m (thick lines every 500 m). 986 = ODP Site 896. Bottom: MCS (Left) Line EG-01A and (Right) Cross-Line SV15-03 showing stratigraphic section (Top: clean; Bottom: interpreted). Ages of seismic reflectors: R1 = 0.2 Ma, R2 = 0.4 Ma, R3 = 0.75 Ma, R4 = 1.1 Ma, R4A = 1.3 Ma.

Site ISD-03A (Isfjorden Drift)

Priority:	Alternate
Position:	77.49732°N 9.70293°E
Water depth (m):	1733.8
Target drilling depth (mbsf):	337
Approved maximum penetration (mbsf):	387
Survey coverage (track map; seismic profile):	EG_01A.segy; SV15_03.segy
Objective(s):	Seismic reflector R4A (1.5 My), Quaternary climatic transitions, paleo SBSIS dynamic
Coring program:	Hole A: APC/HLAPC/XCB to 387 mbsf - 4 APCT measurements Hole B: APC/HLAPC/XCB to 387 mbsf Hole C: APC/HLAPC/XCB to 387 mbsf Hole D: APC/HLAPC/XCB to 387 mbsf
Downhole measurements program:	Hole D: Wireline log with Triple Combo; FMS-sonic; VSI
Nature of rock anticipated:	Fine grained contourites and glaciomarine sediments

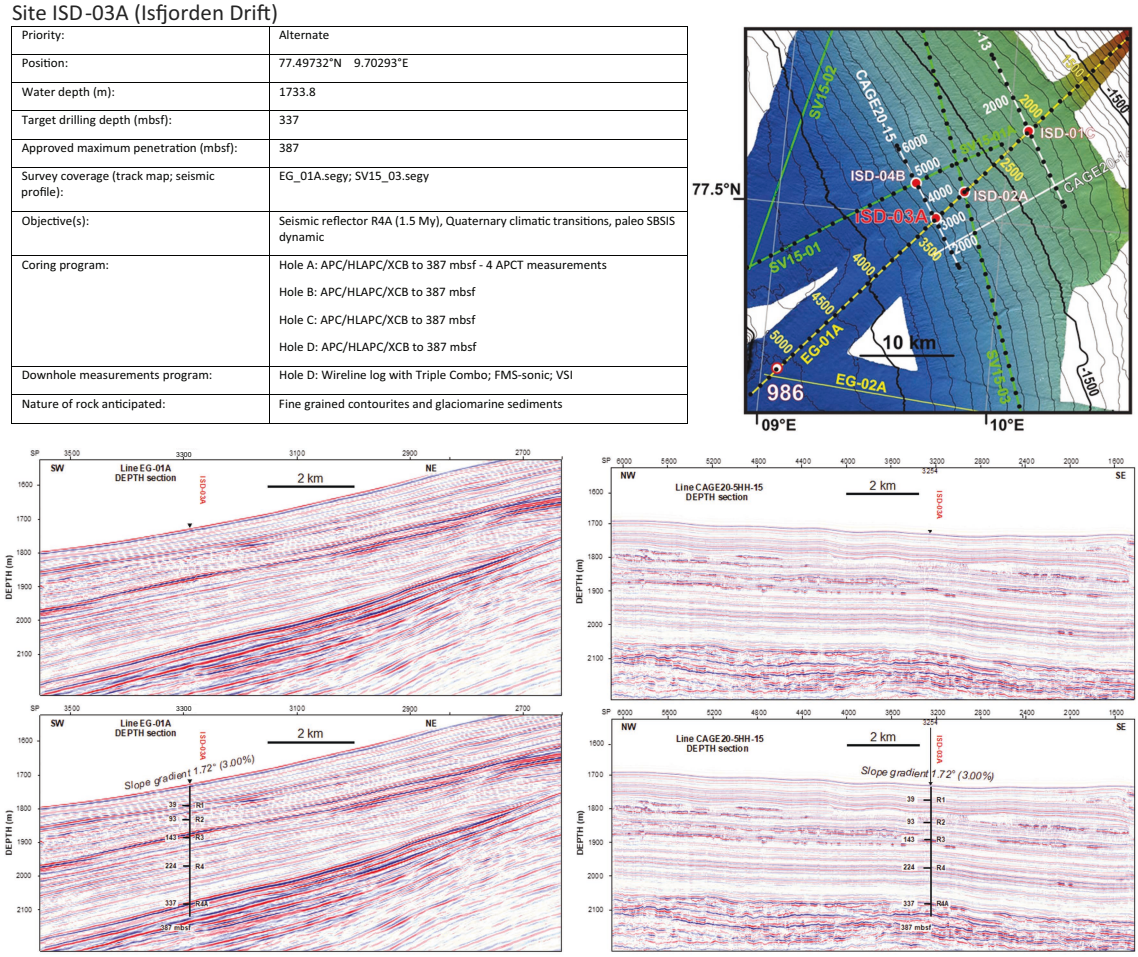

Figure AF6. Top: multibeam bathymetric map with location of alternate Site ISD-03A on Isfjorden drift and crossing multichannel seismic (MCS) lines. Contour interval = 50 m (thick lines every 500 m). 986 = ODP Site 896. Bottom: MCS (Left) Line EG-01A and (Right) Cross-Line CAGE20-5HH-15 showing stratigraphic section (Top: clean; Bottom: interpreted). Ages of seismic reflectors: R1 = 0.2 Ma, R2 = 0.4 Ma, R3 = 0.75 Ma, R4 = 1.1 Ma, R4A = 1.3 Ma.

Site ISD-04B (Isfjorden Drift)

Priority:	Alternate
Position:	77.52897°N 9.61072°E
Water depth (m):	1720
Target drilling depth (mbsf):	352
Approved maximum penetration (mbsf):	402
Survey coverage (track map; seismic profile):	SV15_01.segy; CAGE20_5HH-15.segy
Objective(s):	Seismic reflector R4A (1.5 My), Quaternary climatic transitions, paleo SBSIS dynamic
Coring program:	Hole A: APC/HLAPC/XCB to 402 mbsf - 4 APCT measurements Hole B: APC/HLAPC/XCB to 402 mbsf Hole C: APC/HLAPC/XCB to 402 mbsf Hole D: APC/HLAPC/XCB to 402 mbsf
Downhole measurements program:	Hole D: Wireline log with Triple Combo; FMS-sonic; VSI
Nature of rock anticipated:	Fine grained contourites and glaciomarine sediments

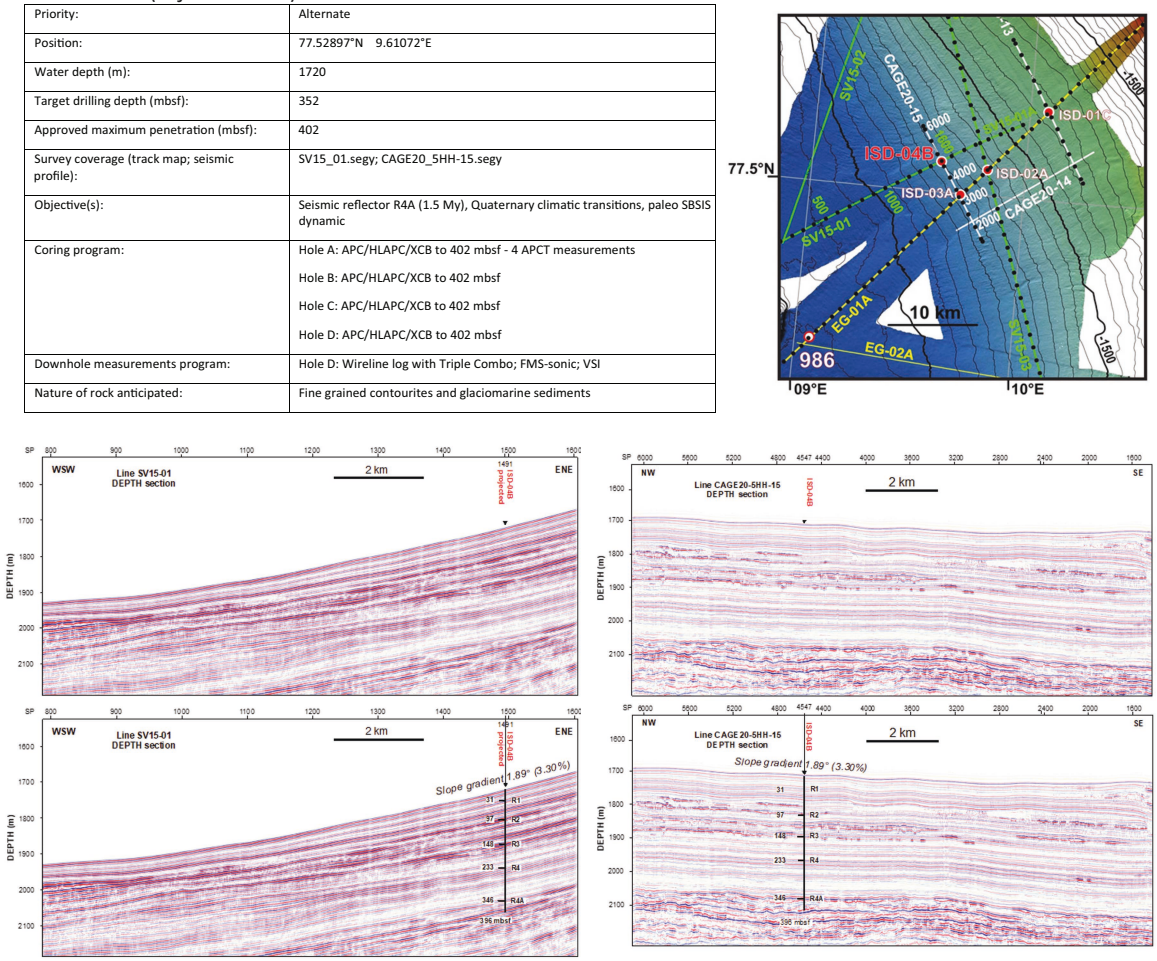

Figure AF7. Top: multibeam bathymetric map with location of alternate Site ISD-04B on Isfjorden drift and crossing multichannel seismic (MCS) lines. Contour interval = 50 m (thick lines every 500 m). 986 = ODP Site 896. Bottom: MCS (Left) Line SV15-01 and (Right) Cross-Line CAGE20-5HH-15 showing stratigraphic section (Top: clean; Bottom: interpreted). Ages of seismic reflectors: R1 = 0.2 Ma, R2 = 0.4 Ma, R3 = 0.75 Ma, R4 = 1.1 Ma, R4A = 1.3 Ma.

Site VRE-01B (Vestnesa Ridge East Termination)

Priority:	Alternate
Position:	79.03208°N 7.05774°E
Water depth (m):	1293
Target drilling depth (mbsf):	616
Approved maximum penetration (mbsf):	618
Survey coverage (track map; seismic profile):	CAGE19-1-HH-051-2D.segy; CAGE19-1-HH-052-2D.segy
Objective(s):	Seismic reflector R8 (5.8 My), Late Miocene Transition, Plio-Quaternary climatic transitions, sediment tectonic stress, evolution of the Molloy Transform Fault
Coring program:	Hole A: APC/HLAPC/XCB to 400 mbsf - 4 APCT measurements Hole B: APC/HLAPC/XCB to 400 mbsf Hole C: APC/HLAPC/XCB to 400 mbsf Hole D: APC/HLAPC/XCB to 400 mbsf
Downhole measurements program:	Hole D: Wireline log with Triple Combo; FMS-sonic; VSI
Nature of rock anticipated:	Fine grained contourites and glaciomarine sediments

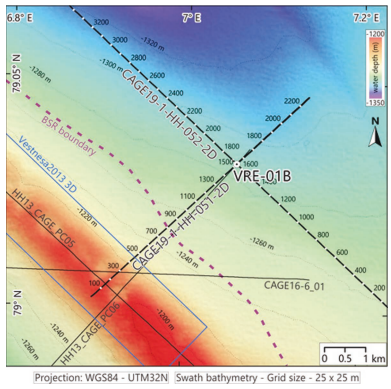

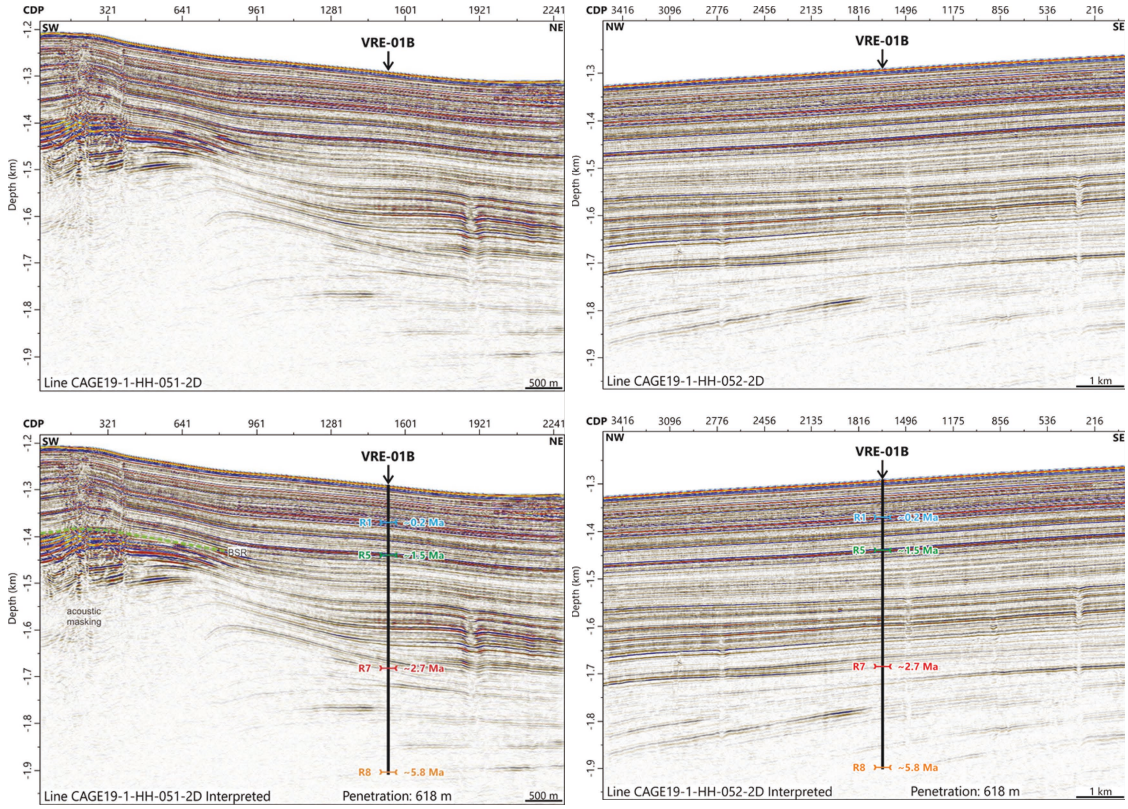

Figure AF8. Top: multibeam bathymetric map with location of proposed alternate Site VRE-01B on Vestnesa Ridge east termination and intersecting multichannel seismic (MCS) lines. Hydrates occur along narrow corridor only at crest of Vestnesa Ridge. Contour interval = 20 m. Bottom: MCS (Left) Line CAGE19-1-HH-051-2D and (Right) Line CAGE19-1-HH-052-2D showing stratigraphic section (Top: clean; Bottom: interpreted). Stratigraphic markers are correlated from ODP Site 912 further north on Yermak Plateau (Mattingsdal et al., 2014). CDP = common depth point.

Site VRE-03A (Vestnesa Ridge East Termination)

Priority:	Primary
Position:	78.94845°N 7.47311°E
Water depth (m):	1201
Target drilling depth (mbsf):	538
Approved maximum penetration (mbsf):	738
Survey coverage (track map; seismic profile):	CAGE20-5-HH-08-2D.segy; CAGE20-5-HH-02-2D.segy
Objective(s):	Seismic reflector R8 (5.8 My), Late Miocene Transition, Plio-Quaternary climatic transitions, sediment tectonic stress, evolution of the Molloy Transform Fault
Coring program:	Hole A: APC/HLAPC/XCB to 400 mbsf - 4 APCT measurements Hole B: APC/HLAPC/XCB to 400 mbsf Hole C: APC/HLAPC/XCB to 400 mbsf Hole D: APC/HLAPC/XCB to 738 mbsf
Downhole measurements program:	Hole D: Wireline log with Triple Combo; FMS-sonic; VSI
Nature of rock anticipated:	Fine grained contourites and glaciomarine sediments

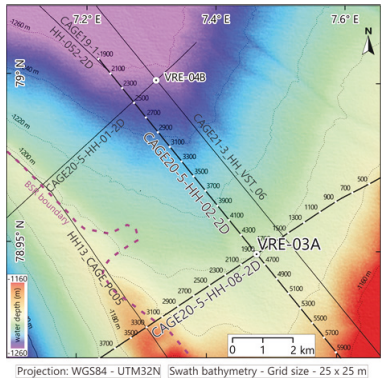

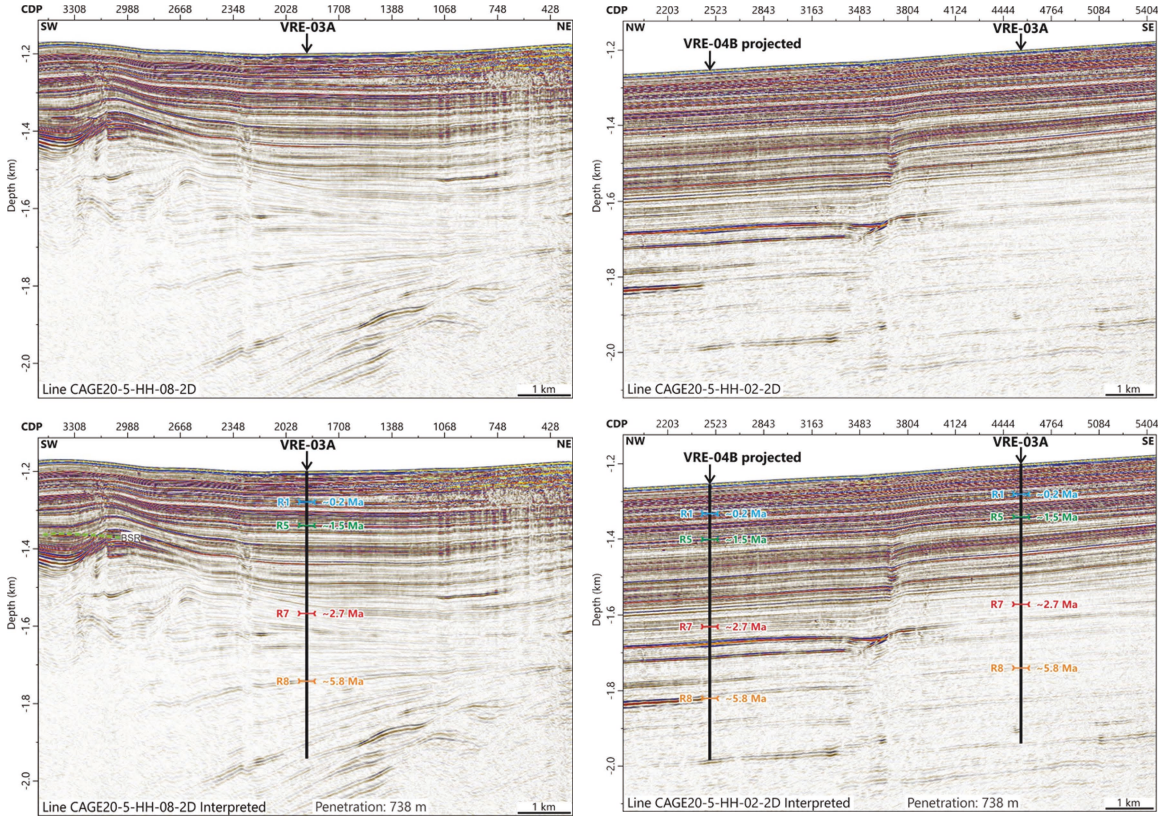

Figure AF9. Top: multibeam bathymetric map with location of primary Site VRE-03A on Vestnesa Ridge east termination and intersecting multichannel seismic (MCS) lines. Hydrates occur along narrow corridor only at crest of Vestnesa Ridge. Contour interval = 20 m. Bottom: MCS (Left) Line CAGE20-5-HH-08-2D and (Right) Line CAGE20-5-HH-02-2D showing stratigraphic section (Top: clean; Bottom: interpreted). Stratigraphic markers are correlated from ODP Site 912 further north on Yermak Plateau (Mattingsdal et al., 2014). CDP = common depth point.

Site VRE-04B (Vestnesa Ridge East Termination)

Priority:	Alternate
Position:	78.99940°N 7.31070°E
Water depth (m):	1257
Target drilling depth (mbsf):	557
Approved maximum penetration (mbsf):	730
Survey coverage (track map; seismic profile):	CAGE20-5-HH-01-2D.segy; CAGE21-3-HH-VST-06.segy
Objective(s):	Seismic reflector R8 (5.8 My), Late Miocene Transition, Plio-Quaternary climatic transitions, sediment tectonic stress, evolution of the Molloy Transform Fault
Coring program:	Hole A: APC/HLAPC/XCB to 400 mbsf - 4 APCT measurements Hole B: APC/HLAPC/XCB to 400 mbsf Hole C: APC/HLAPC/XCB to 400 mbsf Hole D: APC/HLAPC/XCB to 730 mbsf
Downhole measurements program:	Hole D: Wireline log with Triple Combo; FMS-sonic; VSI
Nature of rock anticipated:	Fine grained contourites and glaciomarine sediments

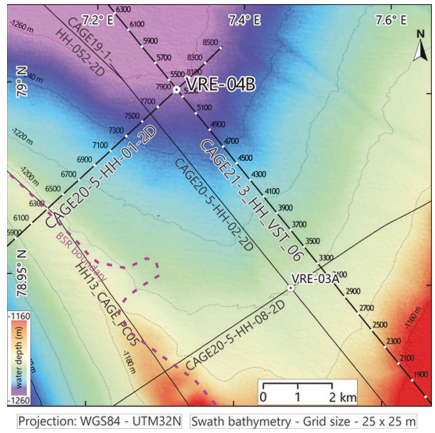

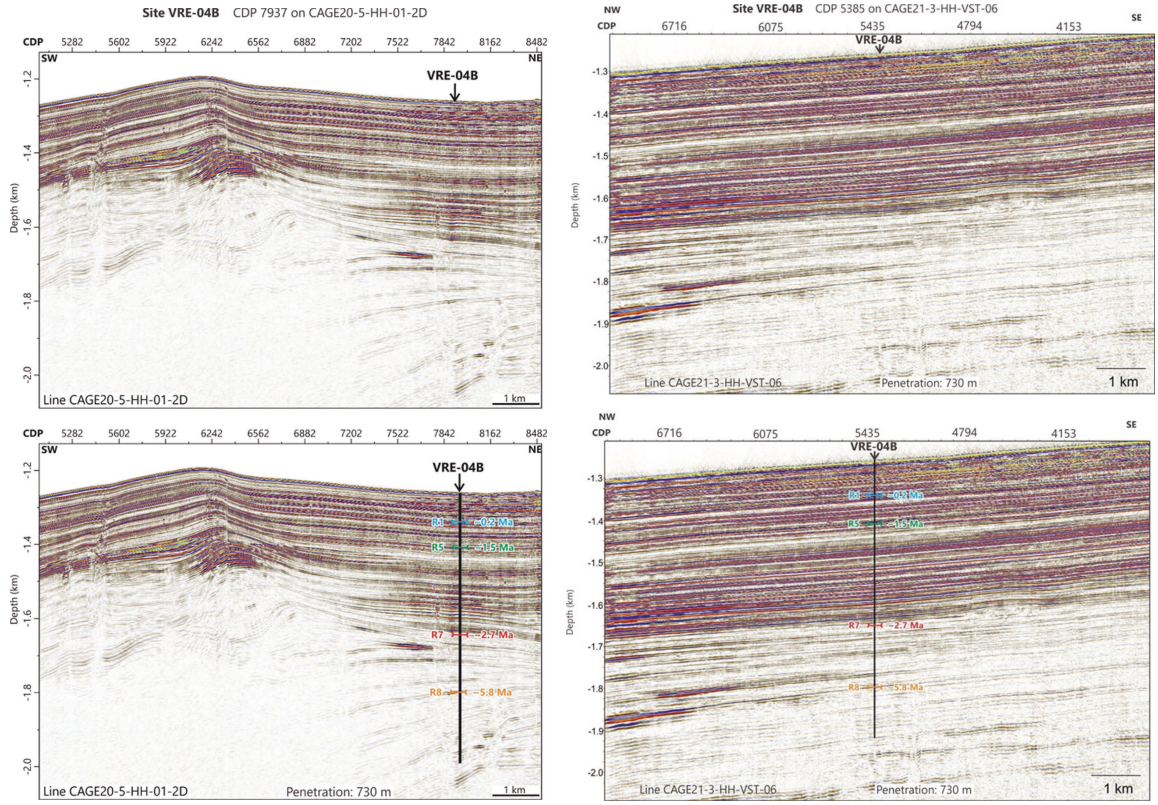

Figure AF10. Top: multibeam bathymetric map with location of alternate Site VRE-04B on Vestnesa Ridge east termination and intersecting multichannel seismic (MCS) lines. Hydrates occur along narrow corridor only at crest of Vestnesa Ridge. Contour interval = 20 m. Bottom: MCS (Left) Line CAGE20-5-HH-01-2D and (Right) Line CAGE21-3-HH-VST-06 showing stratigraphic section (Top: clean; Bottom: interpreted). Stratigraphic markers are correlated from ODP Site 912 further north on Yermak Plateau (Mattingsdal et al., 2014). CDP = common depth point.

Site VRW-02B (Vestnesa Ridge West Termination)

Priority:	Alternate
Position:	79.15870°N 4.62165°E
Water depth (m):	1607
Target drilling depth (mbsf):	531
Approved maximum penetration (mbsf):	677
Survey coverage (track map; seismic profile):	CAGE18-4_08.segy; CAGE20-5-HH-09-2D.segy
Objective(s):	Seismic reflector R8 (5.8 My), Late Miocene Transition, Plio-Quaternary climatic transitions, sediment tectonic stress, evolution of the Molloy Transform Fault
Coring program:	Hole A: APC/HLAPC/XCB to 400 mbsf - 4 APCT measurements Hole B: APC/HLAPC/XCB to 400 mbsf Hole C: APC/HLAPC/XCB to 400 mbsf Hole D: APC/HLAPC/XCB to 677 mbsf
Downhole measurements program:	Hole D: Wireline log with Triple Combo; FMS-sonic; VSI
Nature of rock anticipated:	Fine grained contourites and glaciomarine sediments

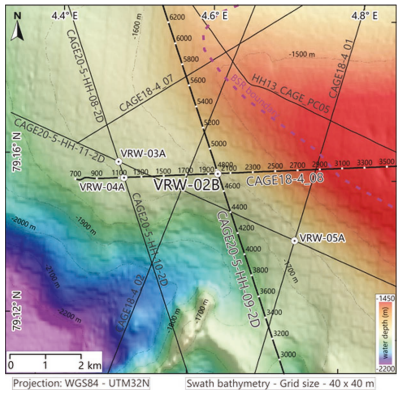

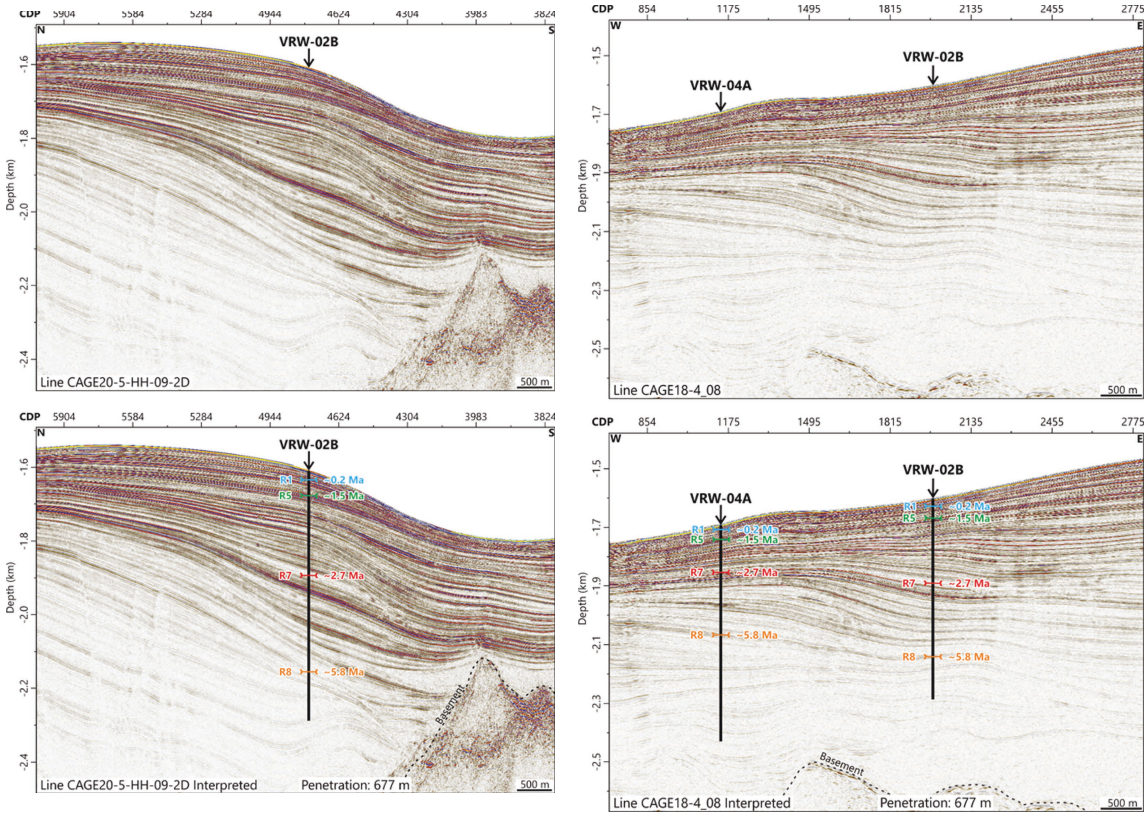

Figure AF11. Top: multibeam bathymetric map with location of alternate Site VRW-02B on Vestnesa Ridge west termination and intersecting multichannel seismic (MCS) lines. Hydrates occur along narrow corridor only at crest of Vestnesa Ridge. Contour interval = 100 m. Bottom: MCS (Left) Line CAGE20-5-HH-09-2D and (Right) Line CAGE18-4_08 showing stratigraphic section (Top: clean; Bottom: interpreted). Stratigraphic markers are correlated from ODP Site 912 further north on Yermak Plateau (Mattingsdal et al., 2014). CDP = common depth point.

Site VRW-03A (Vestnesa Ridge West Termination)

Priority:	Primary
Position:	79.15985°N 4.48874°E
Water depth (m):	1681
Target drilling depth (mbsf):	364
Approved maximum penetration (mbsf):	696
Survey coverage (track map; seismic profile):	CAGE20-5-HH-11-2D.segy; CAGE20-5-HH-10-2D.segy
Objective(s):	Seismic reflector R8 (5.8 My), Late Miocene Transition, Plio-Quaternary climatic transitions, sediment tectonic stress, evolution of the Molloy Transform Fault
Coring program:	Hole A: APC/HLAPC/XCB to 400 mbsf - 4 APCT measurements Hole B: APC/HLAPC/XCB to 400 mbsf Hole C: APC/HLAPC/XCB to 400 mbsf Hole D: APC/HLAPC/XCB to 696 mbsf
Downhole measurements program:	Hole D: Wireline log with Triple Combo; FMS-sonic; VSI
Nature of rock anticipated:	Fine grained contourites and glaciomarine sediments

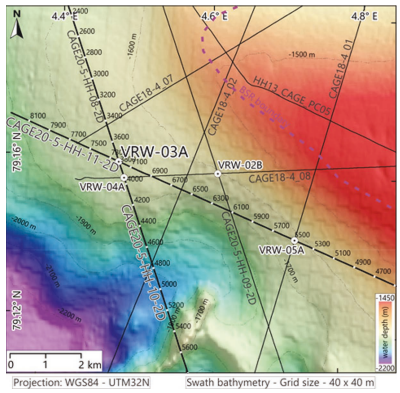

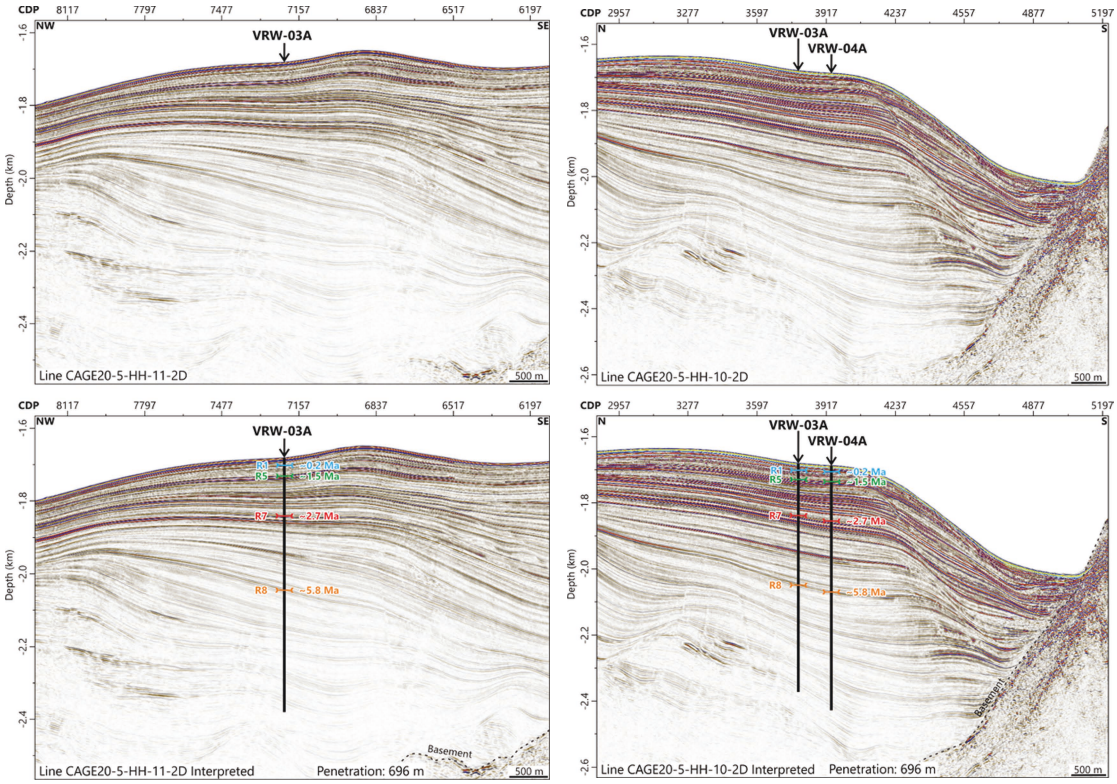

Figure AF12. Top: multibeam bathymetric map with location of primary Site VRW-03A on Vestnesa Ridge west termination and intersecting multichannel seismic (MCS) lines. Hydrates occur along narrow corridor only at crest of Vestnesa Ridge. Contour interval = 100 m. Bottom: MCS (Left) Line CAGE20-5-HH-11-2D and (Right) Line CAGE20-5-HH-10-2D showing stratigraphic section (Top: clean; Bottom: interpreted). Stratigraphic markers are correlated from ODP Site 912 further north on Yermak Plateau (Mattingsdal et al., 2014). CDP = common depth point.

Site VRW-04A (Vestnesa Ridge West Termination)

Priority:	Alternate
Position:	79.15593°N 4.49753°E
Water depth (m):	1690
Target drilling depth (mbsf):	375
Approved maximum penetration (mbsf):	740
Survey coverage (track map; seismic profile):	CAGE18-4_08.segy; CAGE20-5-HH-10-2D.segy
Objective(s):	Seismic reflector R8 (5.8 My), Late Miocene Transition, Plio-Quaternary climatic transitions, sediment tectonic stress, evolution of the Molloy Transform Fault
Coring program:	Hole A: APC/HLAPC/XCB to 400 mbsf - 4 APCT measurements Hole B: APC/HLAPC/XCB to 400 mbsf Hole C: APC/HLAPC/XCB to 400 mbsf Hole D: APC/HLAPC/XCB to 740 mbsf
Downhole measurements program:	Hole D: Wireline log with Triple Combo; FMS-sonic; VSI
Nature of rock anticipated:	Fine grained contourites and glaciomarine sediments

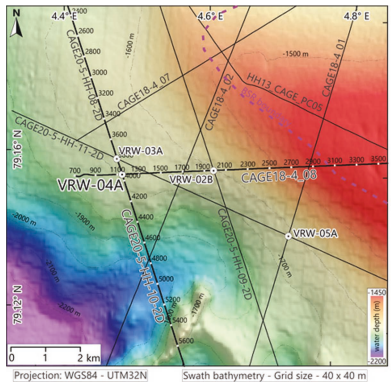

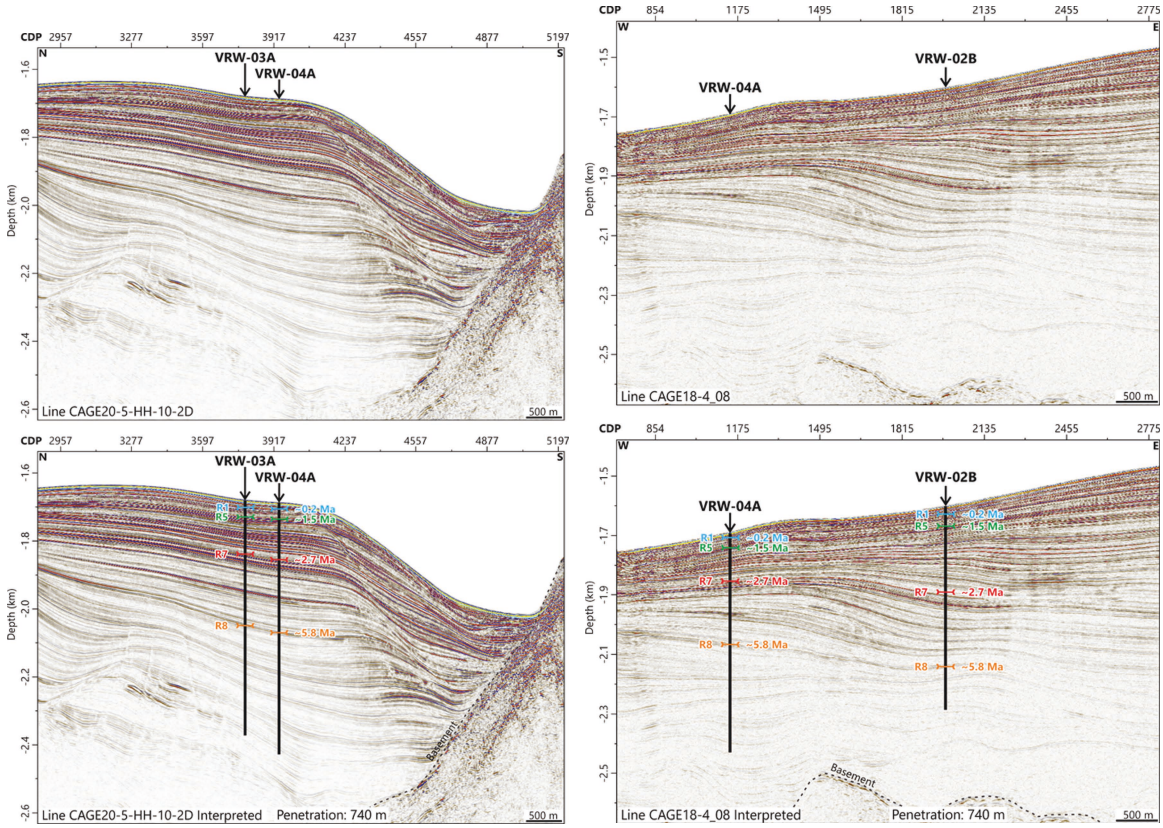

Figure AF13. Top: multibeam bathymetric map with location of alternate Site VRW-04A on Vestnesa Ridge west termination and intersecting multichannel seismic (MCS) lines. Hydrates occur along narrow corridor only at crest of Vestnesa Ridge. Contour interval = 100 m. Bottom: MCS (Left) Line CAGE20-5-HH-10-2D and (Right) Line CAGE18-4_08 showing stratigraphic section (Top: clean; Bottom: interpreted). Stratigraphic markers are correlated from ODP Site 912 further north on Yermak Plateau (Mattingsdal et al., 2014). CDP = common depth point.

Site VRW-05A (Vestnesa Ridge West Termination)

Priority:	Alternate
Position:	79.14327°N 4.73000°E
Water depth (m):	1621
Target drilling depth (mbsf):	625
Approved maximum penetration (mbsf):	669
Survey coverage (track map; seismic profile):	CAGE20-5-HH-11-2D.segy; CAGE18-4-01.segy
Objective(s):	Seismic reflector R8 (5.8 My), Late Miocene Transition, Plio-Quaternary climatic transitions, sediment tectonic stress, evolution of the Molloy Transform Fault
Coring program:	Hole A: APC/HLAPC/XCB to 400 mbsf - 4 APCT measurements Hole B: APC/HLAPC/XCB to 400 mbsf Hole C: APC/HLAPC/XCB to 400 mbsf Hole D: APC/HLAPC/XCB to 669 mbsf
Downhole measurements program:	Hole D: Wireline log with Triple Combo; FMS-sonic; VSI
Nature of rock anticipated:	Fine grained contourites and glaciomarine sediments

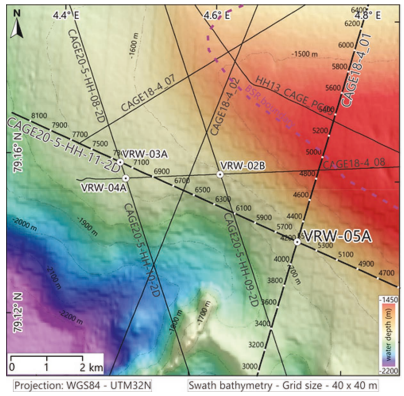

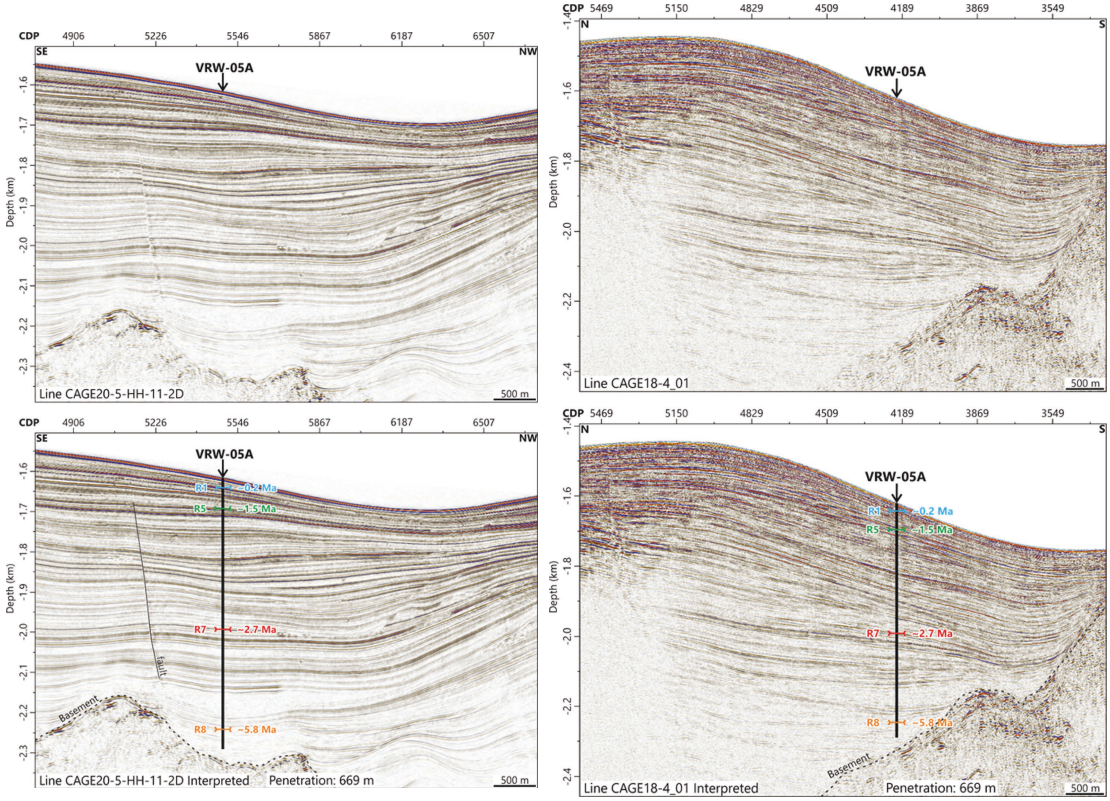

Figure AF14. Top: multibeam bathymetric map with location of alternate Site VRW-05A on Vestnesa Ridge west termination and intersecting multichannel seismic (MCS) lines. Hydrates occur along narrow corridor only at crest of Vestnesa Ridge. Contour interval = 1000 m. Bottom: MCS (Left) Line CAGE20-5-HH-11-2D and (Right) Line CAGE18-4_01 showing stratigraphic section (Top: clean; Bottom: interpreted). Stratigraphic markers are correlated from ODP Site 912 further north on Yermak Plateau (Mattingsdal et al., 2014). CDP = common depth point.

Site SVR-03A (Svyatogor Ridge)

Priority:	Primary
Position:	78.2718209°N 5.889665°E
Water depth (m):	1581
Target drilling depth (mbsf):	108
Approved maximum penetration (mbsf):	616
Survey coverage (track map; seismic profile):	Svyatogor2014-3D-XL222.segy; CAGE21-3HH_SVR-IODP-01.segy
Objective(s):	Seismic reflector R7 (2.7 My), Onset of NHG, Quaternary climatic transitions, sediment tectonic stress, evolution of the Molloy Transform Fault
Coring program:	Hole A: APC/HLAPC/XCB to 400 mbsf - 4 APCT measurements Hole B: APC/HLAPC/XCB to 400 mbsf Hole C: APC/HLAPC/XCB to 616 mbsf
Downhole measurements program:	Hole C: Wireline log with Triple Combo; FMS-sonic; VSI
Nature of rock anticipated:	Fine grained contourites and glaciomarine sediments

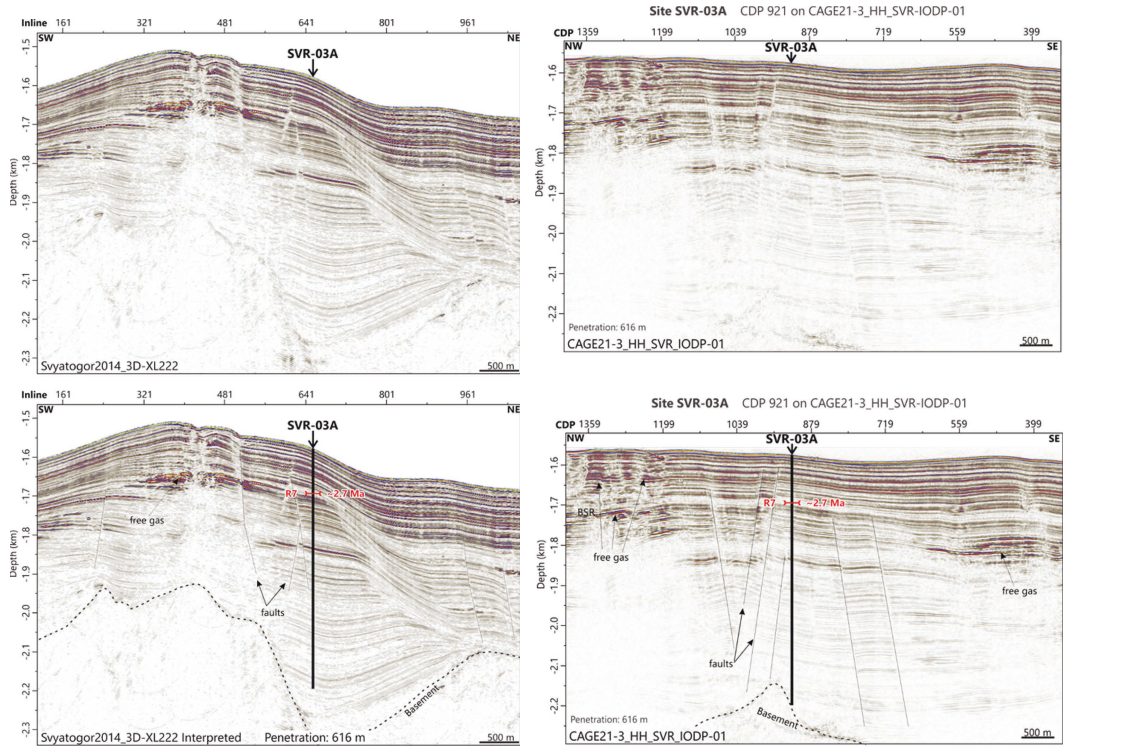

Figure AF15. Top: multibeam bathymetric map with location of primary Site SVR-03A on Svyatogor Ridge and intersecting Svyatogor 2014 3-D seismic lines. Indications for hydrates occur only at crest of Svyatogor Ridge. Contour interval = 10 m. Bottom: (Left) Cross-Line 222 and (Right) In-Line CAGE21-3-HH-SVR-IODP-01 from Svyatogor 2014 3-D seismic data showing stratigraphic section (Top: clean; Bottom: interpreted). Stratigraphic marker from Waghorn et al. (2018). CDP = common depth point.

Site SVR-04A (Svyatogor Ridge)

Priority:	Alternate
Position:	78.2641°N 5.9231°E
Water depth (m):	1594
Target drilling depth (mbsf):	123
Approved maximum penetration (mbsf):	745
Survey coverage (track map; seismic profile):	Svyatogor2014-3D-XL46.segy; CAGE21-3HH_SVR-IODP-01.segy
Objective(s):	Seismic reflector R7 (2.7 My), Onset of NHG, Quaternary climatic transitions, sediment tectonic stress, evolution of the Molloy Transform Fault
Coring program:	Hole A: APC/HLAPC/XCB to 400 mbsf - 4 APCT measurements Hole B: APC/HLAPC/XCB to 400 mbsf Hole C: APC/HLAPC/XCB to 745 mbsf
Downhole measurements program:	Hole C: Wireline log with Triple Combo; FMS-sonic; VSI
Nature of rock anticipated:	Fine grained contourites and glaciomarine sediments

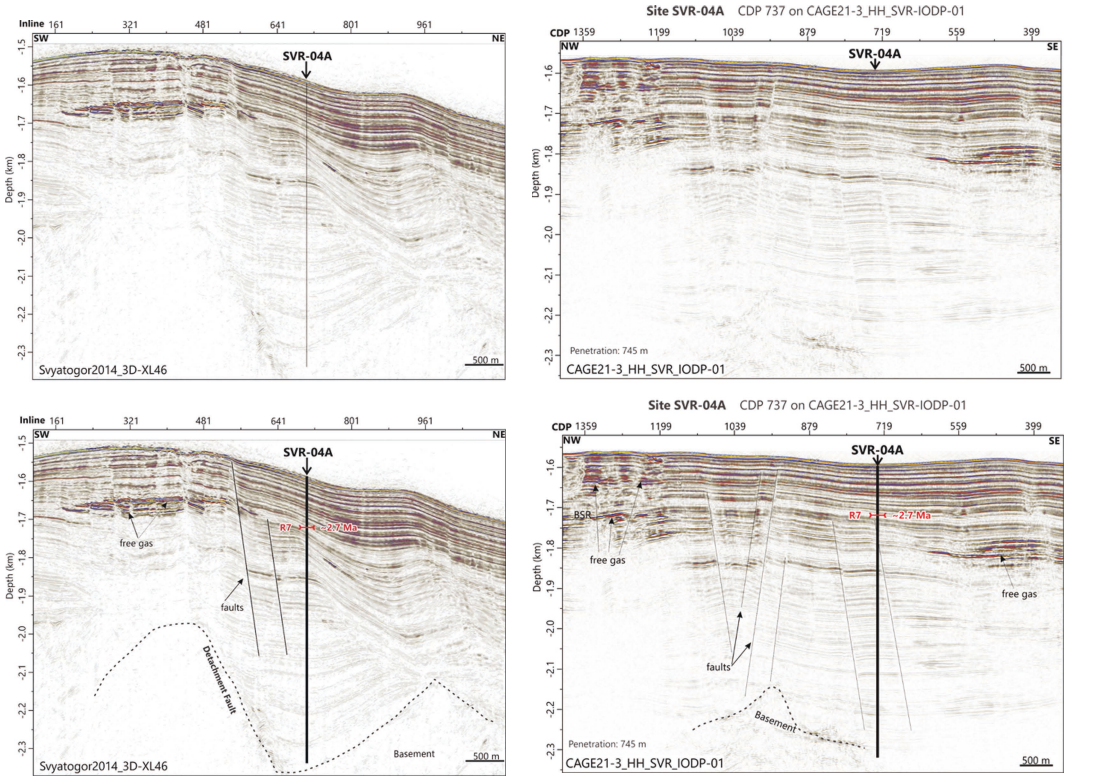

Figure AF16. Top: multibeam bathymetric map with location of alternate Site SVR-04A on Svyatogor Ridge and intersecting Svyatogor 2014 3-D seismic lines. Indications for hydrates occur only at crest of Svyatogor Ridge. Contour interval = 10 m. Bottom: (Left) Cross-Line 46 from Svyatogor 2014 3-D seismic data and (Right) Line CAGE21-3_HH_SVR-IODP-01 showing stratigraphic section (Top: clean; Bottom: interpreted). Stratigraphic marker from Waghorn et al. (2018). CDP = common depth point.

Site SVR-05A (Svyatogor Ridge)

Priority:	Alternate
Position:	78.2688°N 5.9095°E
Water depth (m):	1600
Target drilling depth (mbsf):	108
Approved maximum penetration (mbsf):	738
Survey coverage (track map; seismic profile):	Svyatogor2014-3D-XL143.segy; Svyatogor2014-3D-IL707.segy
Objective(s):	Seismic reflector R7 (2.7 My), Onset of NHG, Quaternary climatic transitions, sediment tectonic stress, evolution of the Molloy Transform Fault
Coring program:	Hole A: APC/HLAPC/XCB to 400 mbsf - 4 APCT measurements Hole B: APC/HLAPC/XCB to 400 mbsf Hole C: APC/HLAPC/XCB to 738 mbsf
Downhole measurements program:	Hole C: Wireline log with Triple Combo; FMS-sonic; VSI
Nature of rock anticipated:	Fine grained contourites and glaciomarine sediments

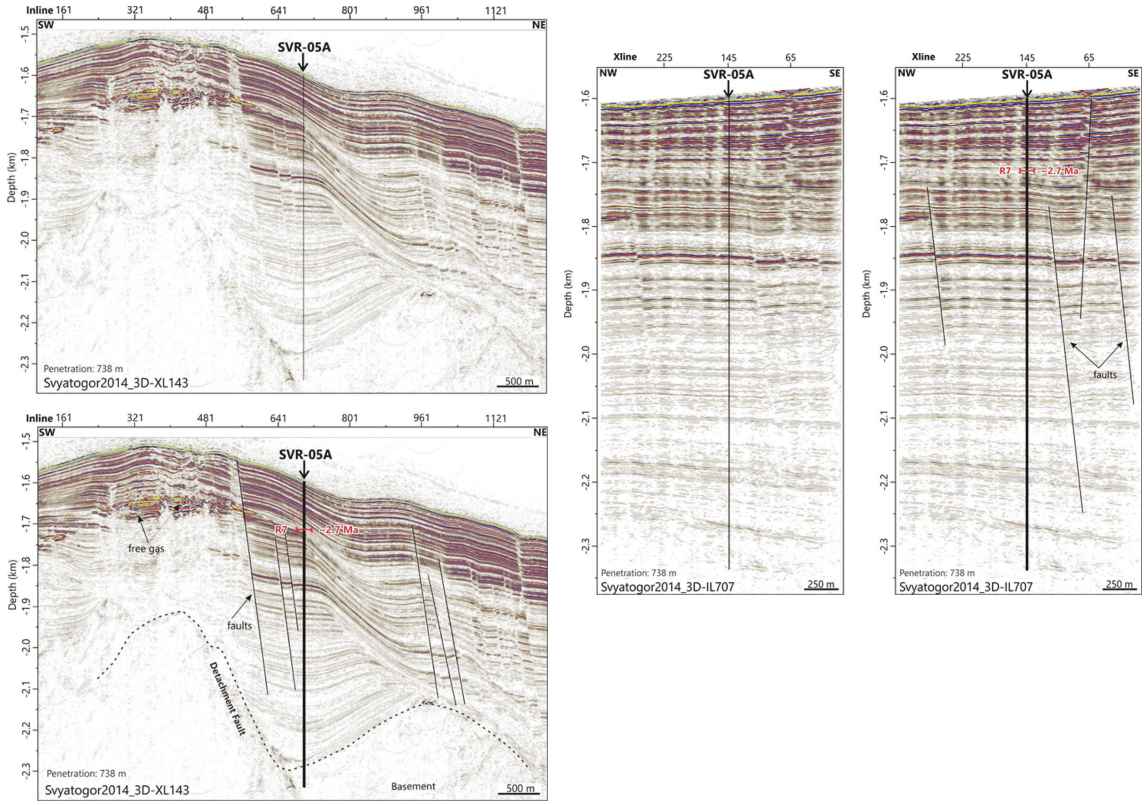

Figure AF17. Top: multibeam bathymetric map with location of alternate Site SVR-05A on Svyatogor Ridge and intersecting Svyatogor 2014 3-D seismic lines. Indications for hydrates occur only at crest of Svyatogor Ridge. Contour interval = 10 m. Bottom: (Left) Cross-Line 143 and (Right) In-Line 707 from Svyatogor 2014 3-D seismic data showing stratigraphic section (Top: clean; Bottom: interpreted). Stratigraphic marker from Waghorn et al. (2018). CDP = common depth point.